



ADVANCED MASTERS IN STRUCTURAL ANALYSIS
OF MONUMENTS AND HISTORICAL CONSTRUCTIONS

Master's Thesis

Christopher Potter

Seismic Analysis of a Typical Masonry Building from Barcelona's Eixample District



UNIVERSITAT POLITÈCNICA
DE CATALUNYA



UNIVERSITY OF PADOVA



Education and Culture

Erasmus Mundus



ADVANCED MASTERS IN STRUCTURAL ANALYSIS
OF MONUMENTS AND HISTORICAL CONSTRUCTIONS



Master's Thesis

Christopher Potter

Seismic Analysis of a Typical Masonry Building from Barcelona's Eixample District

This Masters Course has been funded with support from the European Commission. This publication reflects the views only of the author, and the Commission cannot be held responsible for any use which may be made of the information contained therein.

DECLARATION

Name: Christopher Potter

Email: cpotter.eng@gmail.com

Title of the MSc. Dissertation: Seismic Analysis of a Typical Masonry Building from Barcelona's Eixample District

Supervisor(s): Professor Pere Roca

Year: 2011

I hereby declare that all information in this document has been obtained and presented in accordance with academic rules and ethical conduct. I also declare that, as required by these rules and conduct, I have fully cited and referenced all material and results that are not original to this work.

I hereby declare that the MSc Consortium responsible for the Advanced Masters in Structural Analysis of Monuments and Historical Constructions is allowed to store and make available electronically the present MSc Dissertation.

University: Universitat Politècnica de Catalunya

Date: 15 July 2011

Signature:



This page is left blank on purpose.

ACKNOWLEDGEMENTS

I would like to thank the SAHC Consortium for selecting me to be part of this wonderful Erasmus Mundus programme. I would also like to acknowledge the financial support provided throughout the course.

I am grateful to my supervisor, Professor Pere Roca, for his kind and focused guidance during the preparation of this dissertation. I would also like to thank him for being able to work with his PhD students and for providing me access to the analysis software both on campus and at home.

My gratitude goes out to each of the professors and guest lecturers of the course. In particular, I recognise the efforts of Professor Claudio Modena, who organised and guided two incredible site visits during my coursework at the University of Padova.

My thanks also goes to all the PhD students who helped throughout my coursework and dissertation. In particular, from the University of Padova I recognise Bruno Silva and Filippo Lorenzoni. From the Universitat Politècnica de Catalunya I especially would like to thank Yohei Endo and Ahmed Elyamani.

I also feel incredibly fortunate to have had such wonderful classmates in Padova and Barcelona. It is them more than anything that has made the course so enjoyable.

Finally, above all else I would like to acknowledge the unending love and support of my wife and family.

This page is left blank on purpose.

ABSTRACT

The historic Eixample district of Barcelona is characterised by its beautiful avenues, laid out in grid across the city. At first impression, the buildings lining these avenues appear identical, an unending façade built to house the new Barcelona of the 20th Century. The unreinforced masonry buildings that typify the development remain in use today, largely unaltered since their construction.

Unreinforced masonry buildings are among the most vulnerable structures to damage from seismic actions. For the masonry buildings of the Eixample that house over 15% of the population of Barcelona, this is no exception. This study performs a seismic analysis on a typical masonry building of the Eixample to estimate and assess this damage. By doing so, it aims to estimate the likely damage due to seismic actions, to identify critical elements of the structures and to quantify the need for seismic risk maintenance and response plans.

The analysis uses the N2 Capacity Spectrum Method (Fajfar, 2000), adopted by Eurocode 8, to determine the displacement demand of possible earthquake scenarios. A seismic hazard analysis determines the seismic demand using deterministic, probabilistic and current European and Spanish code provisions. The seismic demand is then compared to the results of a non-linear pushover analysis completed using software DIANA (Version 9.4). The model geometry was based upon plans of a building that well represents the typical unreinforced masonry buildings of the Eixample.

Results indicate a displacement demand to Spanish code provisions that corresponds to a substantial level of damage, in accordance with the European Macroseismic Scale (EMS 98) damage criteria. A moderate level of damage is derived from the probabilistic seismic scenario. Similar to previous studies, these results indicate a significant risk of seismic damage. The analysis has isolated critical structural elements that control the global response and damage during seismic action. This information can be used to develop inspection and maintenance plans to limit the risk of seismic damage.

This study highlights the real risk of seismic damage to the typical unreinforced masonry buildings of the Eixample district. It determines appropriate building maintenance procedures, and reinforces the need for seismic response planning to best manage the significant expected social and infrastructure demands should such a disastrous event ever occur.

This page is left blank on purpose.

RESUMEN

El histórico distrito de Eixample en Barcelona se caracteriza por sus hermosas avenidas, organizadas en una cuadrícula casi perfecta a lo largo de la ciudad. A primera vista, sus edificios parecen idénticos, formando una larga fachada sin fin construida para albergar la nueva Barcelona del Siglo XX. Los edificios de mampostería no reforzada que tipifican esta área de la ciudad continúan en uso hoy en día y la gran mayoría de ellos sin sufrir ningún tipo de alteración desde su construcción.

Los edificios de mampostería no reforzada se clasifican entre las estructuras más vulnerables a los eventos sísmicos. Los edificios del distrito de Eixample, que albergan más del 15% de la población de Barcelona, no son la excepción. En el presente estudio se lleva a cabo un análisis sísmico de un edificio típico de mampostería no reforzada del área de Eixample con el fin de estimar y evaluar el nivel de daño. De esta forma, el objetivo del estudio es el de estimar el posible daño causado por un sismo, identificar los elementos críticos de la estructura y cuantificar la necesidad de realizar un mantenimiento de riesgo sísmico y de diseñar planes de respuesta.

El análisis utiliza el Método del Espectro de Capacidad N2 (Fajfar, 2000), adoptado por el Eurocodigo 8, para determinar el desplazamiento de demanda ante diferentes escenarios sísmicos. Mediante un análisis de riesgo sísmico se determina la demanda sísmica usando métodos determinísticos y probabilísticos; asimismo, las provisiones vigentes del código Europeo y Español son usadas para definir escenarios de demanda sísmica adicionales. Una vez determinada la demanda sísmica, esta es comparada con los resultados obtenidos de un análisis no lineal de tipo pushover realizado con el programa DIANA (Versión 9.4). La geometría utilizada en el modelo se basa en los planos de un edificio representativo de la geometría típica encontrada en los edificios de mampostería no reforzada del distrito de Eixample.

Para el caso en el cual el espectro de demanda es definido de acuerdo a las provisiones del código Español, los resultados obtenidos indican un desplazamiento de demanda que corresponde a un nivel de daño sustancial (basado en los criterios de daño establecidos por la Escala Macrosísmica Europea, EMS 98). Por otra parte, un nivel de daño moderado es obtenido para el caso en el cual el espectro de demanda se define basado en métodos probabilísticos. De forma similar a lo observado en estudios desarrollados por otros investigadores en el pasado, estos resultados indican un riesgo significativo de daño sísmico. Durante el análisis se identifican ciertos elementos estructurales que son críticos y que controlan el comportamiento global y el nivel de daño durante un evento sísmico. Esta información puede ser utilizada para diseñar planes de inspección y mantenimiento para limitar el riesgo de daño sísmico.

El presente estudio destaca el riesgo real de daño sísmico para un edificio típico de mampostería no reforzada del distrito de Eixample. Se determinan procedimientos apropiados para el mantenimiento de edificios, y se recalca la necesidad de diseñar planes de respuesta para manejar mejor las significativas demandas sociales y de infraestructura que se presentarían en el caso de un evento sísmico.

This page is left blank on purpose.

TABLE OF CONTENTS

1.	INTRODUCTION AND OBJECTIVES	1
1.1	Introduction	1
1.2	Objectives	3
1.3	Work Organisation	4
2.	STRUCTURAL ASSESSMENT – STATE OF THE ART	7
2.1	Introduction	7
2.2	Structure Identification	8
2.3	Historical Investigation	8
2.4	Geometrical and Structural Systems Survey	8
2.5	Damage Survey and Identification of Actions	9
2.5.1	Mechanical Actions	9
2.5.2	Physical Actions	10
2.5.3	Chemical and biological actions	10
2.6	Material Characterisation	10
2.7	Monitoring	11
2.8	Previous Studies	12
2.9	Structural Analysis Techniques	12
2.9.1	Kinematic Limit Analysis	13
2.9.2	Non-linear Time History Analysis	15
2.9.3	Non-linear Pushover Analysis	16
2.9.4	Applicability of Pushover Methods	18
2.9.5	Non-linear Modelling	19
2.10	Diagnosis and Vulnerability Assessment	20
2.11	Maintenance and Interventions	24
3.	SEISMIC HAZARD ASSESSMENT – STATE OF THE ART	25
3.1	Introduction	25
3.2	Site Geology	27
3.3	Deterministic Approach	29
3.4	Probabilistic Approach	32
3.5	Code Recommendations	33
3.5.1	Eurocode 8	33
3.5.2	NCSE-02	34
4.	CAPACITY SPECTRUM METHOD – STATE OF THE ART	37
4.1	Introduction	37

4.2	Step 1 – Seismic Demand	37
4.3	Step 2 – Pushover Curve.....	38
4.4	Step 3 – Capacity Spectrum	40
4.5	Step 4 – Displacement Demand.....	41
4.5.1	Case 1 – Elastic demand	42
4.5.2	Case 2 – Inelastic demand, $T^* > T_c$	42
4.5.3	Case 3 – Inelastic demand, $T^* < T_c$	44
5.	STRUCTURAL ASSESSMENT – CASE STUDY.....	47
5.1	Structure Identification	47
5.2	Historical Investigation.....	48
5.3	Geometrical and Structural Systems Survey.....	51
5.4	Previous Studies.....	55
5.5	Damage Survey and Identification of Actions.....	56
5.5.1	Damage.....	56
5.5.2	Loading	57
5.6	Monitoring	58
6.	SEISMIC HAZARD ASSESSMENT – CASE STUDY	59
6.1	Introduction	59
6.2	Site Geology	59
6.3	Smoothed Acceleration Response Spectra.....	63
6.4	Deterministic Approach.....	65
6.5	Probabilistic Approach	68
6.6	Code Recommendations	71
6.6.1	Eurocode 8.....	71
6.6.2	NCSE-02.....	73
6.7	Discussion of Results	75
7.	STRUCTURAL ANALYSIS – CASE STUDY	77
7.1	Introduction	77
7.2	Model Geometry and Constraints.....	77
7.2.1	Model Descriptions	78
7.2.2	Model Simplifications and Assumptions	80
7.2.3	Finite Element Discretisation	86
7.3	Material Characteristics and Behavioural Models	88
7.4	Analysis Procedure.....	90
7.4.1	Step 1 – Seismic Demand	90
7.4.2	Step 2 – Pushover Curve.....	90

7.4.3	Step 3 – Capacity Spectrum	95
7.4.4	Step 4 – Displacement Demand.....	96
7.5	Model Results and Damage Probability Assessment	97
7.5.1	Gravity Analysis	99
7.5.2	Case 1 and Case 2	103
7.5.3	Case 3.....	109
7.5.4	Case 4 and Case 5	113
7.5.5	Case 6.....	118
7.5.6	Case 7.....	120
7.5.7	Case 8.....	125
7.6	Discussion of Results	128
7.7	Results of Kinematic Limit Analysis.....	129
8.	CONCLUSIONS	131
9.	REFERENCES	133
10.	APPENDICES.....	137
10.1	Appendix A	137

Figures Index

Figure 1.1: The Eixample, Barcelona (CCCB, 2009)	1
Figure 2.1: Two out-of-plane façade mechanisms for a typical unreinforced masonry building (NIKER D3.1, 2010).....	14
Figure 2.2: In-plane façade failure mechanisms for an unreinforced masonry building (DDPC, 2006)	15
Figure 2.3: Typical pushover curve	16
Figure 2.4: Simplified representation of capacity and demand spectra in ADRS format (FEMA 440, 2005)	17
Figure 2.5: Damage grades (EMS-98)	21
Figure 2.6: Vulnerability index distribution for Barcelona by census zone (Lantada, 2006)	22
Figure 2.7: Definition of damage threshold limits for idealised capacity curve (mod. Irizarry, 2004)....	23
Figure 2.8: Fragility curves for mid-rise unreinforced masonry buildings in Barcelona (Barbat et al., 2006)	24
Figure 3.1: Acceleration Response Spectrum – El Centro, California 1979 (Chopra, 1981).....	25
Figure 3.2: Diagrammatic Smoothed Response Spectrum (Irizarry, 2004)	26
Figure 3.3: Influence of soil classification on acceleration response spectrum (Eurocode 8)	28
Figure 3.4: Relationship between MSK intensity and local magnitude (M_L) (Irizarry et al., 2011)	30
Figure 3.5: Type I and Type II elastic acceleration spectra for soil classifications (Eurocode 8)	34
Figure 4.1: Typical lateral load distributions	39

Figure 4.2: Typical pushover curve for Eixample unreinforced masonry building	39
Figure 4.3: Bilinear elasto perfectly plastic idealisation of pushover curve	41
Figure 4.4: Intersection of capacity and demand spectrum within elastic range	42
Figure 4.5: Intersection in the inelastic range where $T^* > T_C$ (Fajfar, 2000)	43
Figure 4.6: Intersection in the inelastic range where $T^* < T_C$ (Fajfar, 2000)	44
Figure 5.1: Barcelona location	47
Figure 5.2: Districts of Barcelona city (Pujades et al., 2010)	48
Figure 5.3: Plan for Eixample development, Ildefons Cerda, 1859 (CCCB, 2009)	49
Figure 5.4: Typical Eixample block layout (CCCB, 2009)	50
Figure 5.5: Street elevation of typical Eixample block (NIKER D3.1, 2010)	51
Figure 5.6: Façade of 629 Gran Via de la Catalanes	52
Figure 5.7: Plan of 629 Gran Via de la Catalanes (Refer Appendix A)	53
Figure 5.8: 3D representation of 629 Gran Via de la Catalanes	53
Figure 5.9: Section of typical floor system of Eixample buildings (mod. Gutierrez, 2010)	54
Figure 5.10: Floor system of 629 Gran Via de la Catalanes	54
Figure 6.1: Geological map of Barcelona region (Irizarry, 2004)	60
Figure 6.2: Barcelona districts and soil zonation determined by Cid et al. (2001), (Pujades et al., 2010)	61
Figure 6.3: Soil amplification factors for Barcelona for Ambraseys relationship (Irizarry, 2004)	62
Figure 6.4: Diagrammatic smoothed response spectrum – functions after Lagomarsino (2002) (Irizarry, 2004)	64
Figure 6.5: Location of reference earthquakes (Irizarry et al., 2004)	65
Figure 6.6: Deterministic acceleration response spectra for Barcelona – Ambraseys relationship (Irizarry, 2004)	66
Figure 6.7: Deterministic smoothed acceleration response spectra for Barcelona	67
Figure 6.8: Deterministic ADRS demand spectra for Barcelona	67
Figure 6.9: Seismotectonic zonation for Catalonia region (Irizarry, 2004)	68
Figure 6.10: Probabilistic acceleration response spectra for each Barcelona soil zone (Irizarry, 2004)	69
Figure 6.11: Probabilistic smoothed acceleration response spectra for Barcelona	70
Figure 6.12: Probabilistic ADRS demand spectra for Barcelona	70
Figure 6.13: Comparison of probabilistic response spectra to Eurocode 8 Type I and Type II spectra for rock (Irizarry, 2004)	71
Figure 6.14: Comparison of probabilistic response spectra for Zones II and III to Eurocode 8 spectrum Type II, soil class B (Irizarry, 2004)	72
Figure 6.15: Elastic acceleration response spectra for Barcelona soil zones, to NCSE-02	73
Figure 6.16: ADRS demand spectra for Barcelona soil zones, to NCSE-02	74

Figure 6.17: Comparison of demand spectra for the Eixample district, Barcelona by different approaches.....	75
Figure 7.1: Model 1 wall panels.....	78
Figure 7.2: Model 2 wall panels.....	79
Figure 7.3: Model 1 – Axis of symmetry constraints	85
Figure 7.4: Model 2 – Vertical constraints at removed ground floor walls	86
Figure 7.5: Characteristics of a curved shell element (DIANA Ver.9.4, 2009)	87
Figure 7.6: Nodal degrees of freedom for a curved shell element (DIANA Ver.9.4, 2009)	87
Figure 7.7: The CQ40S quadrilateral curved shell element (DIANA Ver.9.4, 2009).....	87
Figure 7.8: Linear tension softening (Lourenço, 2010)	88
Figure 7.9: Drucker Prager yield surface (Lourenço, 2010)	89
Figure 7.10: Model 1 – Deflected shape of first mode of vibration.....	91
Figure 7.11: Secant (or Quasi Newton-Raphson) iteration method.....	94
Figure 7.12: Deflected shape– Ultimate gravity loading.....	99
Figure 7.13: Base reaction – displacement curve, Ultimate gravity loading	100
Figure 7.14: Maximum principal strains – Ultimate gravity loading.....	100
Figure 7.15: Minimum principal strains – Ultimate gravity loading.....	101
Figure 7.16: Maximum principal stresses – Ultimate gravity loading.....	101
Figure 7.17: Minimum principal stresses – Ultimate gravity loading.....	102
Figure 7.18: Deflected shape at yield – Case 1	103
Figure 7.19: Pushover curve – Case 1.....	104
Figure 7.20: Comparison of capacity spectrum and demand spectra – Case 1	105
Figure 7.21: Maximum principal strains at substantial damage state – Case 1.....	106
Figure 7.22: Minimum principal strains at substantial damage state – Case 1.....	107
Figure 7.23: Maximum principal stresses at substantial damage state – Case 1	107
Figure 7.24: Minimum principal stresses at substantial damage state – Case 1	108
Figure 7.25: Pushover curve – Case 3.....	109
Figure 7.26: Comparison of capacity spectrum and demand spectra – Case 3	110
Figure 7.27: Maximum principal strains at substantial damage state, internal view – Case 3	111
Figure 7.28: Minimum principal strains at substantial damage state, internal view – Case 3	112
Figure 7.29: Minimum principal stresses at substantial damage state, internal view – Case 3.....	112
Figure 7.30: Deflected shape at yield – Case 4	113
Figure 7.31: Pushover curve – Case 4.....	114
Figure 7.32: Comparison of capacity spectrum and demand spectra – Case 4	114
Figure 7.33: Maximum principal strains at substantial damage state – Case 4.....	115
Figure 7.34: Minimum principal strains at substantial damage state – Case 4.....	116
Figure 7.35: Maximum principal stresses at substantial damage state – Case 4.....	116
Figure 7.36: Minimum principal stresses at substantial damage state – Case 4.....	117

Figure 7.37: Pushover curve – Case 6	118
Figure 7.38: Comparison of capacity spectrum and demand spectra – Case 6	119
Figure 7.39: Deflected shape – Case 7	120
Figure 7.40: Pushover curve – Case 7	121
Figure 7.41: Comparison of capacity spectrum and demand spectra – Case 7	121
Figure 7.42: Maximum principal strains at substantial damage state – Case 7	122
Figure 7.43: Minimum principal strains at substantial damage state – Case 7	123
Figure 7.44: Maximum principal stresses at substantial damage state – Case 7	123
Figure 7.45: Minimum principal stresses at substantial damage state – Case 7	124
Figure 7.46: Deflected shape – Case 8	125
Figure 7.47: Pushover curve – Case 8	126
Figure 7.48: Comparison of capacity spectrum and demand spectra – Case 8	126

Tables Index

Table 2.1: Damage threshold limits (Lagomarsino, 2002)	23
Table 3.1: General sub-soil classifications (Eurocode 8, NCSE-02)	27
Table 3.2: Values of parameters for attenuation relationship (Ambraseys et al., 1996)	31
Table 3.3: Values of soil parameters for soil classification (Ambraseys et al., 1996)	31
Table 5.1: Dead and live loads	57
Table 5.2: Load combination factors (EC 1990:2002)	57
Table 6.1: Comparison of measured subsoil characteristics to soil classifications	61
Table 6.2: Values of parameters – functions developed by Lagomarsino (2002) (Irizarry, 2004)	64
Table 6.3: Surface wave magnitude of reference earthquakes	66
Table 7.1: Material characteristics	88
Table 7.2: Results of first mode of vibration for each model	91
Table 7.3: Normalised lateral load distributions (kN) for each model	92
Table 7.4: Summary of analysis cases	93
Table 7.5: Modal participation factors for each model and load distribution	96
Table 7.6: Comparison of normalised modal and non-linear analysis deflections – Case 1	104
Table 7.7: Results of displacement demand – Case 1	105
Table 7.8: Comparison of normalised modal and non-linear analysis deflections – Case 3	109
Table 7.9: Results of displacement demand – Case 3	110
Table 7.10: Results of displacement demand – Case 4	115
Table 7.11: Results of displacement demand – Case 6	119
Table 7.12: Results of displacement demand – Case 7	122
Table 7.13: Results of displacement demand – Case 8	127
Table 10.1: Drawing Register	137

1. INTRODUCTION AND OBJECTIVES

1.1 Introduction

The historic Eixample district of Barcelona is an iconic region of the city, representing its growth and prosperity. In the mid 1800s Barcelona was overcrowded and unhygienic. Global industrialisation was underway but the city, constrained by its city walls, could not respond. In 1869, a plan to remove the walls and extend the city won approval and the Eixample (the enlargement) began. Its construction would take 60 years and provide the foundation of a new Barcelona for the 20th Century.

The plan, by a local engineer Ildefons Cerda, was for a well organised and above all healthy extension to the city. It was characterised by a structured layout of avenues laid out in grid across the development (Figure 1.1). The roads were to be wide, with equal space assigned for pedestrians and traffic, and each city block was to house an inner courtyard or garden for additional light and space. In reality these aspects were largely retained, primarily due to strict planning controls on the development.

Building design was also strictly controlled and before long rows of near identical façades lined each avenue. The buildings are typically five or six storeys, of unreinforced masonry construction, with a central stair and light wells. They are constructed immediately adjacent their neighbour and are considered less as individual buildings, but as part of each city block.



Figure 1.1: The Eixample, Barcelona (CCCB, 2009)

Unreinforced masonry constructions are among the most vulnerable structures to seismic damage. Such damage can be related to both the global and local element responses of the structure and can range from minor cracking to total collapse. Recent studies of seismic damage to unreinforced

masonry buildings have confirmed their vulnerability and reinforced the need for assessment of each building's seismic demand and response. By completing this assessment, the likely risk of damage for each building can be quantified and plans can be developed to reduce the risk.

The particular risk of seismic damage to the cultural heritage of European cities has also been identified (RISK-UE, 2004). This is due to the typical layout and composition of such cities, often comprising unreinforced masonry structures of cultural significance, as both individual buildings and building aggregates. In response, the RISK-UE project was established which produced a methodology for seismic risk assessment and encouraged seismic response planning.

The present study involves the seismic analysis of a typical unreinforced masonry building of the Eixample district, Barcelona. It characterises the building's response to seismic actions and identifies the expected levels of damage for a range of seismic scenarios.

In accordance with the recommendations of the RISK-UE project, the seismic hazard analysis is identified using deterministic, probabilistic and current European code approaches. Structural response is defined by a non-linear pushover analysis procedure using finite element software DIANA (Version 9.4). The structural analysis has then been performed using a capacity spectrum method, in accordance with Eurocode 8 (2004).

The seismic analysis forms only one part of a broader structural assessment which must also consider:

- The history of the Eixample district and its development.
- The characteristics of its building typologies.
- Possible sources of damage and their consequences to the buildings of the district.
- Appropriate alternative methods to assess seismic hazard and each building's seismic response.
- A means to quantify and minimise the risk of seismic damage.

This broader assessment helps to ensure an accurate representation of the typical structures of the Eixample district in the seismic analysis and places the results in the context of other possible damages. As such, it allows the development of appropriate strategies to maintain the structures and reduce the risk of damage both from seismic events and other actions.

Previous studies have been completed on the seismic vulnerability of the buildings of Barcelona, including those of the Eixample district. A specific study of the Eixample district buildings used a 3D macroelement approach and identified a risk of significant seismic induced damage to the structures. This result confirms the need to undertake likewise studies using a variety of approaches to accurately define the seismic risk and the likely levels of damage to these buildings.

1.2 Objectives

The primary objective of this study is to determine the seismic performance of a typical unreinforced masonry building of the Eixample district of Barcelona, for a variety of seismic scenarios.

As stated above, this objective will be achieved by applying a capacity spectrum method of seismic analysis. Seismic hazard will be quantified by deterministic, probabilistic and current European code approaches. Structural response will then be defined by a non-linear pushover analysis, using finite element software DIANA (Version 9.4). The seismic analysis will form part of a broader structural assessment approach.

To complete the primary objective, a number of secondary objectives must also be defined, as follows:

- To review recommended approach methodologies for the structural assessment of historical constructions. This will enable the formation of an appropriate assessment methodology for the present study.
- To investigate the historical development of the Eixample district and its impact on the building typologies.
- To obtain plans of an unreinforced masonry building of the Eixample district. It will then be necessary to ensure that the building is representative of the typical constructions of the district.
- To characterise the form of the structural systems and the material composition in the building. This will include defining the load supporting elements, floor systems and material characteristics.
- To review previous studies of the analysis and assessment of similar constructions, particularly those studies focussed on Barcelona, and the Eixample district.
- To identify likely actions to the structure and to assess the possibility of damage by these actions.
- To present a seismic hazard analysis in accordance with the recommendations of the RISK-UE project and determine likely seismic scenarios for the Eixample district.
- To complete a state of the art review of suitable structural analysis methods commonly used to assess the response of structures to seismic actions. To consider the applicability of each to the present study and to select an appropriate method. This method will comprise two components; the building's response to seismic actions; and, comparison of the response to the previously defined seismic scenarios.
- To create a mathematical model of the building using the determined analysis method. The model must well represent the true form and material characteristics of the building. For a non-linear finite element analysis, the element type and discretisation, material behavioural models, and non-linear solution procedures must be carefully selected to ensure representative results.

- To complete the structural analysis and compare to the identified seismic scenarios for the site. This will determine the expected level of damage to the building for each scenario.
- To review the analysed performance of the building at the identified damage level. For non-linear finite element analysis, this will involve comparing the principal strains and stresses at the displacement demand to the expected level of damage. This review will help to validate both the model and the damage level determination.
- To define the performance of the structure under seismic actions and to identify appropriate maintenance strategies to limit the risk of seismic damage.

1.3 Work Organisation

This report comprises eight chapters, based upon the assessment methodology adopted for the study. Chapters two, three and four provide a state of the art investigation of the assessment methodology and analysis. Chapters five, six and seven are devoted to their application to the case study. A synopsis of each chapter is provided below.

The first chapter provides a brief introduction to the topic of the study and defines the relevance and importance of the case study. The primary and secondary objectives of the study are also outlined, along with a description of the work contents and organization.

Chapter two defines an appropriate approach methodology for the structural assessment. Each stage of the methodology is discussed, focussing on its contribution to the global understanding of the structure and its application to unreinforced masonry constructions of cultural significance.

Chapter three comprises a state of the art description of the seismic hazard analysis used for this study. Three analysis approaches are detailed; a deterministic approach; a probabilistic approach; and two current code approaches, Eurocode 8 (2004) and NCSE-02 (2002). The influences of local geology and earthquake type on the form of the response spectra are also discussed.

In chapter four, a detailed description is presented of the selected capacity spectrum method of analysis. The primary steps involved are clearly identified and the formulations and methodology for each step are presented.

Chapter five contains the structural assessment of the unreinforced masonry buildings in the Eixample district. Each stage is presented in a separate sub-section. The stages include the historical investigation; the geometrical and structural systems survey; a review of previous studies; the damage survey and identification of actions; and monitoring.

The sixth chapter details the application of the seismic hazard analysis to Barcelona. Regional and local geology is defined, followed by an assessment of its influence on the seismic demand. Response and demand spectra are then presented for each seismic hazard analysis approach and for the variety of soil types in Barcelona.

Chapter seven presents the application and results of the capacity spectrum method, using a non-linear finite element pushover approach. Model geometry and constraints are detailed, along with a discussion of the model assumptions. Material characteristics and behavioural models are then identified. The analysis results are presented both in terms of seismic displacement demand and in the overall response of the structure to the imposed actions. Finally, critical elements of the building are identified for routine inspection and maintenance to limit the risk of seismic damage.

The final chapter provides an overview of how the selected assessment methodology has enabled the clear determination of seismic performance for the building. A summary of the seismic analysis results is presented and compared to the results of previous studies. Conclusions regarding the modelling and analysis procedures are also provided.

This page is left blank on purpose.

2. STRUCTURAL ASSESSMENT – STATE OF THE ART

This chapter defines an appropriate approach methodology for the structural assessment. Firstly, the specific nature of structural assessments to heritage structures is introduced. Each stage in the methodology is then discussed, focussing on its application and its contribution to the overall structural assessment.

2.1 Introduction

The structural assessment of existing structures involves an approach that is substantially different to the design of new structures. Furthermore, the skills and knowledge required for the assessment are not often taught and are not included in standard building codes. These concepts have formed the basis for the development of recent standards such as ISO 13822:2010, the 'Assessment of Existing Structures' which recognise the need for a considered approach to the assessment that will ensure the ongoing safe and serviceable use of structures.

The assessment of heritage structures must be made in this context. Heritage structures can be defined as those structures of cultural significance. As such, their assessment must also involve a detailed investigation of the cultural values of the structure, and consider the likely physical and cultural impacts of proposed interventions.

A number of approaches and recommendations have been developed to guide this assessment. More recently, the International Scientific Committee on the Analysis and Restoration of Structures of Architectural Heritage (ISCARSAH) published the 'Recommendations for the Analysis, Conservation and Structural Restoration of Architectural Heritage' (2005), which provide both general principles for the assessment and guidelines for their application. Additional guidance for cultural and structural assessment, including considerations for interventions, can be found in the Charters of the International Council on Monuments and Sites (ICOMOS). These include the international 'Venice Charter' (1964) and national charters such as the Australian 'Burra Charter' (1999).

An approach methodology for structural assessment can be developed from these guidelines. The methodology should include the following:

- Structure Identification
- Historical Investigation
- Geometrical and Structural Systems Survey
- Damage Survey and Identification of Actions
- Material Characterisation
- Monitoring
- Structural Analysis

- Diagnosis and Vulnerability Assessment
- Recommendations for Maintenance, Interventions and Monitoring.

The following sections identify the primary considerations for each part of the methodology as they relate to the present study.

2.2 Structure Identification

The typology of the structure should be identified (church, house, tower, bridge, etc.) as well as whether the structure is isolated or part of an aggregate of structures. Identification of the structural typology enables an initial understanding of implicit vulnerabilities as well as the likely mechanical characteristics and morphology of the materials.

The structure's location, title, current and intended use, and the nature and topography of its surrounds should also be described. These details provide a base level of knowledge for the structure that is used for each later stage of the assessment.

2.3 Historical Investigation

The historical investigation should include a detailed assessment of the construction history and its change in use over time. A description of past events that affected the structure is also required, including fires, floods, earthquakes, wars, etc. From these works, a phase analysis can be developed whereby each primary stage of construction history can be described. When represented graphically, this can prove to be of assistance on site to help characterise observed irregularities and damage.

The historical context of the structure's construction and use, and a detailed description of its cultural significance is required. From a structural perspective, these details provide the basis for a qualitative study of the material composition and of damage to similar structures. For a specific project, they can also provide the basis for protection from inappropriate development and interventions, and can help to establish those in the local community that have most interest in the conservation and use of the structure.

An overview of any past reports and monitoring at the site should be completed. This can provide details of previous interventions and of the changing conditions of the structure and can help guide future monitoring strategies.

A detailed historical investigation will use both written and verbal sources and its results will be invaluable to support both the structural and cultural understanding of the structure.

2.4 Geometrical and Structural Systems Survey

The architectural and structural form and layout of the structure should be documented. This can initially be achieved approximately on site so that site observations can be easily recorded and

preliminary analysis and assessment can be established. This is of particular use for the design and documentation of emergency works.

A more detailed survey can be completed which can include the identification of individual structural elements (walls, columns, lintels, trusses, ties, etc.) and the development of detailed plans, sections and elevations. In addition, a description of the structural systems should be made such as the expected load paths for vertical and lateral actions. This can then be used as a basis for a detailed analysis of the structure, to help define observed damage and irregularities in the structure, and to allow an accurate representation of intervention works.

The geometrical survey can be combined with the historical investigation to develop the graphical representation of the phase analysis, described above.

2.5 Damage Survey and Identification of Actions

An initial damage survey should be completed during the first inspection of a structure. This is imperative to ensure that any unsafe structural elements are observed and that any appropriate emergency works can be provided.

Following the initial assessment, a more detailed damage survey can be completed utilising the information from the historical investigation and the geometrical survey. Both the characteristics and the observed extent of damage must be recorded. These can then be used to identify possible failure mechanisms and to help guide a suitable testing and monitoring regime to evaluate in more detail the extent of damage and characterise the composition of the most affected and vulnerable structural elements.

The damage characteristics can be directly related to the cause of the damage. For heritage structures, the typical causes of damage are mechanical, physical and chemical / biological actions, as detailed below. The characterisation of actions is also required prior to undertaking a detailed structural analysis.

A description of methods used to assess the extent of damage is provided in Section 2.10, as part of the description of the vulnerability analysis.

2.5.1 Mechanical Actions

Mechanical actions include direct static loading and indirect static actions such as settlements, thermal effects and creep. Dynamic actions such as seismic accelerations, wind and the effects of machinery and traffic can also be considered mechanical actions. The result of mechanical actions is dependent on the structural form and system, the materials composition, condition and morphology and the scale of the imposed action. Typically for unreinforced masonry structures, damage resulting from mechanical actions is characterised by deformations and cracking or crushing of the masonry due to excessive stresses.

For the present study, the focus of the analysis is the seismic vulnerability of the buildings. As such, a detailed seismic hazard assessment is required to determine the relevant seismic actions. The procedures used to define the seismic hazard are presented in Section 3 'Seismic Hazard Assessment – State of The Art'.

2.5.2 Physical Actions

Physical actions can include environmental effects such as freeze-thaw, water penetration and erosion, air humidity, lightning or fire. Anthropogenic effects also often result in physical actions to the structure such as inappropriate interventions that remove or damage existing fabric. For unreinforced masonry structures physical actions can typically result in the direct loss of material (such as for erosion or physical removal of elements), or in direct damage and modification of the mechanical characteristics of the materials caused by freeze-thaw effects and fire.

2.5.3 Chemical and biological actions

Chemical and biological actions include natural effects such as moisture penetration, salt penetration and decay, vegetation growth, fungal attack and attack by pests such as termites, borers and beetles. They can also be the result of anthropogenic actions such as the application of inappropriate coatings or other materials within a structure that are chemically incompatible with the original fabric. For unreinforced masonry structures, chemical and biological actions typically include mechanical decay due to the penetration of moisture and salts to the masonry, often encouraged by inappropriate surface coatings. Other impacts include the fracturing of masonry elements by vegetation growth and the biological decay of timber elements within the structure such as floor and roof framing.

2.6 Material Characterisation

The material characterisation initially involves identifying the different material typologies within a structure. By doing so, it is possible to limit the scope of on-site testing to best characterise the materials. A plan of non-destructive tests (NDT) and minor-destructive tests (MDT) should then be developed taking into account material typology and those elements identified by the damage survey as being most vulnerable to continuing deterioration. The tests selected should be complementary, such that the outcomes of various tests can be calibrated to help verify the results.

Material properties to be considered include:

- Physical (porosity, density, timber species, colour, etc.).
- Chemical (Percentage of salts, silica and other compounds, types of salts and their likely origin, percentage of carbonation within concrete, etc.).
- Mechanical (yield stress, compressive strength, shear modulus, elastic modulus, etc.).

The testing regime should consider not only the material being tested and the desired parameters, but also the accessibility for on-site testing, or any limitations for sampling for laboratory testing.

In addition to material properties, the testing should provide a detailed understanding of the morphology of each identified typology and how the materials perform and interact as individual components and as composites.

For the unreinforced masonry buildings of the present study, a masonry testing regime may include:

- Localised sampling of the masonry to determine mean physical and mechanical properties.
- Survey of sampled areas to clarify wall morphology.
- The use of single and double flat jacks to verify assumed load distribution.

2.7 Monitoring

Monitoring is used to assess the time-dependent variation of quantities related to structural behaviour.

Static monitoring can be used to study the evolution of structural damage such as the development of cracking or of out-of-plumb measurements. These results can help to guide appropriate interventions, as the damage may have been caused by a past action or may be continuing. If monitoring indicates that a quantity is stable, the observed damage may still limit structural capacity under certain load conditions, such as the development of a macroelement or local stresses due to geometrical non-linearity. Hence monitoring itself is not a measure of structural safety, the results must be interpreted as part of the overall structural assessment.

Indirect actions such as temperature and humidity variations can also be monitored to determine any cyclical variation in the measured quantities.

Dynamic monitoring is typically used to record more intense records of sudden variations such as structural vibrations due to ground accelerations or anthropogenic actions. Dynamic monitoring may be continuous, time dependent or trigger-activated, where the monitoring records are retained following a certain threshold of excitation. The results of dynamic monitoring can help to calibrate mathematical models by determining the natural frequencies, mode shapes and modal damping of a structure. They can also be used to help characterise global and local behaviour and to help verify building integrity.

Similar to material testing, structural monitoring requires a detailed implementation plan based upon the geometrical and structural systems survey, the mechanical typology assessment and the damage survey. The results of preliminary mathematical modelling are also used to help determine suitable locations for dynamic monitoring.

The results of both static and dynamic monitoring can be used to help assess the long-term suitability and effectiveness of past and current interventions.

2.8 Previous Studies

As discussed in Section 2.3, an overview of previous monitoring, interventions and reports at the subject site should form part of the knowledge phase of any structural assessment. In addition to site specific studies, it is of benefit to undertake a review of previous studies of the specific building typology and of similar assessments of structures in the local region.

Both the studies of the subject site and those with a more general focus contribute to the knowledge and understanding of the structure and assist in the interpretation of observed damages and modifications. As such, they can help guide appropriate monitoring, testing and analysis techniques for the structure. Furthermore, previous studies of the local seismic actions, soil and wind conditions can be directly used for the analysis works.

2.9 Structural Analysis Techniques

Structural analysis uses the data from previous stages of the assessment to develop a mathematical representation of the structure. Such data should include geometry, identified structural systems, observed damages, morphology and material characteristics.

The results of the analysis may be used in conjunction with other qualitative and quantitative results for the following:

- As a basis for understanding the structural behaviour.
- Define a level of safety for the structure.
- Check hypothesis for observed damage, both the initial causes and evolution.
- Locate concealed damages through correlation with dynamic monitoring.
- Identify critical structural elements that may require monitoring, testing or remediation.
- Model the influence of past alterations and forecast effectiveness of proposed interventions.
- As part of a long-term monitoring strategy, the analysis can help to evaluate long-term structural performance.

The structural analysis of historical constructions requires an approach fundamentally different to that of the design of new structures. For new works both geometry and material characteristics are clearly defined and controlled and code recommendations are readily available for the design of each structural element. For heritage works, the building geometry, the form and function of the structural systems and the material properties are somewhat variable quantities, not only between structures of similar typology but within the one structure. In addition, alterations, interventions and damage can significantly impact the strength and effectiveness of structural elements.

Hence, the selection of appropriate structural analysis techniques must account for these uncertainties.

For the present study, the focus of the assessment is the seismic analysis of a typical unreinforced masonry building in the Eixample district, Barcelona. As such, the following sections contain both a brief description of the commonly used seismic analysis techniques for both new and heritage structures, together with a brief discussion regarding the suitability of the techniques to the present study.

A detailed description of the procedures for the selected seismic analysis technique, the capacity spectrum method is provided in Section 4.

For this study it was decided to select a performance based approach, whereby the level of serviceability and safety is characterised by the structural performance determined by the analysis. This approach can also be used to define required ductility and capacity of structural elements from an estimation of the likely deformations. It is in contrast to a capacity based (or strength based) design approach, where the linear elastic capacity of structural elements is checked to resist elastic equivalent seismic actions. The equivalent forces are usually determined by code formulations and are designed to account for structural ductility (Aydinoglu et al., 2010).

Performance based design can take many forms, the most common approaches applied to seismic assessment are:

- Kinematic limit analysis: Linear and geometrically non-linear.
- Non-linear time history analysis.
- Non-linear pushover analysis.

2.9.1 Kinematic Limit Analysis

Kinematic limit analysis involves the analysis of discretised local elements, or 'macroelements', of a structure. Each macroelement is selected upon the basis that it has homogeneous constructive characteristics and exhibits a rigid structural behaviour (Roca, 2010). The elements are selected based upon identified failure mechanisms for the structural typology and are often described in terms of architectural features or components, such as the façade, parapet, bell-tower, etc.

For each macroelement, the capacity of each identified failure mechanism is determined either by linear analysis considering only the seismic acceleration required to instigate the mechanism, or by geometrical non-linear analysis considering both the initial acceleration required and the final displacement (or rotation) of the element at overturning. A limiting displacement level can also be considered.

The identification of suitable macroelements and failure mechanisms developed from the observations of seismic induced damage. In particular, large scale damage surveys were completed following the earthquake of Ortigia in Sardinia, Italy in 1995, and the Umbria and Marches earthquake of 1997 in central Italy (Binda et al. 1999). Following these works, a systematic classification system was developed for seismic induced damages to Churches, together with detailed studies into the causes of the observed damages and recommendations for appropriate intervention strategies.

An index of failure mechanisms has since been developed for both unreinforced masonry churches and buildings. These indexes are used not only to identify possible failure mechanisms, but are used as part of the damage survey following a seismic event to help record the extent of damage, to document the extent of emergency works, and to aid in the planning of long-term assessment and rehabilitation projects.

For the present study of the Eixample buildings, a kinematic limit analysis is being performed within a concurrent dissertation project. The primary results of the kinematic limit analysis are recorded in Section 7.7 and comparisons are made to the results of the current work.

For the typical unreinforced masonry buildings of the Eixample district, the kinematic limit analysis defines the structure as a composition of macroelements that are classified in terms of their position within the structure. For example, the façade, lateral side walls, internal walls, light wells, etc. For each building element, a number of possible rigid block failure mechanisms have been considered.

Two failure mechanisms for the façade of the current structural typology are presented in Figure 2.1.

- a) The out-of-plane rotation of the full façade of a building and part lateral wall, with rotation at the base of the wall.
- b) The out-of-plane rotation of a portion of the façade, with rotation at the base of the wall.

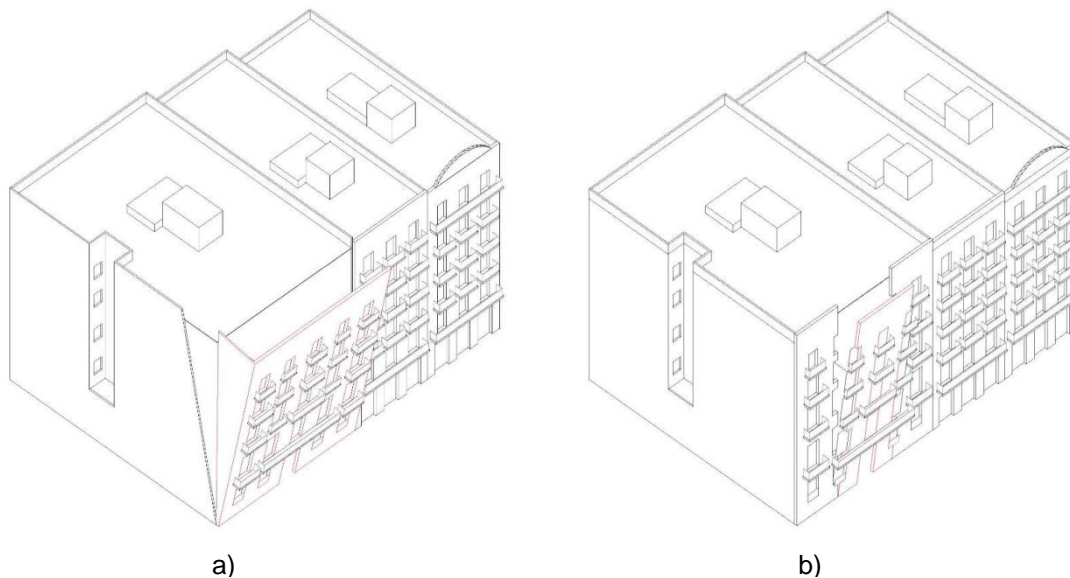


Figure 2.1: Two out-of-plane façade mechanisms for a typical unreinforced masonry building (NIKER D3.1, 2010)

The assumptions of this analysis include:

- Seismic damage of the structure is consistent with the rigid blocks defined.
- Structural capacity is governed by the collapse or excessive deformation of rigid blocks of unlimited strength capacity.

- Floors are deformable, that is, that mechanisms are considered where there is no assumed contribution by floor restraint to the lateral capacity of the walls.

For each mechanism, the capacity diagram developed is compared against the elastic seismic response curves for the site. By doing so, for the linear analysis it is possible to determine whether the ground accelerations caused by the likely seismic actions are sufficient to develop the mechanisms. For geometrical non-linear analysis, a seismic demand displacement is determined. This is then checked against a calculated ultimate displacement, related to the displacement at overturning. It is also possible to calculate a safety ratio for each mechanism.

The primary benefit of kinematic limit analysis for the buildings of the Eixample district is that in contrast to the non-linear methods described below, it considers the local mechanisms of building elements due to seismic actions. Such local mechanisms may be out-of plane, as shown in Figure 2.1, or in-plane as shown below (Figure 2.2). This is of critical importance in the understanding of the likely seismic response and vulnerability of the building, as local mechanisms are often the most prevalent failure mode observed during the seismic damage assessment of unreinforced masonry structures.

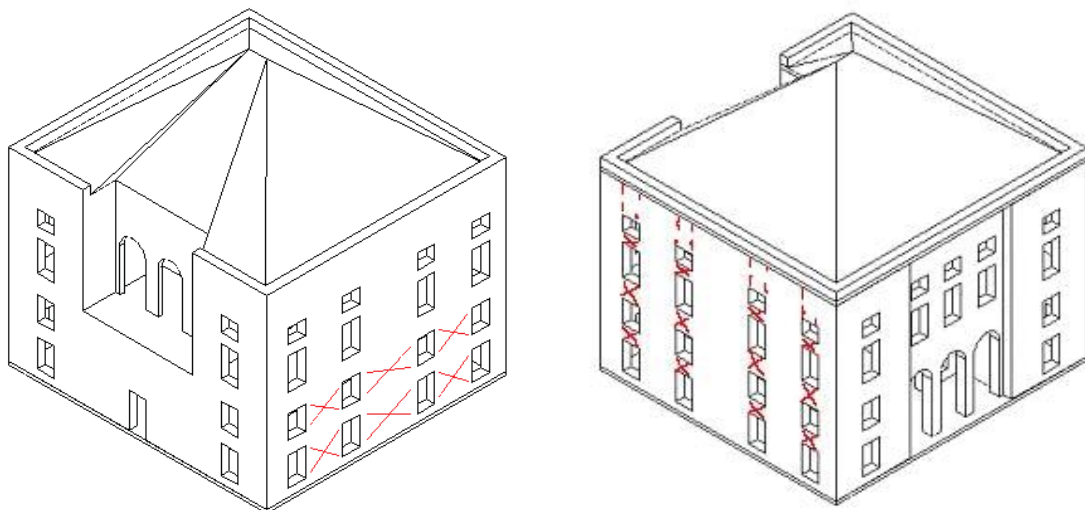


Figure 2.2: In-plane façade failure mechanisms for an unreinforced masonry building (DDPC, 2006)

2.9.2 Non-linear Time History Analysis

A non-linear time history analysis involves the application of imposed variations in accelerations to a non-linear mathematical model of the structure to simulate ground acceleration during a seismic event. The acceleration record imposed may be equal to that measured from a seismic event, or may be artificially generated based upon the seismicity and local geological composition of the site.

Non-linear time history analysis therefore requires the accurate determination of seismic accelerations for a likely seismic event at the subject site. It also requires precise understanding of the non-linear properties of the materials, including the hysteretic damping characteristics. Furthermore, the level of

accuracy is reliant on a detailed geometrical representation of the structure, its restraints and the mechanical relationships between materials and elements.

For the present unreinforced masonry structure, the subject site is in an area of low seismic risk with very few and imprecise records of past seismic actions that caused structural damage (refer Section 6). Hence any definition of seismic accelerations would be a significant approximation and the assumptions of the seismic assessment would have a significant impact on the analysed structural response. In terms of material and geometrical characteristics, the present study is intended to provide an understanding of the vulnerability of a building typology, not the seismic assessment of a particular structure. As such, the level of accuracy in the analysis should be comparable with the level of building knowledge which will ensure a good representation of the likely response of a typical building.

For the assessment of the current building typology there is significant variability in building geometry, materials, morphology and in the element and material relationships. Hence, the required precision of a non-linear time history analysis would be unsuitable for this study.

Non-linear time history analysis is more suited to the analysis of a particular existing structure where the geometrical and material characteristics can be more clearly defined, or to a new structural design. It is also more suited to areas where there is more significant seismic risk and where an accurate estimation can be made of seismic accelerations during an earthquake.

2.9.3 Non-linear Pushover Analysis

Non-linear pushover analysis is used to analyse the lateral capacity of a structure, determine the displacement demand of seismic actions for a structure and to assess the structure's vulnerability to seismic damage.

The procedure consists of applying lateral actions to a non-linear mathematical model of the structure to determine a relationship between the resultant lateral displacement and reaction. This relationship defines the response of the structure in the linear elastic and non-linear ranges. A typical force-displacement graph, or 'pushover curve', developed from this procedure is presented in Figure 2.3.

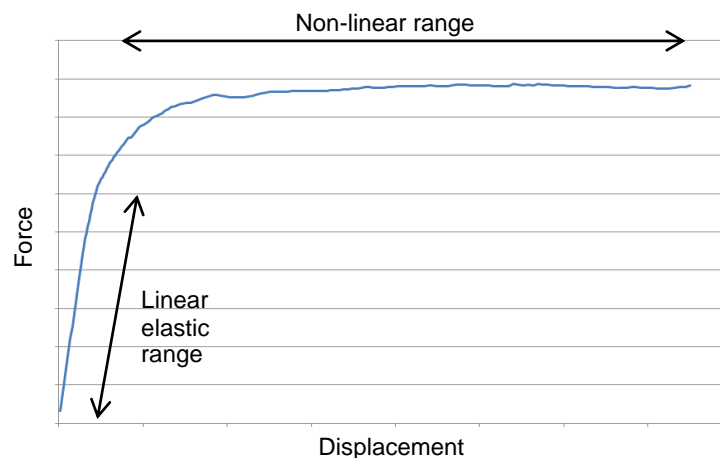


Figure 2.3: Typical pushover curve

The key components of the pushover curve are the gradient and extent of the linear response, the form of the non-linear response (smooth or jagged, positive or negative gradient), the extent of the non-linear response, and whether unloading can be defined at the maximum displacement.

To assess the displacement demand of a seismic action, the pushover curve is compared to a seismic demand curve. To do so, the multi-degree of freedom (MDOF) pushover curve is converted to a single degree of freedom (SDOF) capacity spectrum in acceleration – displacement (ADRS) format and the elastic acceleration response spectrum derived from the seismic hazard analysis is converted to an elastic demand spectrum, also in ADRS format. These can then be plotted on the same graph (Figure 2.4). Conceptually, the intersection of the two spectra then determines the displacement demand of the seismic action on the structure.

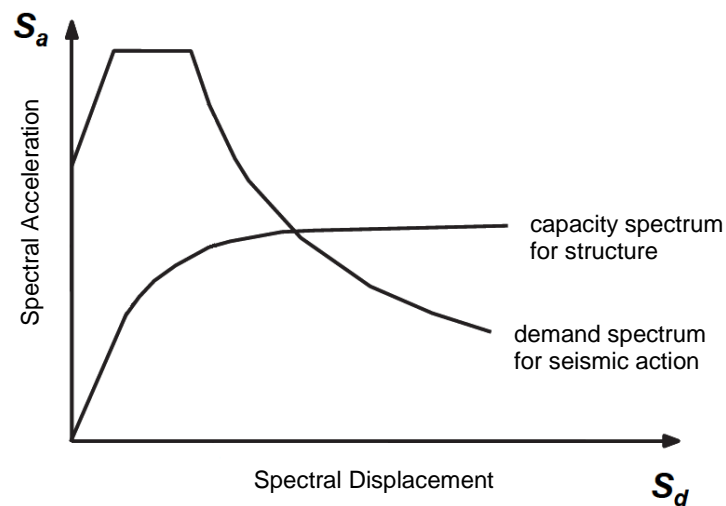


Figure 2.4: Simplified representation of capacity and demand spectra in ADRS format (FEMA 440, 2005)

In practice, modifications are required to both spectra to ensure compatibility between the inelastic range of the capacity spectrum and the elastic demand spectrum. A number of approaches are available for these modifications. Similarly, a number of methods have been proposed for the development of the pushover curve including force-based methods, displacement-based methods and monotonic or adaptive increases in the applied actions.

The majority of the pushover analysis procedures were developed in the past 20 years. It is an area of continuing development, with recent alterations and extensions to existing methods, and the ongoing publication of newly proposed methods. The following sections briefly describe the most commonly used methods and discuss the practicality and suitability of each to the present study.

Pushover methods can be broadly classified by the following:

- Force-based pushover techniques, with monotonically increasing distribution of lateral loads. For example:
 - o Capacity Spectrum Method (CSM) (ATC 40, 1997; FEMA 440, 2005).
 - o N2 method, currently employed in Eurocode 8 (Fajfar, 2000; Eurocode 8, 2004).
- Force-based pushover techniques, with combination of results from several applications of monotonically increasing load. Load distribution based upon elastic modes of vibration. For example:
 - o Modal Pushover Analysis (MPA) method (Goel and Chopra, 2004).
- Force-based pushover techniques, with step-wise adaptive modal-based increases in lateral loads. For example:
 - o Adaptive Modal Combinations (AMC) method (Kalkan and Kunnath, 2006).
- Displacement based pushover techniques, with stepwise adaptive modal-based increases in displacements. For example:
 - o Displacement Adaptive Pushover (DAP) method (Antoniou and Pinho, 2004).

It is of interest to note that there are no methods that apply a monotonic increase in displacements. As discussed by Antoniou and Pinho (2004), if a monotonic increase of displacements were applied to a structure, then the structural response (the displacement response) due to induced stresses is predetermined and controlled. As such, the form of the response would not alter with the inelastic deterioration of the structure and it will not represent the true building response. The only way to ensure the structural response is in accordance with the induced stresses and inelastic deterioration is to adaptively update the vertical distribution of displacements at regular intervals, to match the changing modal characteristics of the structure.

2.9.4 Applicability of Pushover Methods

For each of the modal-based techniques, the structure must have clearly definable, global, modal responses. The number of modes to be considered is determined by the displacement contribution to the system after applying actions in accordance with each mode. Usually the final application (or step) is one that causes a change in displacement below a certain threshold, or that develops a total displacement above a predetermined target displacement.

For the MPA method, the lateral loads are monotonically increased and the displacement demand for each mode is calculated in accordance with the CSM or N2 methods. The contributions of displacement from each mode are then combined by square root sum of the squares (SRSS). For the step-wise, adaptive modal based methods, the increases in lateral forces or displacements are calculated based upon the changing inelastic modal characteristics of the structure. The step sizes are determined by monitoring the total displacement against the total energy demand of the imposed

forces or displacements at each step (Kalkan and Kunnath, 2007). The resultant pushover curve therefore incorporates each step and the contribution of each mode.

An elastic modal analysis was completed on the models of the building in the present study (refer Section 7.4). The results indicate that there is one clearly dominant global mode of vibration for the structure in the longitudinal direction of loading. Other modes in this direction are characterised by the local responses of the masonry façade and internal walls and no other clearly definable global modes were observed. As such, it was not suitable to apply a modal combination method, such as the MPA method, to this structure.

The adaptive force and displacement methods each require specific mathematical algorithms to progressively update the imposed forces and displacements in accordance with the changing inelastic characteristics of the structure. For this reason, specific software has been developed by the proponents of such methods to enable its application. To date both the software and the methods have been developed for application to reinforced concrete and steel moment-resisting frame structures. These structures typically have well definable modes of vibration and the results of the methods when applied to these structures compare well to the results of non-linear time history analysis. As such, it is not suitable to apply these methods to the present building.

The most applicable pushover methods therefore are the capacity spectrum methods. For the present study the N2 capacity spectrum based method was selected (Fajfar, 2000; Eurocode 8, 2004). A detailed description of this method is provided in Section 4.

2.9.5 Non-linear Modelling

Both the time history analysis and the pushover analysis described above require the prior development of a representative non-linear mathematical model of the structure. As discussed, this model is based upon data from previous stages of the assessment including structural geometry, observed damages and material characteristics.

An appropriate approach is to develop a non-linear finite element model. The method involves the mathematical discretisation of the structural components into small elements. The element may be various shapes including square, triangular or cubic and each element contains a number of nodes positioned at the element boundary. An additional node may be located at the centre of the element. The stresses and strains are calculated taking into consideration the form and stiffness of the structural components, the degrees of freedom specified to each node, the applied actions, boundary conditions and the stress and strain history of the analysis. The response of each element, hence the overall structural response, is based upon the computation results of integration functions at a number of integration points between the nodes. For shell elements, a number of integration points may also be prescribed in the thickness of the element.

The benefits of using finite element analysis are in the calculation of structural response at a large number of locations throughout each structural component and that the responses can be preconfigured to represent the linear or non-linear characteristics of the materials observed on site.

The results of the analysis can be compared with in-situ damage observations, stress testing, and static and dynamic monitoring to help understand structural performance, and to help calibrate the model.

A description of the finite element model and the behavioural models used for each material is presented in Section 7.

2.10 Diagnosis and Vulnerability Assessment

Diagnosis involves the review of all previously obtained qualitative and quantitative data from the structural assessment. From this review, it will be possible to determine whether additional testing, modelling, monitoring or other works are required to better comprehend the form and behaviour of the structure.

Another part of the diagnosis is to determine the level of safety and risk of damage for the structure. The outcomes of this work form the basis for selecting appropriate maintenance strategies and interventions.

A vulnerability assessment is a key part of this diagnosis, as it provides a determination of the probability of a certain level of damage to the structure over a given period of time. The starting point for any vulnerability assessment is to classify the likely types and levels of damage (Section 2.5).

The focus of the present study is the damage caused by seismic actions on the structure. As such, it can be characterised as a mechanical action which can result in excessive deformations and mechanical damage due to excessive stress levels. It is imperative that the seismic assessment of any building also includes a thorough investigation of the current damage levels and sources, as these ultimately impact the structure's strength and its capacity to resist seismic actions.

The classification of seismic damage typically incorporates two components; classification of the damage mechanism, and the level of damage. Damage mechanisms can either be related to local or global seismic damage. Local damage is typically characterised by out-of-plane or in-plane failure of isolated sections (or macroelements) of the structure due to excessive seismic actions. Structural analysis of the failures of such macroelements is based upon limit-state concepts. The application of these concepts to the unreinforced masonry buildings of the Eixample district forms the basis of a concurrent thesis. The results of this analysis are compared with those of the present study in Section 7.7. Global seismic damage refers to the damage caused by the global response of the structure to seismic actions, the focus of the present study. The effects of a global response are not limited to overall deformations, but can include local deterioration such as excessive stresses and buckling failures.

The extent of damage is typically characterised by a damage grade which have been developed to enable a clearer relationship between the observed level of damage and the magnitude of the seismic event. The damage grades were developed within the RISK-UE project and are incorporated into the European Macroseismic Scale 1998 (EMS-98). The damage grades are:

- Grade 1: Negligible to slight damage.
- Grade 2: Moderate damage.
- Grade 3: Substantial to heavy damage.
- Grade 4: Very heavy damage.
- Grade 5: Destruction.

A pictorial description of each of these grades applicable to unreinforced masonry buildings is provided below (Figure 2.5).






Classification of damage to masonry buildings	
	<p>Grade 1: Negligible to slight damage (no structural damage, slight non-structural damage) Hair-line cracks in very few walls. Fall of small pieces of plaster only. Fall of loose stones from upper parts of buildings in very few cases.</p>
	<p>Grade 2: Moderate damage (slight structural damage, moderate non-structural damage) Cracks in many walls. Fall of fairly large pieces of plaster. Partial collapse of chimneys.</p>
	<p>Grade 3: Substantial to heavy damage (moderate structural damage, heavy non-structural damage) Large and extensive cracks in most walls. Roof tiles detach. Chimneys fracture at the roof line; failure of individual non-structural elements (partitions, gable walls).</p>
	<p>Grade 4: Very heavy damage (heavy structural damage, very heavy non-structural damage) Serious failure of walls; partial structural failure of roofs and floors.</p>
	<p>Grade 5: Destruction (very heavy structural damage) Total or near total collapse.</p>

Figure 2.5: Damage grades (EMS-98)

A structure's damage vulnerability is then a measure of the probability of exceedance of a certain level of damage over a given period of time.

There are two common methods of assessing the vulnerability of a structure to a level of damage. One method is termed the vulnerability index method and is based upon the overall vulnerability of a building typology and region to damage (Lantada, 2009). The vulnerability index is quantified by a numerical representation of a vulnerability class for each building typology, a region modifier and factors to account for individual peculiarities of a building including the number of storeys, building condition, horizontal and vertical irregularity of the structure and physical relationship to adjacent structures. By determining the vulnerability index for each typology and area of a city it is possible to develop a map of the mean vulnerability index. The mean vulnerability index map for Barcelona is provided below (Figure 2.6), where higher levels of the index indicate increased susceptibility to damage.

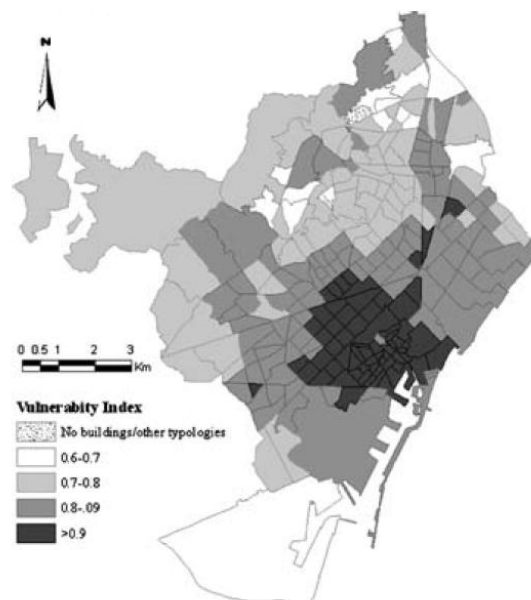


Figure 2.6: Vulnerability index distribution for Barcelona by census zone (Lantada, 2006)

An alternate method is to categorise the moderate level of damage for a particular structure based upon the results of a pushover analysis. The probability of exceedance of the other levels of damage can then be estimated by means of fragility curves defined by lognormal probability distributions (Lantada, 2009). Lagomarsino (2003) defined damage threshold limits for each level of damage dependant on the yield and ultimate spectral displacements of an idealised bilinear capacity curve.

The threshold limits for each level of damage are provided in Table 2.1 and represented graphically in Figure 2.7.

Table 2.1: Damage threshold limits (Lagomarsino, 2002)

	Damage Grade	Damage Threshold Limit	Relationship to idealised capacity curve
1.	Slight	S_{d1}	$0.7S_{dy}$
2.	Moderate	S_{d2}	S_{dy}
3.	Substantial to Heavy	S_{d3}	$0.125S_{du}$
4.	Very Heavy	S_{d4}	$0.25S_{du}$
5.	Destruction	S_{d5}	$0.5S_{du}$

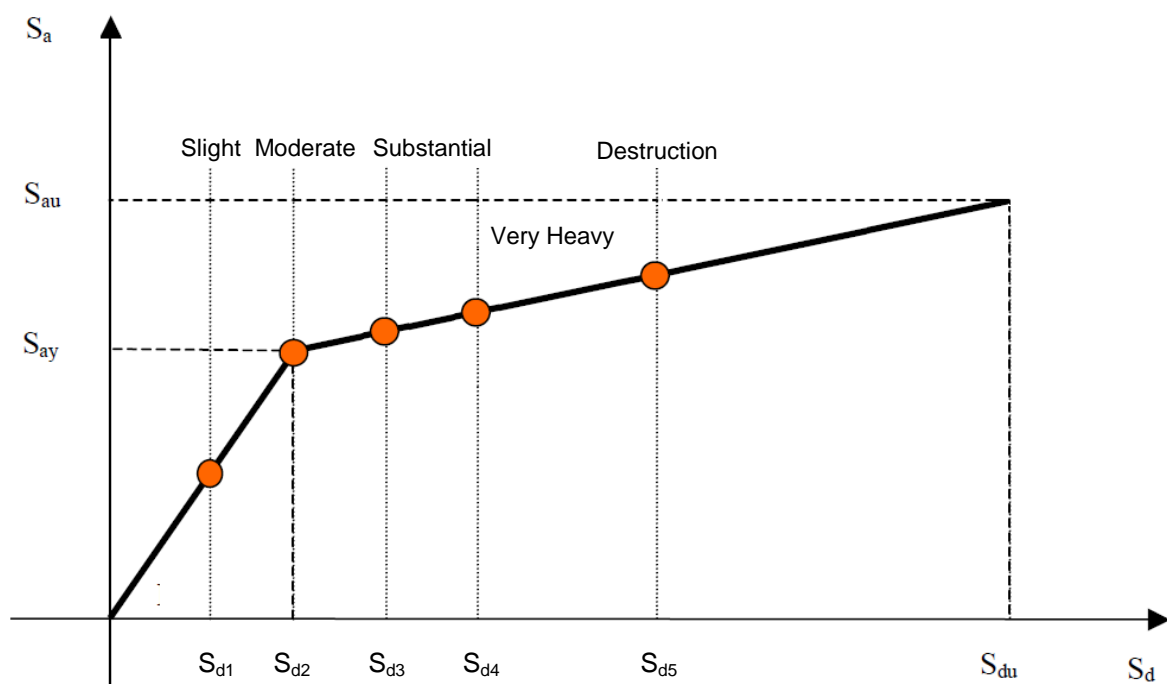


Figure 2.7: Definition of damage threshold limits for idealised capacity curve (mod. Irizarry, 2004)

These limits provide an estimate of the total displacement demand required to illicit a certain level of damage to the structure. The vulnerability of the structure to each level of damage can then be determined using fragility curves.

Once the value of the spectral displacement due to seismic demand has been determined from the pushover analysis, the vulnerability of the structure to other damage levels is obtained as the probability of exceedance shown by the fragility curves. Fragility curves developed from a previous study of mid-rise (3-5 storey) unreinforced masonry buildings in Barcelona are presented below (Figure 2.8). The fragility curves are dependent on the results of the non-linear pushover analysis and so would be slightly different for the present study.

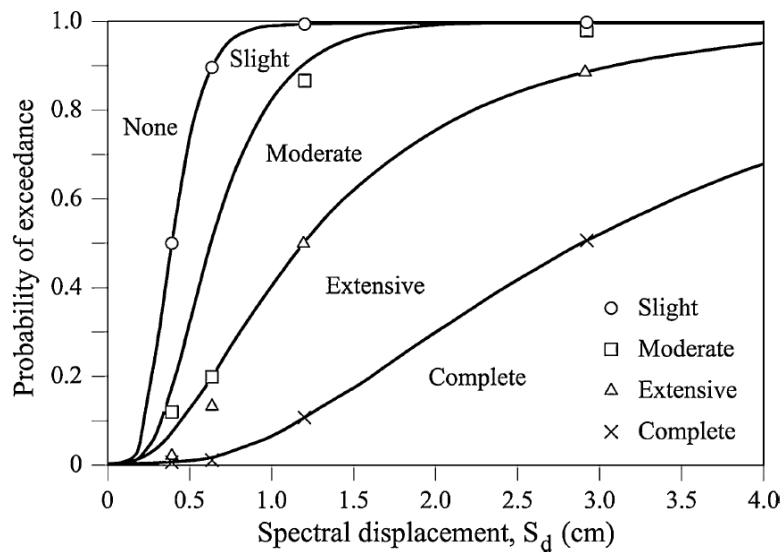


Figure 2.8: Fragility curves for mid-rise unreinforced masonry buildings in Barcelona (Barbat et al., 2006)

A damage assessment has been completed in this study based upon the results of the non-linear structural analysis of a typical unreinforced masonry building. The results of this assessment are presented in Section 7.5.

2.11 Maintenance and Interventions

In the present study, the focus is on the seismic performance assessment of a typical unreinforced masonry construction of the Eixample district. As such, any recommendations must be framed within the context of being able to be applied to a building typology, rather than a specific building. It is therefore intended to determine a general recommendation for the inspection and maintenance of the buildings to limit seismic damage.

In terms of the general application of interventions, the following aspects must be considered:

- They should ensure an adequate level of safety to the structure, whilst minimising the impact on the existing fabric.
- Any changes to the existing structural system and morphology should be limited or prevented.
- If possible, the intervention should integrate with and support the existing behaviour of the structure.
- The intervention must be chemically, physically and mechanically compatible with the existing construction. In this respect, they should also be durable.
- If possible, the intervention should be removable.
- It is preferable if the intervention can be applied incrementally and that its installation is accompanied by a programme of monitoring to assess its effectiveness.

3. SEISMIC HAZARD ASSESSMENT – STATE OF THE ART

This chapter provides a background to the development of the acceleration response spectra and demand spectra. The influences of local geology and the earthquake type on the magnitude and form of the calculated spectra are also presented and discussed.

In accordance with the recommendations of the RISK-UE project (2004), three methods are detailed to develop the spectra; the deterministic approach; the probabilistic approach; and, two current code approaches: Eurocode 8 (2004) the Spanish seismic code (NCSE-02, 2002).

3.1 Introduction

Earthquake action can be measured by the horizontal and vertical ground actions resulting from a seismic event. The scale of these actions is dependent on the seismic magnitude, seismic mechanism, the location and depth of the event relative to the subject site, the geology of the path of the seismic waves between the event and the site, and the local site geological conditions.

A common representation of seismic action is that of an acceleration response curve, which describes the measured or expected peak horizontal acceleration of a single degree of freedom system as a function of the structural period. A typical acceleration response spectrum is presented below, as determined from the El Centro, California earthquake of 15th October 1979, measuring $M_S=6.9$ (Figure 3.1).

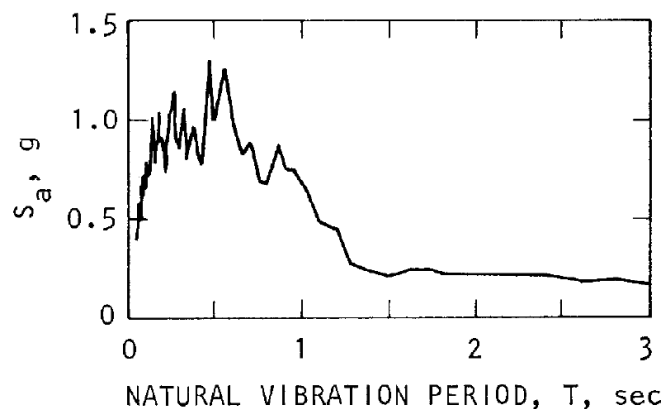


Figure 3.1: Acceleration Response Spectrum – El Centro, California 1979 (Chopra, 1981)

A response spectrum may be developed from measured earthquake motions, or a spectrum for expected acceleration responses may be devised.

To enable earthquake resistant analysis and design of current and new structures, it is necessary to have a clear understanding of the likely earthquake actions at a subject site. To do so, common practice is to develop a smoothed earthquake response spectrum which can readily be compared to

the analysed structural performance and from which design actions can be easily developed. The smoothed response spectrum typically consists of a number of straight and curved lines that are defined to best represent the form of the measured or expected response spectrum. A diagrammatic representation of a smoothed acceleration response spectrum is provided in Figure 3.2.

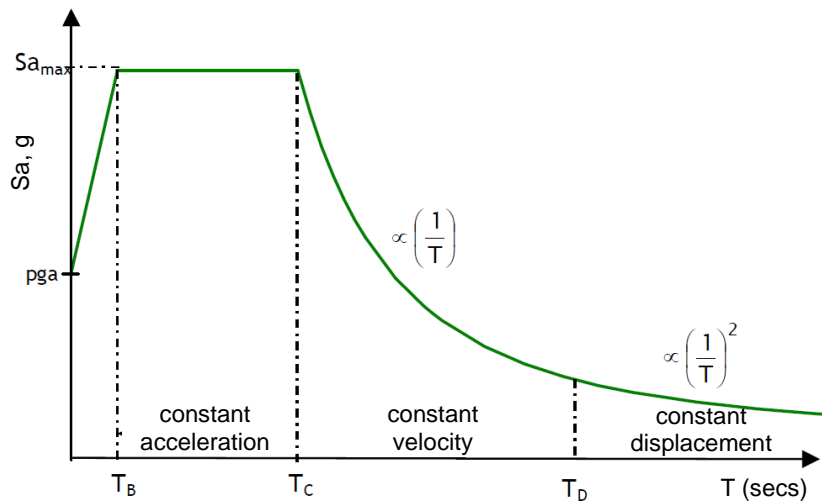


Figure 3.2: Diagrammatic Smoothed Response Spectrum (Irizarry, 2004)

The key parameters of a smoothed acceleration response spectrum are as follows:

- The peak ground acceleration (PGA), defined as the maximum acceleration at the ground surface, where the structural response period is zero.
- The maximum spectral acceleration ($S_{a,max}$).
- Definition of ranges of the structural period to define the start values for the constant acceleration response (T_B), for a constant velocity response (T_C), and for a constant displacement response (T_D).

A number of approaches are available to develop acceleration response spectra for a site. For Barcelona, which is in an area of low seismicity, the following approaches have been selected:

- Deterministic Approach. Method to develop response spectra from past earthquake events and local geological conditions, refer Section 3.3.
- Probabilistic Approach. Method to develop response spectra from all available seismological data of the region and local geological conditions, refer Section 3.4.
- Code formulations, including Eurocode 8 and NCSE-02. Methods to develop response spectra using recommended peak ground accelerations for the local area and local geological conditions, refer Section 3.5.

3.2 Site Geology

The local geology of a site has a significant influence on the ground motions developed by a seismic event. In particular, a local soil profile consisting of a layer of soft soils can have a pronounced amplification effect of the motions at surface level compared to stiff soils or rock (Borcherdt, 1994).

A general description of the classification and effects of the site geology on response spectra is provided below. A discussion of the site geology for the Eixample district of Barcelona and a suitable soil classification is presented in Section 6.2.

A typical method of defining the local geology is by a soil classification depending on the soil shear wave velocity (V_s). Correlations to the shear wave velocity can be made from results of cone penetration testing or to the undrained cohesive strength of the material.

As the effect of local soil conditions is so pronounced, each method used to develop an acceleration response spectrum includes parameters that are dependent on the soil profile. Furthermore, each method utilises slightly different ranges of shear wave velocity to classify the sub-soil characteristics. The specific sub-soil classifications and values for the parameters for each method are presented in the detailed descriptions of each method. In general however, there are four common classifications for the characteristics of the sub-soil, as presented below (Table 3.1). Additional special soil classifications are also contained within Eurocode 8 to account for shallow alluvium layers underlain by stiffer materials, deposits of soft cohesive soils of high plasticity index and water content, and liquefiable soils.

Table 3.1: General sub-soil classifications (Eurocode 8, NCSE-02)

Soil classification	V_s (m/s)	N_{SPT} (blows/30cm)	c_u (kPa)
Rock, with limited weaker material at ground surface.	> 750 to 800	-	-
Very stiff clay, very dense sand or gravel, or highly fractured rock. Increasing stiffness with depth.	from 350 – 400 to 750 – 800	> 50	> 250
Stiff clay, or medium-dense sand or gravel of significant thickness.	from 180 – 200 to 350 – 400	15 – 50	70 – 250
Soft cohesive soils, or loose cohesionless soil	< 180 – 200	< 15	< 70

As stated above, a local soil profile of soft soils ($V_s < 200$) will have a pronounced amplification effect on the ground motions caused by an earthquake event compared to a rock soil profile ($V_s > 750$). For soil classifications between these ranges, amplification of the ground motions also occurs, but to a

lesser extent. This effect is clearly represented by the influence to the acceleration response spectra, as shown in Figure 3.3. As shown, not only is there an amplification of the acceleration with reduced soil strength, but there is generally an increase in the range of the structural period for the maximum spectral acceleration.

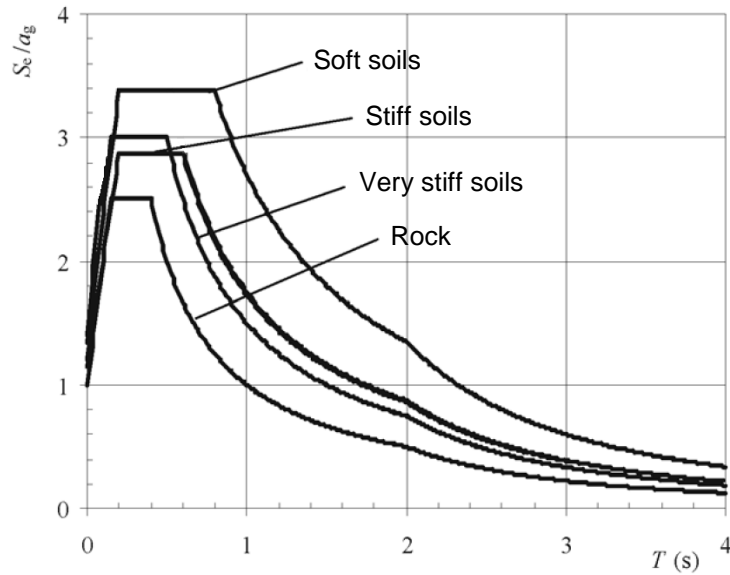


Figure 3.3: Influence of soil classification on acceleration response spectrum (Eurocode 8)

3.3 Deterministic Approach

The deterministic approach develops a hazard assessment based upon data from past seismic events that represent the maximum past impact to the subject site. For sites where seismic events are fairly regular and there are sufficient recent records of seismic action, the assessment can be based directly on the measured magnitude of the events. For sites where there are fewer recorded events of significant impact, such as Barcelona, the assessment can be based upon the recorded macroseismic intensity of the earthquakes and the relative distance of these events to the site.

The general procedure is provided below for using a deterministic hazard assessment to develop a response spectrum from recorded seismic intensities. A description of the application of this procedure to Barcelona, and the development of a smoothed response spectrum, are provided in Section 6.4.

Earthquake intensity is a qualitative description of the magnitude of a seismic event. Various macroseismic intensity scales have been developed, with the most commonly used scales being the Modified Mercalli Intensity (MMI) scale and the Medvedev Sponheuer Karnik (MSK) scale. The MSK scale has an advantage over the MMI scale, as the intensity is classified not only by the observed damage but also by vulnerability classes of structures, dependent on the composition of the structural materials (Molin, 1995). The intensity scales range in values of increasing levels of damage from I to XII, with I referring to no observed damage, and XII to total damage of structures and significant, lasting ground displacements.

To utilise the recorded intensities for a hazard assessment, the intensity values must first be correlated to an earthquake magnitude scale, then an acceleration response spectra can be developed using an appropriate attenuation relationship.

Earthquake magnitude scales represent a quantitative description of the size of the earthquake and can be related to the total seismic energy of the event. A number of magnitude scales have been developed including:

- Richter local magnitude (M_L), for shallow earthquakes less than 600km from the subject site.
- Surface wave magnitude (M_S), for shallow more distant earthquakes of significant scale.
- Body wave magnitude (M_B), for shallow intraplate earthquakes.

A commonly utilised scale within the Risk-UE project is the surface wave magnitude, which enables the development of hazard assessments from data of distant earthquakes.

To convert the intensity values to M_S values, two relationships can be employed (Irizarry, 2004). Firstly, the values are correlated to the local magnitude scale (M_L) using a relationship developed for the Catalonia region by Gonzalez (2000), which was modified by Irizarry (2004) to account for varying depths of seismic action, h , (Figure 3.4).

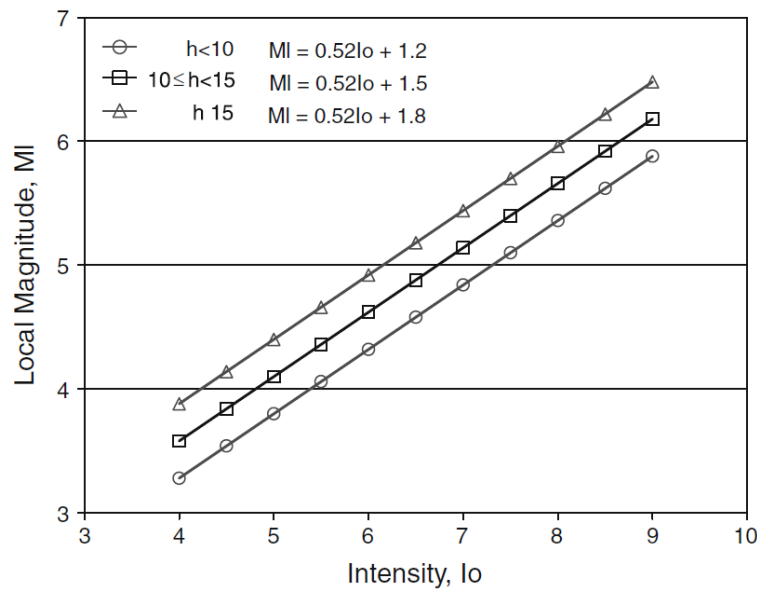


Figure 3.4: Relationship between MSK intensity and local magnitude (M_L) (Irizarry et al., 2011)

Secondly, the M_L value is used to obtain an approximate M_S value using a magnitude relationship scale developed by Dufumier (2002), as follows, where the M_B value is assumed to be similar to the M_L value for the selected events.

$$M_S = 1.75 \cdot M_B - 4.3 \quad (\text{Eqn. 3.1})$$

Once a representative value of the earthquake magnitude (M_S) has been obtained, this can be used to generate an acceleration response spectrum using an appropriate attenuation relationship. One such relationship is that developed by Ambraseys et al. (1996) which used data from 157 earthquakes in Europe with surface wave magnitudes between 4.0 and 7.9 and focal depths less than or equal to 30km.

The benefits of this relationship for application to Barcelona are: (Faccioli, 2006)

- Relationship is largely based upon European data.
- Appropriate for various earthquake source mechanisms.
- Uses a simplified soil classification system consisting of rock ($V_S > 750$ m/s), stiff soils ($V_S: 360-750$ m/s) and soft soils ($V_S: < 360$ m/s).
- Can be used for various source distances and magnitudes.

The formulation is as follows:

$$\log(y) = C_1 + C_2 \cdot M + C_4 \cdot \log(r) + C_A \cdot S_A + C_S \cdot S_S + \sigma \cdot P \quad (\text{Eqn. 3.2})$$

$$r = \sqrt{d^2 + h_0^2} \quad (\text{Eqn. 3.3})$$

Where:

- y : Peak ground acceleration (PGA).
- $C_1, C_2, C_4, C_A, C_S, \sigma$ and h_0 : Factors dependant on the structural period.
- S_A, S_S : Factors dependant on the local soil conditions.

- P: Parameter to adjust standard deviation of results, set to zero for mean values.
- M: Surface wave magnitude of past event (M_S).
- d: Distance of past event to subject site, km.

Values for the abovementioned parameters are presented below in Table 3.2 and Table 3.3.

Table 3.2: Values of parameters for attenuation relationship (Ambraseys et al., 1996)

T	C_1	C_2	h_0	C_4	C_A	C_S	σ
0	-1.48	0.266	3.5	-0.922	0.117	0.124	0.25
0.1	-0.84	0.219	4.5	-0.954	0.078	0.027	0.27
0.15	-0.98	0.247	4.7	-0.938	0.143	0.085	0.27
0.2	-1.21	0.284	4.2	-0.922	0.135	0.142	0.27
0.28	-1.46	0.326	4.4	-0.946	0.134	0.158	0.29
0.32	-1.63	0.349	4.2	-0.932	0.125	0.161	0.31
0.4	-1.94	0.377	3.6	-0.888	0.139	0.172	0.31
0.5	-2.25	0.42	3.3	-0.913	0.147	0.201	0.32
0.6	-2.49	0.438	2.5	-0.881	0.124	0.212	0.32
0.7	-2.67	0.463	3.1	-0.914	0.116	0.214	0.33
0.8	-2.86	0.485	3.7	-0.925	0.127	0.218	0.32
0.9	-3.03	0.502	4.0	-0.920	0.124	0.225	0.32
1.0	-3.17	0.508	4.3	-0.885	0.128	0.219	0.32
1.4	-3.52	0.522	3.4	-0.839	0.109	0.197	0.31
1.6	-3.68	0.52	2.5	-0.781	0.108	0.206	0.31
1.8	-3.79	0.514	2.4	-0.730	0.104	0.204	0.32
2.0	-3.79	0.503	3.2	-0.728	0.101	0.182	0.32

Table 3.3: Values of soil parameters for soil classification (Ambraseys et al., 1996)

Soil classification	S_A	S_S
Rock	0	0
Stiff soil	1	0
Soft soil	0	1

The soil parameters in Table 3.3 only provide an initial estimate of the influence of local geological conditions. The spectra derived from the Ambraseys relationship must then also be calibrated to the soils at the subject site and amplification factors derived to mathematically describe the varying seismic response of each local soil type. The soil amplification factors derived from this calibration for Barcelona, for a range of structural periods, are presented in Section 6.2. Once completed, the final response spectra can be used in conjunction with the spectra from a probabilistic approach and those from code recommendations to assess the likely seismic hazard for the site.

The benefits of the deterministic approach are that an approximate hazard assessment can be constructed relatively easily, based upon data from only those past events that had the most significant impact on the subject site. This is in contrast to probabilistic approaches that consider local geological and seismological data for the full range of ground motions that could affect the subject site. The drawbacks are that the past events may have occurred some hundreds of years ago and as such the intensities developed may be somewhat unreliable. Also, the recorded damages from the time may overestimate the likely damages to more modern structures, even to those comprising similar materials which may lead to a conservative hazard assessment.

3.4 Probabilistic Approach

In contrast to the deterministic approach which considers only those past events that had the maximum seismic effect at the subject site, the probabilistic approach considers all seismic sources that could possibly affect the site.

The following section briefly describes the methodology for the probabilistic approach. The seismotectonic zonation, results of previous probabilistic assessments and development of a smoothed response spectrum are presented in Section 6.5.

The probabilistic approach requires a thorough understanding of the seismotectonic characteristics of the local region to develop the hazard assessment. Firstly, the local region is divided into seismic source zones for which the frequency, relative magnitude, type and location of seismic events is defined. Using appropriate attenuation relationships, a seismic parameter can then be developed to describe the seismic hazard from each source zone to the subject site.

The seismic hazard for the subject site is then defined by the probability of exceedance of a certain level of the seismic parameter resulting from a contribution of each source zone (Irizarry et al., 2011).

The probability of exceedance utilised is 10% in 50 years, or a return period of 475 years.

The Risk-UE project and other previous studies in Barcelona have utilised the CRISIS 99-18 computer code in combination with the Ambraseys attenuation relationship to evaluate a probability model that considers the temporal distribution, magnitude and location of the seismic actions from each zone.

Similar to the deterministic approach, once the response spectra are obtained from the CRISIS 99-18 program, they must be calibrated to account for the individual nature of the local soil conditions. Appropriate soil amplification factors to be applied to the Ambraseys response spectra for Barcelona are presented in Section 6.2.

The primary benefits of the probabilistic approach are that it considers all possible seismic sources for the subject site and it derives the hazard probability from the temporal variation of all past actions, as well as their mechanism and magnitude. In this regard, the probabilistic approach encompasses a far more detailed description of the seismicity of the subject site.

3.5 Code Recommendations

Two code recommended approaches have been included in this study, Eurocode 8 (2004) and that from the Spanish earthquake design code, NCSE-02 (2002). This section provides a brief description of the methodology of each code to develop acceleration response spectra.

The elastic acceleration response spectra obtained for Barcelona from each code are presented in Section 6.6.

3.5.1 Eurocode 8

Acceleration response spectra are developed in accordance with parametric functions that describe the shape of the spectrum between specific ranges of the structural period; that for constant acceleration, constant velocity and constant displacement. A diagrammatic representation of the acceleration response spectrum with the ranges of the periods is presented in Figure 3.2.

The parametric functions for the horizontal acceleration of an elastic single degree of freedom system are as follows:

$$0 \leq T \leq T_B \quad S_e(T) = a_g \cdot S \cdot \left[1 + T/T_B (\eta \cdot 2.5 - 1) \right] \quad (\text{Eqn. 3.4})$$

$$T_B \leq T \leq T_C \quad S_e(T) = a_g \cdot S \cdot \eta \cdot 2.5 \quad (\text{Eqn. 3.5})$$

$$T_C \leq T \leq T_D \quad S_e(T) = a_g \cdot S \cdot \eta \cdot 2.5 \cdot \left[T_D/T \right] \quad (\text{Eqn. 3.6})$$

$$T_D \leq T \leq 4 \text{secs} \quad S_e(T) = a_g \cdot S \cdot \eta \cdot 2.5 \cdot \left[T_C \cdot T_D / T^2 \right] \quad (\text{Eqn. 3.7})$$

$$a_g = \gamma_I \cdot a_{gR}; \quad \eta = \sqrt{10 / (5 + \xi)} \geq 0.55 \quad (\text{Eqns. 3.8; 3.9})$$

Where:

- S_e : Elastic spectral acceleration.
- T : Vibration period of a linear single degree of freedom system.
- a_g, a_{gR} : Design ground acceleration and reference ground acceleration on rock.
- γ_I : Importance factor for the structure.
- S : Soil factor.
- ξ : Viscous damping ratio.
- T_B, T_C, T_D : Definition of ranges of the structural period to define the start values for the constant acceleration response (T_B), constant velocity response (T_C), and for constant displacement response (T_D).

Eurocode 8 defines two types of elastic spectra, and recommends in general that both types be considered in the seismic analysis (Figure 3.5). An exception to this is for a probabilistic assessment, where the Type II spectra may alone be considered, when earthquakes that contribute most to the

seismic hazard have a value of surface wave magnitude (M_S) less than 5.5. Values for the soil factor, T_B , T_C and T_D for each spectra type are provided within the code.

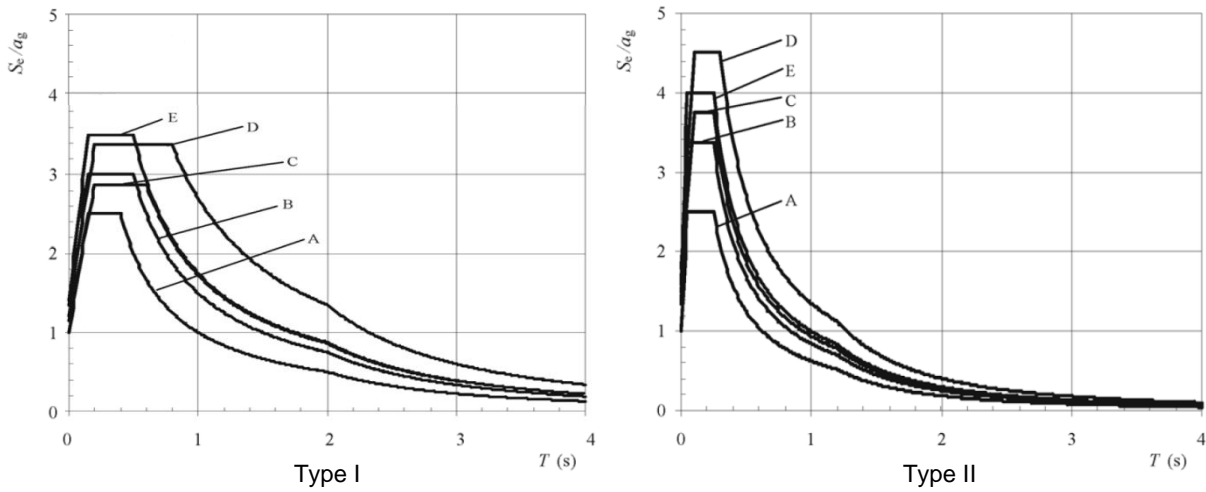


Figure 3.5: Type I and Type II elastic acceleration spectra for soil classifications (Eurocode 8)

In general, spectra Type I is more representative of the effect of larger, more distant seismic actions, whilst Type II is representative of lower magnitude events closer to the subject site.

The elastic response spectra developed for Barcelona from Eurocode 8 (2004) are presented in Section 6.6.

3.5.2 NCSE-02

Similar to Eurocode 8, NCSE-02 provides parametric functions that describe the form of the elastic response spectra between specific ranges of the structural period; that for constant acceleration, constant velocity and constant displacement.

The functions for horizontal acceleration of an elastic single degree of freedom system are as follows:

$$0 \leq T \leq T_B \quad S_e(T) = a_b \cdot \rho \cdot S \cdot \left[1 + 1.5 \cdot T/T_B \right] \quad (\text{Eqn. 3.10})$$

$$T_B \leq T \leq T_C \quad S_e(T) = a_b \cdot \rho \cdot S \cdot 2.5 \quad (\text{Eqn. 3.11})$$

$$T \geq T_C \quad S_e(T) = a_b \cdot \rho \cdot S \cdot K \cdot \left[C/T \right] \quad (\text{Eqn. 3.12})$$

Where:

- S_e : Elastic spectral acceleration.
- T : Vibration period of a linear single degree of freedom system.
- a_b : Base ground acceleration on rock.
- ρ : Importance factor for the structure.
- C : Soil classification factor.
- S : Soil amplification factor, dependent on C .
- K : Coefficient for expected earthquake type for the region.

- T_B, T_C : Definition of ranges of the structural period to define the start values for the constant acceleration response (T_B) and constant velocity response (T_C).

In contrast to Eurocode 8, there is no separate function for a range of structural periods with constant displacement. Also, the values for S , T_B and T_C are dependent on the values of K and C for the local site.

The elastic response spectra for Barcelona developed in accordance with NCSE-02 are presented in Section 6.6.

This page is left blank on purpose.

4. CAPACITY SPECTRUM METHOD – STATE OF THE ART

This chapter describes the general application of a capacity spectrum method to determine the displacement demand on a structure using a nonlinear pushover analysis. The primary steps involved are clearly identified and the formulations and methodology for each step are presented.

4.1 Introduction

As discussed in Section 2.9, the capacity spectrum method (CSM) is a performance based method that determines the displacement on a structure due to imposed seismic actions. This procedure is readily applicable to the unreinforced masonry buildings of the Eixample district and can provide a reasonable estimation of the displacement demand due to seismic actions.

The method involves comparing a capacity spectrum, describing the capacity of the structure, to a demand spectrum, denoting seismic demand. The nominal intersection of these curves is termed the performance point and describes the displacement demand induced in the structure due to a given level of seismic acceleration.

For this study it was decided to use the N2 capacity spectrum method, which is also recommended in Eurocode 8 (2004).

In summary, the steps for determining the displacement demand using the N2 method are:

1. Determine the seismic demand for the site. Plot in ADRS format.
2. Apply lateral forces to non-linear modal and construct pushover curve, idealise as a bilinear capacity curve.
3. Modify capacity curve to a capacity spectrum in ADRS format.
4. Determine location of intersection point. If in inelastic range, develop inelastic demand spectrum. Calculate SDOF spectral displacement demand and convert to MDOF displacement demand.

The following sections detail each step in the procedure.

4.2 Step 1 – Seismic Demand

The initial step is to determine the seismic demand for the site. To do so, the horizontal elastic acceleration response curves for the site must be obtained. The methods to develop these curves are described in Section 3, whilst the resulting acceleration response curves for Barcelona are derived and presented in Section 6.

To enable comparison of the seismic demand with the structural capacity, the response curves must be modified to be in an acceleration-displacement (ADRS) format using the following relationship. The resulting ADRS curves are termed 'demand spectra'.

$$S_{de} = T^2 / 4 \cdot \pi^2 \cdot S_{ae} \quad (\text{Eqn. 4.1})$$

Where:

- S_{de} : Elastic spectral displacement.
- T : Vibration period of a linear single degree of freedom (SDOF) system.
- S_{ae} : Elastic spectral acceleration.

The demand spectra for the Eixample district of Barcelona are presented in Figure 6.17.

4.3 Step 2 – Pushover Curve

The second step is to develop a force-displacement curve from a non-linear pushover analysis of the structure. This curve is a direct result of the response of the multi-degree-of-freedom (MDOF) system.

The starting point to develop this curve is the application of an appropriate distribution of lateral forces to the centre-of-mass of the roof and each floor level. The load distribution should be consistent with the assumed deflected shape of the structure and hence be related to the likely inertial response (refer N2 method, below). The two load distributions that are commonly used are a relative vertical distribution related to the first mode of vibration, and a linear increase in lateral loads with the building height (Fajfar, 2000; FEMA 440, 2005). To determine the lateral load distribution related to the first mode of vibration, first a modal analysis must be completed. For each load distribution, the proportion of lateral force at each level is determined by the following relationship:

$$P_i = m_i \Phi_i \quad (\text{Eqn. 4.2})$$

Where:

- P_i : Lateral load proportion applied at level i .
- m_i : Mass of structure at level i .
- Φ_i : Shape factor for assumed load distribution at level i , either using the first mode of vibration or linear increase in loading with building height. The shape factor is normalised to 1 at roof level.

The two lateral load distributions are represented diagrammatically below (Figure 4.1).

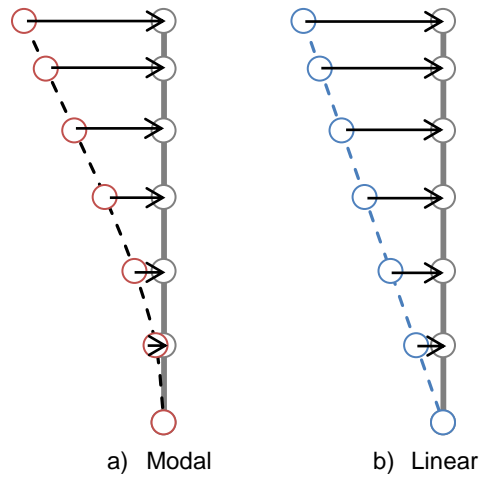


Figure 4.1: Typical lateral load distributions

The pushover curve is a plot of the lateral displacement at roof level in the direction of the applied forces, against the total lateral reaction at the base of the structure. A typical pushover curve for the Eixample unreinforced masonry building is presented below (Figure 4.2). Pushover curves from the analysis of each model are presented in Section 7.5.

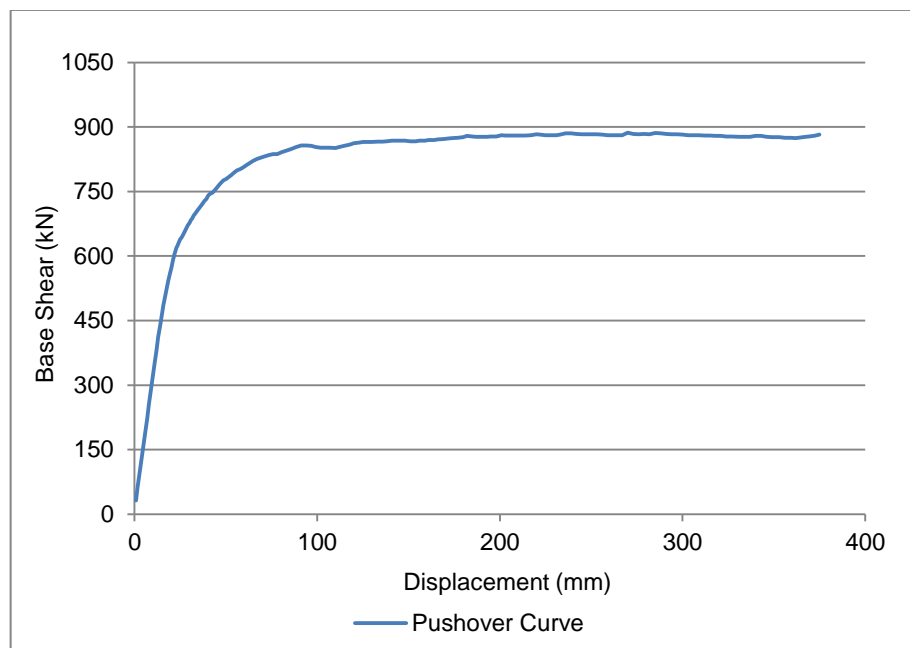


Figure 4.2: Typical pushover curve for Eixample unreinforced masonry building

4.4 Step 3 – Capacity Spectrum

To compare the pushover curve with the demand spectra for the site, it must be converted to an equivalent single-degree-of-freedom system and transformed to acceleration-displacement format. The resulting curve is termed a 'capacity spectrum'. The formulations presented herein are from the N2 methodology described by Fajfar (2000) and form the basis for the transformations described in Eurocode 8 (2004). The relationships are also equivalent to those described in the ATC-40 method and as recommended by Goel and Chopra (2004).

The basis for the transformation from the MDOF system to the SDOF system can be derived by equating the internal and external forces acting on the structure. The resultant equation of motion for the SDOF system is given by:

$$m^* \cdot \ddot{D}^* + F^* = -m^* \cdot a \quad (\text{Eqn. 4.3})$$

Where:

- m^* : Equivalent mass of SDOF system.
- D^* : Lateral displacement of equivalent SDOF system, also termed spectral displacement (S_d).
- F^* : Lateral force of equivalent SDOF system.
- a : Ground acceleration.

The derivation of the above relationship (Fajfar, 2000) permits the development of the following relations for each of the identified parameters:

$$m^* = \sum m_i \Phi_i \quad (\text{Eqn. 4.4})$$

$$D^* = D_r / \Gamma \quad (\text{Eqn. 4.5})$$

$$F^* = V / \Gamma \quad (\text{Eqn. 4.6})$$

$$\Gamma = m^* / \sum m_i \Phi_i^2 = \sum m_i \Phi_i / \sum m_i \Phi_i^2 \quad (\text{Eqn. 4.7})$$

Where:

- Γ : Modal participation factor.

As can be seen from the above, the transformation from a MDOF system to a SDOF system involves reducing the MDOF by a single constant, the modal participation factor. Hence, the relationship between the lateral force and displacement of the pushover curve is retained, and the elastic modulus of elasticity remains unchanged.

The final requirement is to convert the SDOF force-displacement curve to ADRS format by dividing the lateral force of the equivalent SDOF by the equivalent mass, as follows.

$$S_a = F^* / m^* \quad (\text{Eqn. 4.8})$$

For the N2 method, prior to completing the transformation, the pushover curve should be idealised by an equivalent bilinear elasto perfectly plastic pushover curve. It should also be noted that the ATC method requires an idealisation to bilinear elasto plastic form. For the N2 method this idealisation is necessary to facilitate the transformation of the elastic demand spectra to an inelastic form. For the ATC method it ensures consistent pseudo damping of the elastic spectra.

As the N2 method has been selected for this project, the derivation of a bilinear elasto perfectly plastic idealisation is described below.

The primary objective of the idealisation is to ensure that the total energy demand is the same for both the original pushover curve and the bilinear idealisation. This can be determined by equating the areas beneath each curve. Guidance is also provided in FEMA 273 (1997) and FEMA 440 (2005) to suggest that appropriate slope of the elastic portion of the idealisation should be such that the elastic portion of the curve crosses the pushover curve at 60% of the proposed yield force. The completed procedure is shown in Figure 4.3.

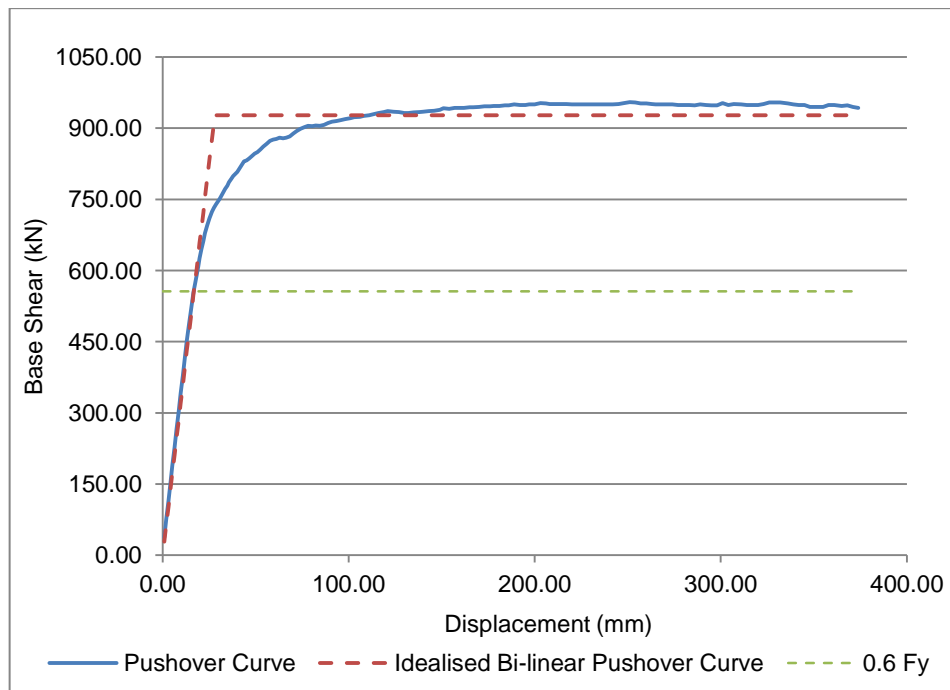


Figure 4.3: Bilinear elasto perfectly plastic idealisation of pushover curve

4.5 Step 4 – Displacement Demand

Once both the demand spectra and the capacity spectra are developed, it is possible to plot them on the same graph and to determine the nominal performance point of the system and hence the displacement demand caused by the seismic action.

There are three different possible cases for the location of the performance point, each will be described briefly below with the relevant formulas to determine the displacement demand.

4.5.1 Case 1 – Elastic demand

The simplest of cases is that the intersection point occurs within the elastic portion of the idealised capacity spectrum (Figure 4.4). In this condition, no adjustment to the elastic demand spectrum is needed, as the structure remains in the elastic range. As such, the coordinates of the intersection with the elastic demand spectrum provide the value for the spectral displacement demand for the equivalent SDOF system.

The displacement of an equivalent MDOF system is then determined using the relationship as described in equation 4.5.

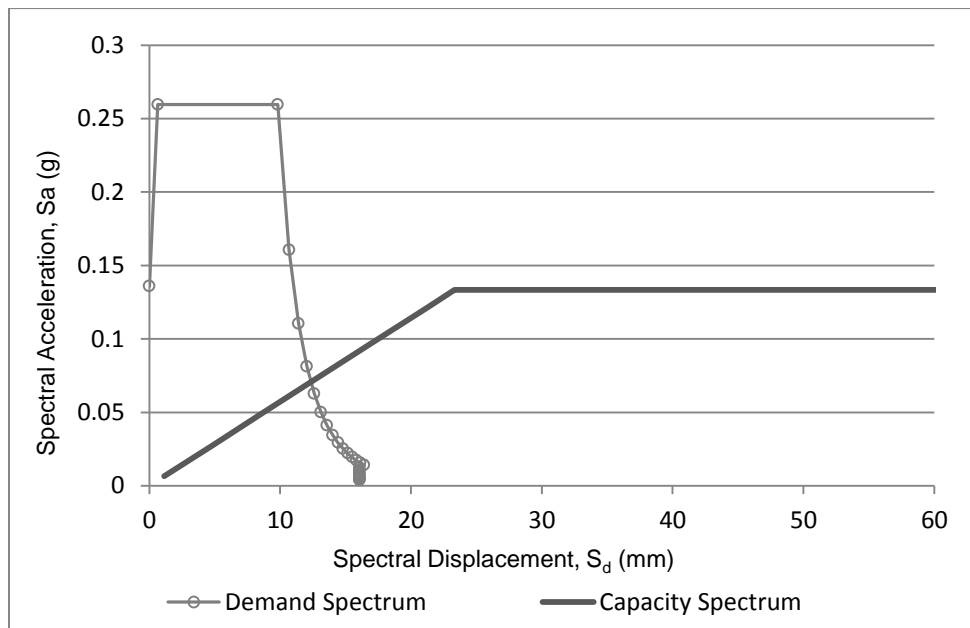


Figure 4.4: Intersection of capacity and demand spectrum within elastic range

4.5.2 Case 2 – Inelastic demand, $T^* \geq T_c$

When the intersection does not occur in the elastic range, the performance point as characterised by the N2 method is no longer the intersection of the capacity and demand spectra. Instead, it is characterised by the intersection of the radial line corresponding to the elastic period of the structure (T^*) and the demand spectrum (Figure 4.5).

The elastic period of the bilinear system can be determined as follows:

$$T^* = 2 \cdot \pi \cdot \sqrt{\frac{m^* \cdot D_y^*}{F_y^*}} \quad (\text{Eqn. 4.9})$$

Where:

- m^* : Equivalent mass of SDOF system.
- D_y^* : Lateral yield displacement of idealised bilinear SDOF system, also termed spectral yield displacement (S_{ay}).
- F_y^* : Lateral yield force of idealised bilinear SDOF system.

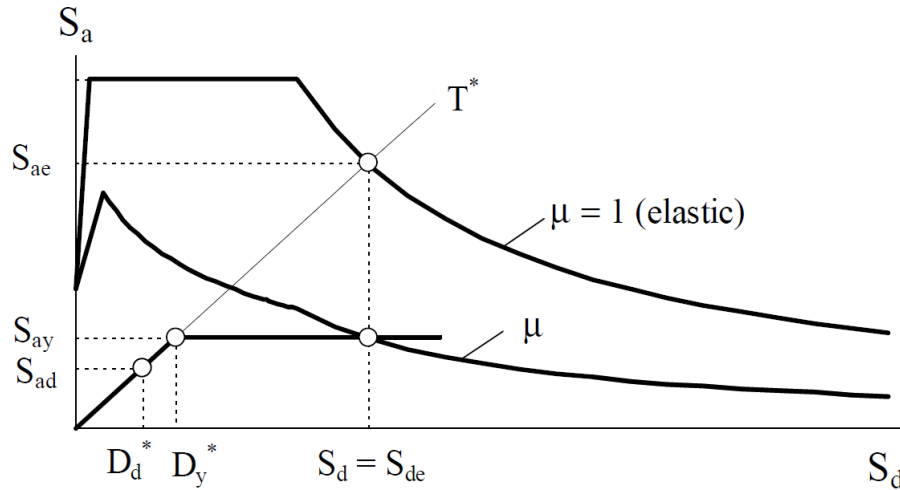


Figure 4.5: Intersection in the inelastic range where $T^* \geq T_c$ (Fajfar, 2000)

In this condition, the intersection point is no longer within the idealised elastic range of the system and as such the elastic demand curve must be modified to an inelastic demand. The procedure presented in the N2 method is to reduce the elastic spectrum by a spectral reduction factor due to the hysteretic damping of the system, which is the energy dissipation with inelastic deformations.

The spectral reduction factor (R_{μ_s}) is calculated by a relationship with the system spectral ductility (μ_s), defined as the ratio of the maximum elastic displacement (S_{de}) for a system with elastic period T^* , to the yield displacement (D_y^* , S_{ay}). These relationships are presented as follows:

$$S_{ai} = S_{ae} / R_{\mu_s} \quad (\text{Eqn. 4.10})$$

$$T < T_c \quad R_{\mu_s} = (\mu_s - 1) \cdot T / T_c + 1 \quad (\text{Eqn. 4.11})$$

$$T \geq T_c \quad R_{\mu_s} = \mu_s \quad (\text{Eqn. 4.12})$$

$$\mu_s = S_{de} / D_y^* \quad (\text{Eqn. 4.13})$$

Where:

- S_{ai} : Spectral inelastic acceleration.
- S_{ae} : Spectral elastic acceleration.
- R_{μ_s} : Spectral reduction factor.

- μ_s : Spectral ductility.
- T_c : Characteristic period of elastic demand spectrum.
- S_{de} : Spectral elastic displacement, for a system with elastic period (T^*).
- D_y^* : Lateral yield displacement of idealised bilinear SDOF system, also termed spectral yield displacement (S_{dy}).

The reduction of the demand spectrum can be visualised in Figure 4.5. As shown, for the case where the elastic period (T^*) is greater than T_c (when the intersection occurs beyond the range of constant acceleration) the displacement demand is equal to the maximum elastic displacement, e.g.

$$T^* \geq T_c \quad S_d = S_{de} \quad (\text{Eqn. 4.14})$$

As for the elastic condition described in Case 1, the displacement of an equivalent MDOF system is then determined using equation 4.5.

4.5.3 Case 3 – Inelastic demand, $T^* < T_c$

Case 3 caters for an inelastic intersection with $T^* < T_c$. Hence, the intersection of the radial line corresponding to the elastic period with the elastic demand spectrum occurs within or prior to the range of constant acceleration (Figure 4.6).

Similarly to Case 2, initially the value of the elastic period (T^*) must be obtained using equation 4.9, then this must be compared to the characteristic period of the demand spectra (T_c).

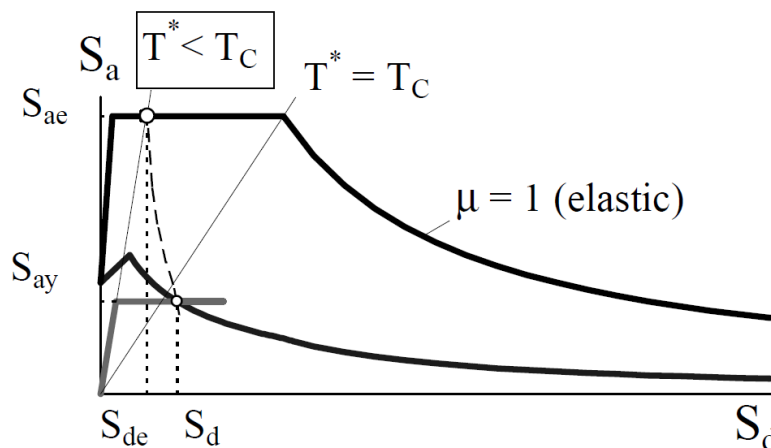


Figure 4.6: Intersection in the inelastic range where $T^* < T_c$ (Fajfar, 2000)

As the intersection point is within the inelastic range, the elastic demand spectra must be modified to the inelastic condition using the same procedure as described for Case 2.

In this case, the spectral displacement is not equal to the elastic displacement, but is dependent on the capacity reduction factor ($R_{\mu c}$). The capacity reduction factor is defined as the ratio between the elastic acceleration of a system with elastic period, T^* , to the yield acceleration of the idealised bilinear system. These relationships can be described as follows:

$$T^* < T_c \quad S_d = \frac{S_{de}}{R_{\mu c}} \cdot \left(1 + (R_{\mu c} - 1) \cdot \frac{T_c}{T^*}\right) \quad (\text{Eqn. 4.15})$$

$$R_{\mu c} = \frac{S_{ae}(T^*)}{S_{ay}} \quad (\text{Eqn. 4.16})$$

Where:

- $R_{\mu s}$: Capacity reduction factor.
- $S_{ae}(T^*)$: Spectral elastic acceleration at the elastic period, T^* .
- S_{ay} : Spectral yield acceleration.
- S_d : Spectral displacement.
- S_{de} : Spectral elastic displacement.
- T_c : Characteristic period of elastic demand spectrum.

This case is shown diagrammatically in Figure 4.6, above. Similarly to Case 1 and Case 2, the equivalent MDOF displacement demand is then calculated using equation 4.5.

This page is left blank on purpose.

5. STRUCTURAL ASSESSMENT – CASE STUDY

This chapter details the application of the structural assessment methodology developed in Section 2. Each stage of the assessment is presented separately beginning with the general identification of the structure and its location. Secondly, an historical investigation describes the development of the Eixample district and the influence of its planning on the building typologies. The key geometrical aspects and structural systems of a typical building are then discussed, followed by the description of a representative building to be used for the seismic analysis. A brief review follows of previous similar studies in the region, including comments on their conclusions.

In the final two sections of the chapter, appropriate methods of applying and using a damage survey and monitoring on the buildings of the Eixample district are discussed. The likely actions to cause damage, and the load actions used for the pushover analysis, are also reported.

5.1 Structure Identification

Barcelona is the capital city of Catalonia, one of Spain's seventeen autonomous communities, or regions. Catalonia is located at the far north-east of Spain and is bordered by France and Andorra to the north and the Mediterranean Sea to the east (Figure 5.1). The city is the second largest in Spain, with a greater metropolitan population of approximately five million people. The greater metropolitan area is bordered by the Llobregat and Besos rivers to the north and south, the Mediterranean Sea to the east and the Collserola Serra mountains to the west.

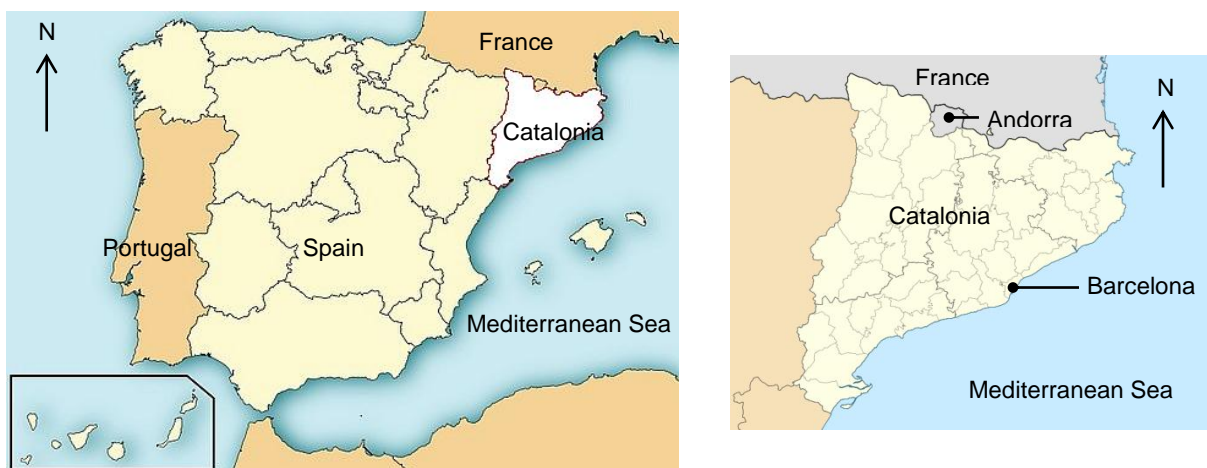


Figure 5.1: Barcelona location

The focus of the present study is the seismic analysis and vulnerability assessment of a typical unreinforced masonry building in the Eixample district. The Eixample, which means the enlargement in Catalan, is one of ten districts of the city of Barcelona (Figure 5.2). It was so named because it

constituted an ambitious extension to the original walled city between 1860 and the early 20th century. The topography is fairly even, with a slight gradient from east to west. The geology is also similar across the district, consisting of Pleistocene clays and gravels (Section 6.2).

The history of the Eixample district, and a detailed description of the building typology of this study are presented in the following sections.



Figure 5.2: Districts of Barcelona city (Pujades et al., 2010)

5.2 Historical Investigation

By the 1850s, Barcelona was a densely populated city contained within walls. The city walls were controlled by the army and development for 1.5km beyond the walls was prohibited. With an ever increasing population, the living conditions within the walled city were poor and there was mounting economic pressure to open the city to the industrial growth of neighbouring towns. Hence, in 1854 a decree was issued for demolition of the walls to allow for development to the towns of Horta, Gracia, San Andres, San Marti, Sarria and Sants.

The planning for this region was issued to public tendering and a plan by a local civil engineer, Ildefons Cerda was officially selected on 8 July 1860 by the Ministry of Public Works (Gutierrez, 2010). Cerda's plan was based upon a detailed study of other cities including Boston, Saint Petersburg and Turin (CCCB, 2009). The concept was to develop a well-structured, open and above all hygienic extension to the walled city (Figure 5.3).

Cerda's plan was for a grid of city blocks with street junctions spaced every 113 metres. The layout is formed by 20, 30 and 50 metre wide roads, each with roughly an equal percentage of space for pedestrian and vehicular traffic. At each road junction, the corners of the city blocks are chamfered,

creating approximately 50 metre diameter open space at the smallest of intersections. A network of primary roads provided easily access both across and within the development and enabled the continued development and integration of the satellite towns. Cerda's previous experience in municipal infrastructure projects also ensured that a sanitation network and public transportation and railway access was also incorporated.

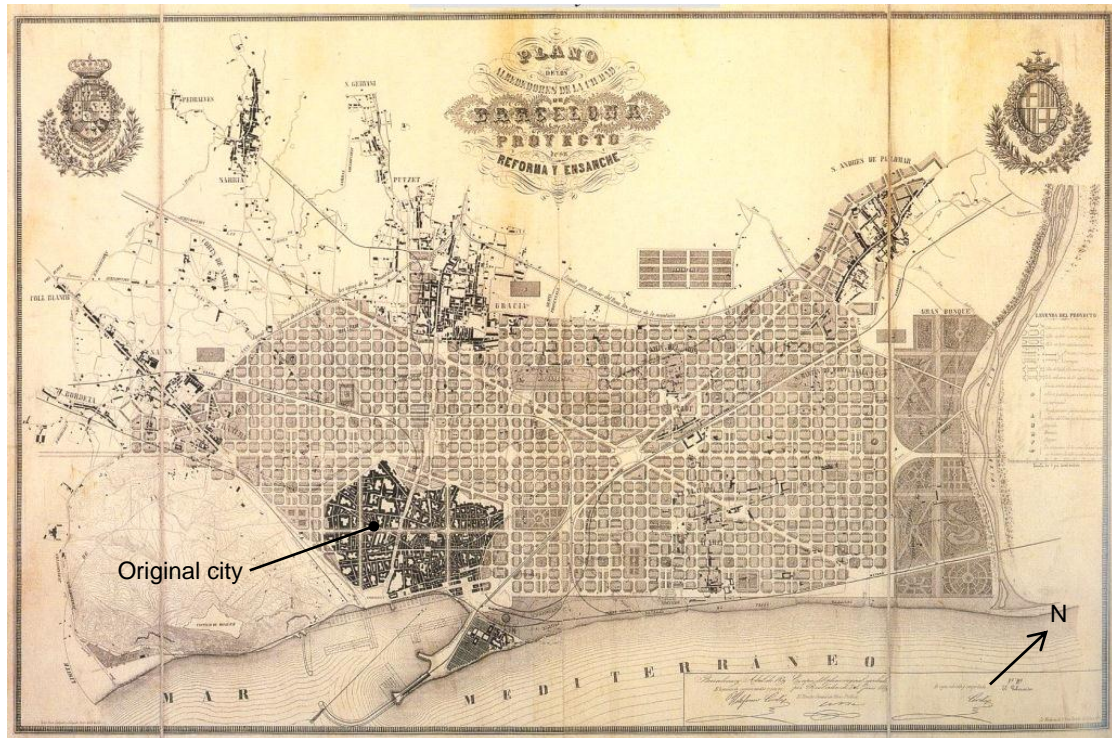


Figure 5.3: Plan for Eixample development, Ildefons Cerda, 1859 (CCCB, 2009)

A significant aspect of the plan was to promote the city's health and living standards. This was to be achieved not only by improved sanitation and the ease of access and space in the road network, but by ensuring cross-ventilation and natural light to each building. Hence, Cerda proposed ideal layouts for the blocks with buildings at the block perimeter and a central open space, which formed the basis for the publication of a set of common construction regulations by the governor of the city in 1859. The regulations changed regularly during the initial stages of development and it was not until 1891 that 'Bylaws for the Eixample' were published and used for the remainder of the development.

The bylaws had a significant impact on the size and nature of the buildings in the Eixample. In particular, the block layout and building typology was influenced by the following bylaws (CCCB, 2009):

- The outermost building line of a block was aligned to the street.
- A maximum building height was to be 22m. Corresponding to a limit of six stories for the buildings and a height to width ratio of approximately 1:1 for 20m wide streets.

- Maximum occupation of multi-storey buildings on a block of 73.6%, which ensured a central open space, but prevented internal façades for the corner buildings. For a standard block, this limited the building depth to 27.9m. The central area could be occupied by single storey buildings.
- Light wells were to be provided to each building in proportion to the gross floor area and number of façades. For one façade, 12%; two façades, 8%; and three façades, 6%.

Changes in the bylaws in the 1930s and 1940s saw an increase in the building height limits to six floors and the provision for one or two additional penthouse levels setback from the street. Accordingly, the average net floor area of the buildings increased from 4.6 times the gross ground area, to 7.1 times by 1947. These modifications were largely retracted by regulations passed in 1976 and the current net floor area ratio stands at 4.4. Unfortunately, development pressures have seen many of the internal spaces reduced by extensions to the perimeter or interior buildings.

The following figure illustrates the typical layout of a group of blocks, largely in accordance with the bylaws of 1891 (Figure 5.4). The influence of bylaws on building typology is discussed in Section 5.3.



Figure 5.4: Typical Eixample block layout (CCCB, 2009)

To this day, Cerda's original plan for the Eixample district is clearly recognisable. The plan has accommodated the increasing population demands on the city extremely well and current planning regulations are looking to once again encourage Cerda's vision of open spaces within each block.

5.3 Geometrical and Structural Systems Survey

Cerda's plans and the bylaws of 1891 not only impacted the block layout, but the dimensions and layouts of individual buildings. In addition, the Eixample development was largely financed by private developers, so both the footprint of each building and the construction methodology was influenced by commercial demands. As such, specific building typologies emerged throughout the district.

As shown in Figure 5.4, the corner of each block comprises one or two triangular shaped buildings with voids positioned within the building footprint and at the internal corner of the block. Between corner buildings along each street frontage are a number of rectangular shaped buildings, with voids typically located centrally and midway along the side perimeter walls. Economic and architectural demands typically resulted in a building width of approximately 15 metres. The following figure presents a typical street elevation at the corner of the Eixample district. Both the triangular building at the corner and the rectangular buildings along the street are clearly visible (Figure 5.5).



Figure 5.5: Street elevation of typical Eixample block (NIKER D3.1, 2010)

One of the most common building typologies in the Eixample is that of the present study, a six storey unreinforced masonry building positioned along the straight side of a typical block. Each rectangular building was constructed as part of the development of the entire block and immediately adjacent to the neighbouring buildings. Therefore each one must be considered part of a building aggregate rather than an isolated structure. To enable structural analysis, the plans, elevations and sections of a representative building were obtained by the Department of Construction Engineering. The selected building is located at 629 Gran Via de la Catalanes, Barcelona (Figure 5.6).



Figure 5.6: Façade of 629 Gran Via de la Catalanes

The building has a height of 21.1m and depth of 27.4m, both in accordance with the bylaws of 1891. Similarly the width of 14m is typical of the rectangular buildings of the Eixample district. The void ratio is 9.6%, which comprises one central and two side voids. This ratio is only slightly above the minimum requirement of the bylaws of 8% for a building with two façades. In some cases, the central void was slightly reduced to include an elevator. In this case, the total void ratio would approach 8%.

All walls comprise brick masonry. At ground level, the façade walls are approximately 600mm thick, whilst the load-bearing internal walls are approximately 300mm thick. Above ground level, the façade walls are approximately 300mm thick, whilst the remaining loadbearing walls are 150mm thick. Non-loadbearing 50mm thick masonry walls are positioned throughout each level to help form the rooms and passages.

A plan and 3D representation of the building are shown below (Figure 5.7, Figure 5.8). A 1:100 scale plan is presented in Appendix A for the building which clearly indicates the voids, wall layout and wall typology (Dwgs. S01, S02, Appendix A).

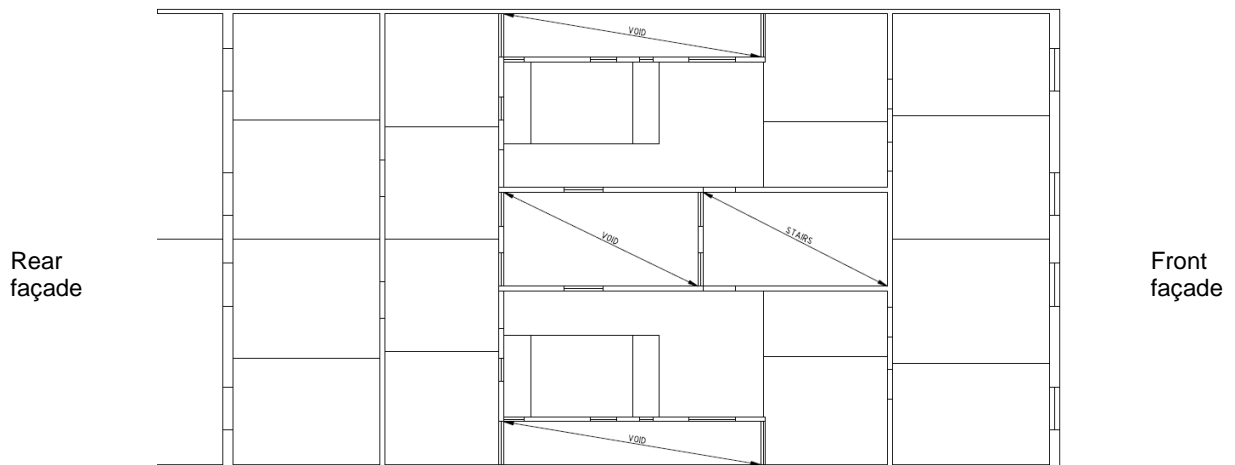


Figure 5.7: Plan of 629 Gran Via de la Catalanes (Refer Appendix A)

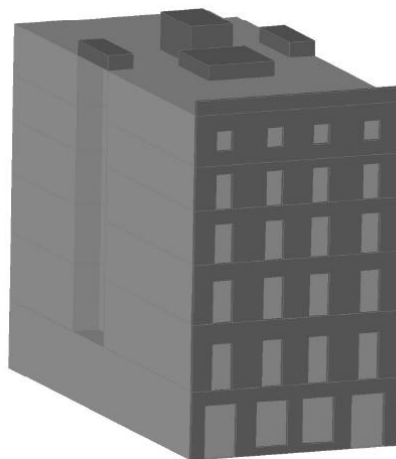


Figure 5.8: 3D representation of 629 Gran Via de la Catalanes

A particular floor structure can be observed throughout the majority of the Eixample buildings. It consists of steel floor joists spaced at approximately 450 millimetre centres, with cross-spanning masonry arches comprising a double layer of thin curved tiles. A layer of rubble and lime mortar is located atop the arches, between the beams. The floor surface is finished with a thin layer of lime-based grout and floor tiles. This typical floor system is shown below (Figure 5.9). The floor structure of the project building was also confirmed to be this system (Figure 5.10).

The floor joists are supported on the loadbearing masonry, with a typical support of about one-third the wall thickness. Joists are typically orientated perpendicular to the façades at the front and rear sections of the building, and perpendicular to the voids and stairs at the central section. The orientation determined by the spacing of the support structure. The typical floor joist orientation is represented on drawings S01 and S02 (Appendix A).

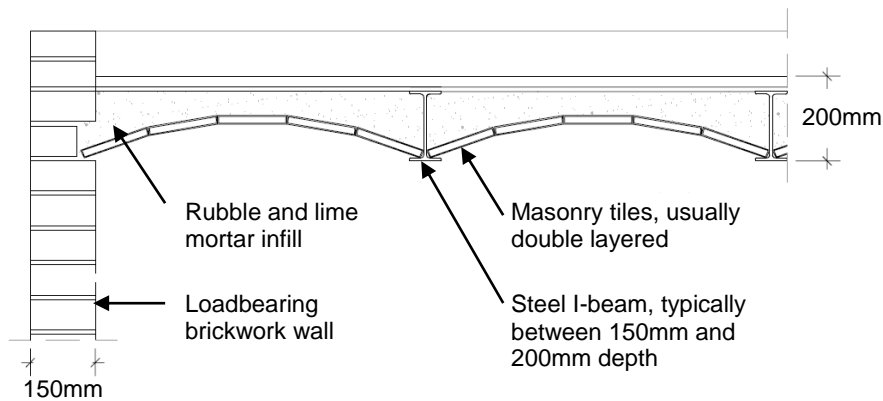


Figure 5.9: Section of typical floor system of Eixample buildings (mod. Gutierrez, 2010)

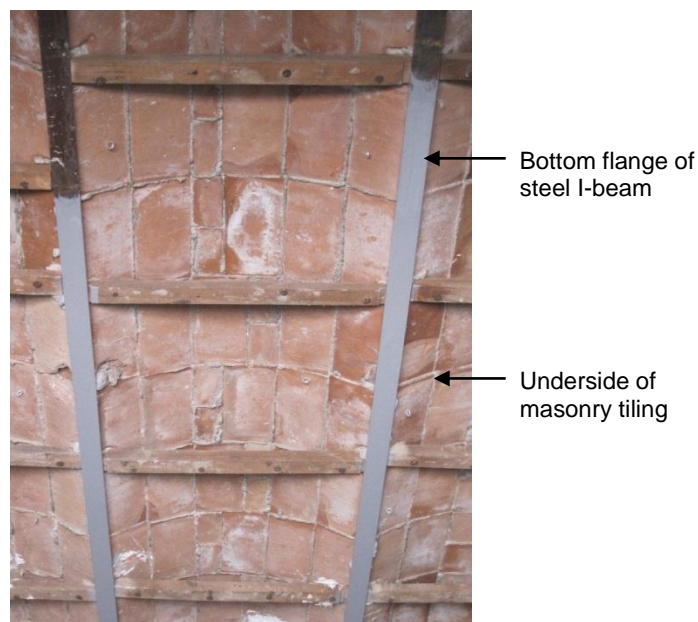


Figure 5.10: Floor system of 629 Gran Via de la Catalanes

As demonstrated above, the typical vertical load path for the structure comprises the force transfer from the steel and masonry floor system to the loadbearing masonry walls. The loadbearing walls are located at the building perimeter, at the surrounds of the voids and stairs, and at approximately 4 metre centres parallel to the façade walls (Figure 5.7). Loads are transferred to stone strip footings at ground level. Lateral forces are ultimately resisted by the in-plane bending, shear and overturning capacity of the loadbearing walls.

In some buildings, there are no internal load-bearing walls at ground floor level. Instead, a system of cast iron or steel beams and columns provides direct support to the loadbearing walls of the levels above. This support system was sometimes erected at the time of construction and sometimes formed part of interventions to the structure. Another typical intervention consists of removing 50mm thick internal non-loadbearing walls to reconfigure the internal areas.

5.4 Previous Studies

There have been a number of previous studies in the seismic analysis of existing structures in Barcelona. These studies include those originating from the RISK-UE project. The RISK-UE was developed by European Commission as part of its 'Framework Programs for Research and Development' (PCRD). The project was established in 2001 and concluded in 2004. It involved the collaboration of research centres from seven European cities, including Barcelona, to establish the likely global impact of a plausible earthquake in each city. The objective was then to advise the appropriate governmental agencies of each city of the likely risk and effects of such an event and to encourage the implementation of management and response plans to reduce this risk (Mouroux et al. 2004).

The outcomes of the RISK-UE project not only included advice for risk management, but identified distinctive features of European cities, established practical methods for seismic hazard identification, and defined specific building vulnerabilities. One outcome of particular relevance to Barcelona, was a seismic risk assessment completed as a PhD thesis at the Universitat Politècnica de Catalunya (Irizarry, 2004).

The thesis applied the framework of the RISK-UE hazard and risk assessment to Barcelona and, more particularly, to a study of the church of Santa Maria del Mar, Barcelona. The results indicate risk of significant seismic damage to a range of unreinforced buildings and monuments across the city. In particular, damage levels mid-way between moderate and substantial damage levels (to EMS-98 classification) were estimated for Santa Maria del Mar and four other churches in the city. Moderate damage levels were estimated for a number of larger unreinforced buildings including the Palau de la Musica Catalana.

The approach defined by RISK-UE, and the seismic hazard identified by Irizarry (2004) have since been applied by researchers at the Universitat Politècnica de Catalunya to complete more general seismic risk assessments of the buildings of Barcelona. The work has developed capacity spectra for both reinforced concrete and unreinforced masonry structures typical of Barcelona. For masonry structures, the analysis utilised a 3D non-linear software program based upon macroelements, considering the major in-plane failure modes of masonry panels (Pujades et al. 2010). To complement this work, the research has included detailed geographic information system (GIS) data for the city to extrapolate the probability of damage to a specific building typology to a vulnerability assessment of the urban centre of Barcelona (Barbat et al. 2008).

The results of these studies indicate that the unreinforced masonry buildings of the Eixample district are susceptible to significant damage during a seismic event. They indicate greater damage from probability scenarios than from deterministic scenarios. The studies have also modelled the typical building in both the longitudinal and transverse directions and as part of a building aggregate. From a review of the results, they have found that the critical motion is that in a longitudinal direction for an isolated structure (Pujades et al. 2010).

The previous assessments provide a general framework for the current study. The seismic hazard assessment of this study has been developed in accordance with the recommendations of RISK-UE and utilises the data developed by Irizarry (2004). The work of Pujades (2010), Barbat (2008) and others at the Universitat Politècnica de Catalunya has provided a solid background on the building typologies of Barcelona, guidance for the damage probability assessment, and a means to compare the results of their analysis.

The current study uses a different analysis tool to that of the previous studies, a 3D finite element analysis. This approach considers the global response of the structure, utilising appropriate non-linear material characteristics and behavioural models. The results will help to develop a clearer understanding of the risk of damage to the unreinforced masonry buildings of the Eixample district and to identify critical elements of the structure to maintain and monitor, to limit such damage.

5.5 Damage Survey and Identification of Actions

5.5.1 Damage

The present study is considering the seismic assessment of a typical building of the Eixample district. As such, it is more suitable to consider the range of possible damages for this building typology and to assess whether these are incorporated into the analysis, rather than undertake a specific damage survey for the representative building.

Unreinforced masonry buildings are by their nature susceptible to cracking or crushing due to excessive stress levels in the masonry. The cause of these stresses may be indirect mechanical actions such as differential settlements, seismic actions, brick expansion and thermal movements, or direct mechanical actions including excessive loading. The effect of masonry cracking can be to limit the in-plane shear resistance of the wall and if out-of-plane deformations occur, the wall may be susceptible to local buckling under high vertical compressive loading. Masonry crushing, often isolated at concentrated actions, can limit the local support capacity of the wall.

For the buildings of the Eixample district, the walls are generally of consistent material composition and regularly proportioned, hence the walls are less susceptible to local stresses from differential movements which can encourage crack development. In addition, the form and mass of the typical floor system limits lateral wall deformations and the development of tensile stresses. The most susceptible elements to cracking are the spandrels above door and window openings. Such cracking is common and is often due to differential movement of the continuous walls at each side of the spandrel. Therefore, for the present study a conservative approach has been to neglect the contribution of the spandrels to the global seismic resistance of the building.

Damage due to physical actions such as fire, water and interventions, and chemical actions such as salt decay will be specific to a building and its effect is likely to be localised. For Barcelona, general

physical actions such as freeze-thaw are not present. As such, these are not considered in the current analysis.

5.5.2 Loading

The static loading for the building has been determined taking into account the typical floor and wall composition, and use of the buildings. The dead and live loads used for the analysis, and the loading factors for gravity and earthquake load cases are presented below (Table 5.1 and Table 5.2). They are based upon the current loading provisions of the European and Spanish codes (EC 1990:2002; CTE-DB-SE-AE, 2007).

Table 5.1: Dead and live loads

Building element	Dead Load (kPa)	Superimposed Dead Load (kPa)	Live Load (kPa)
Floors	2.5 (Joists, masonry arches and rubble fill)	1.16 (Lime grout and tiling, ceiling and fittings)	2 (Residential or light commercial)
Roof	2.5 (Joists, masonry arches and rubble fill)	3.16 (Additional level of joists, masonry arches and rubble fill, roof tiling, ceiling and fittings)	1 -
Solid walls	Thickness x density (Refer Section 7.3 'Material Characteristics')	-	-
50mm thick walls	0.80 (Hollow masonry plus plaster surfacing)	-	-

Table 5.2: Load combination factors (EC 1990:2002)

Load Combination	Dead Load Factor	Live Load Factor
Gravity	1.1	1.5
Earthquake	1	0.3

5.6 Monitoring

Static monitoring of a specific structure is not required as part of the present study, as the focus is on the seismic response of a specific building typology. Should the seismic analysis of a particular structure be required, then static monitoring should be performed at observed damages such as wall cracking, for a sufficient period of time to gauge whether the movements are continuing and to determine any seasonal influences.

Dynamic monitoring however would be of direct benefit to the current study, as it could provide a clear indication of both the frequencies and the shapes of the modes of vibration. These could then be correlated with the mathematical model of the structure. A system of dynamic monitoring within a number of adjacent buildings could also help to assess to what extent they perform as a building aggregate or as individual structures. The results of this assessment could also then be incorporated into the mathematical modelling.

A further use for dynamic modelling for the representative study could be to determine the structural impact of varying levels of damage within a structure. For instance, if the vibrational response of a wall section at each side of cracking is different, it would suggest that the wall will perform as a series of isolated sections during a seismic action rather than as an integrated unit. Such tests could be carried out on a number of representative buildings so that a clear understanding of the effect on the seismic response could be determined and hence applied to future seismic analyses based solely upon observed damage.

At this time, there are no available records of studies in the static or dynamic monitoring of the unreinforced masonry buildings of the Eixample district.

The dynamic monitoring of such structures would in particular be of great benefit to the understanding of the interactions of the adjacent buildings and the impact of observed damages.

6. SEISMIC HAZARD ASSESSMENT – CASE STUDY

This chapter details the application of the seismic hazard assessment presented in Section 3 to Barcelona. Initially, regional and site geology is defined. The results of geological testing are presented and are classified in terms of current code recommendations. The influence of each soil type is then discussed for the codes and for the deterministic and probabilistic approaches.

Described in the second section are the procedures and parameters used to develop smoothed acceleration response spectra for the deterministic and probabilistic approaches.

In the following sections, the application of the deterministic, probabilistic and code-based approaches is separately detailed and the response spectra developed are presented. The smoothed response and demand spectra for each approach are also presented at the end of each section. Comparisons are also made between the spectra derived from each approach.

6.1 Introduction

A detailed seismic hazard assessment is an integral part of any seismic analysis. The seismic actions defined can be used in conjunction with a variety of analysis approaches including strength (capacity) based and performance based methods. In this way the seismic hazard assessment can be used to determine a nominated capacity, or a displacement demand for any given structure.

As discussed in Section 3, the RISK-UE project (2004) has developed a methodology for seismic hazard assessment, specifically designed for European cities. This methodology includes three approaches to determine the likely seismic actions; the deterministic approach, based upon the most significant past seismic events; the probabilistic approach, based upon regional seismicity for a probability of occurrence of 10% in 50 years; and the use of current code recommendations. For each approach, the local site geology and expected type of earthquake have a significant bearing on the results.

The following sections define the local soil geology and its impact on the ground acceleration. The methodology for developing smoothed response spectra is then described. Each approach is then detailed, together with the results of the seismic hazard assessment.

6.2 Site Geology

Barcelona is situated within a region at the north-east of the Iberian Peninsula in a region bounded to the north and north-west by the Pyrenees and to the east by the Balearic / Mediterranean Sea. More locally, the city is located within the Catalan Coastal Range and is bounded to the north by the Besos Delta, to the south by the Llobregat Delta and to the west by the Collserola Serra (Figure 6.1).

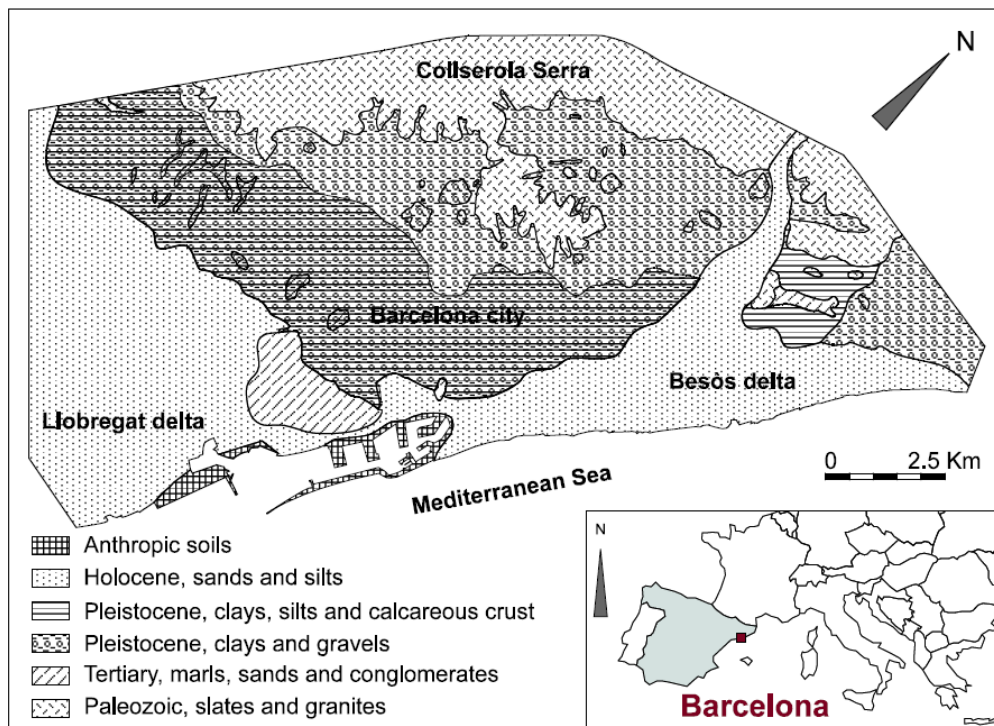


Figure 6.1: Geological map of Barcelona region (Irizarry, 2004)

As shown above, the delta regions to the north and the south of the city comprise Holocene soils, predominantly of sands and silts. In contrast, the majority of the city comprises Pleistocene soils of clays and gravels, whilst a limited region of the city, and the area to the west of Barcelona, have a Paleozoic profile of rock subsoils.

As discussed in Section 3.2, the subsoil conditions have a significant impact on the ground surface response to a seismic event. As such, subsoil classifications dependent on soil stiffness have been defined to enable modification of the acceleration response spectrum for varying subsoil conditions. For Barcelona, the soil profiles demonstrated in Figure 6.1 have been related to the standard soil classifications utilising the shear wave velocities. A map of five subsoil zones derived by Cid et al. (2001), together with the districts of Barcelona is provided below (Figure 6.2).

The average measured shear wave velocities (V_s) for each zone in Figure 6.2 and the equivalent soil classification to Eurocode 8 and NCSE-02 are presented in Table 6.1. As can be seen, the Eixample district is predominantly located within Zone II, which correlates to a Eurocode 8 classification of Class B and an NCSE-02 classification Type III.

The current study considers the seismic analysis of a typical building of the Eixample district, not a specific site where testing could be made. As such, it is prudent to consider the worst likely soil conditions within the district for the analysis. For the Eixample district, the worst likely conditions are Zone I soils which correlate to Eurocode 8 Class C and NCSE-02 classification Type IV. Such sections of the Eixample may include those adjacent to the Sant Marti district, the Raval area to the south-west of the Ciutat Vella, or in areas where significant fill was introduced in the development.

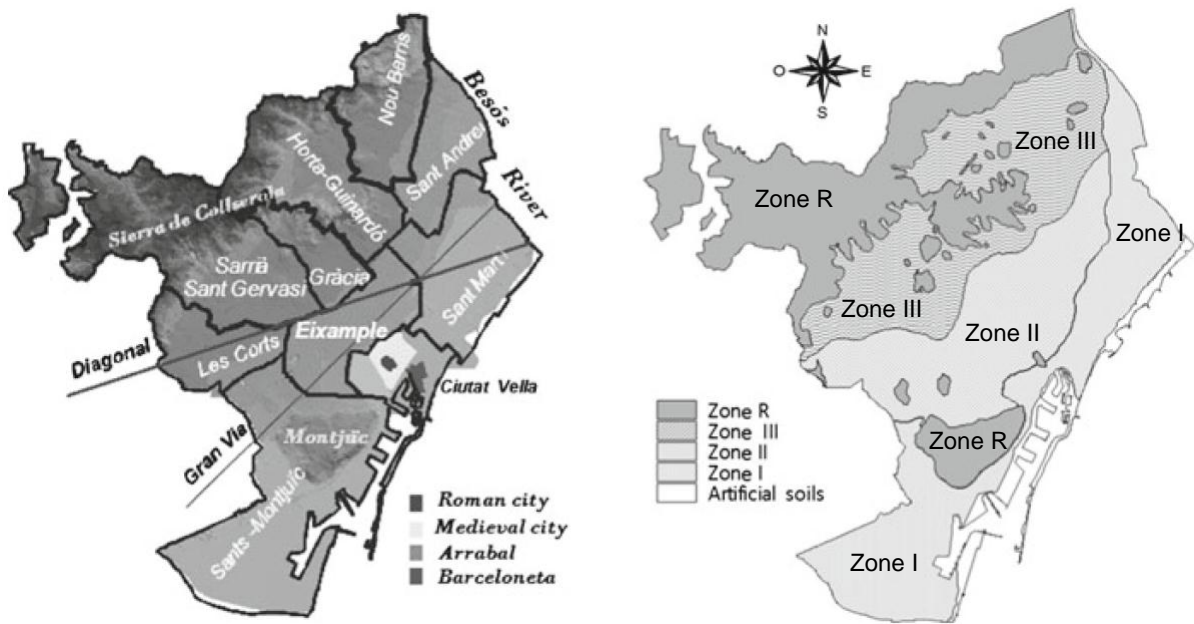


Figure 6.2: Barcelona districts and soil zonation determined by Cid et al. (2001), (Pujades et al., 2010)

Table 6.1: Comparison of measured subsoil characteristics to soil classifications

Soil Zone Cid et al. (2001)	Measured average V_s (m/s)	Eurocode 8 classification	NCSE-02 classification	Description
Zone R	800	Class A	Type I	Rock
Zone III	405	Class B	Type II	Very stiff soils of 10-15m depth underlain by rock.
Zone II	394	Class B	Type III	Very stiff soils underlain by rock at significant depth
Zone I	225	Class C	Type IV	Soft to medium stiffness soils underlain by rock at significant depth

As discussed in Sections 3.3 and 3.4, the Ambraseys et al. relationship can be used to develop approximate response spectra for both the deterministic and probabilistic approaches. The relationship includes factors that are dependent on local soil conditions, however these factors may only be used to establish the general form of the response curve, while the final spectra must be calibrated to the actual geological environment.

For Barcelona, calibration was achieved by Irizarry (2004), by initially calculating a set of transfer functions which describe the relationships between the expected seismic responses of the local rock to that of the soils of Zone I, II and III.

As described by Irizarry (2004), the mean of five actual worldwide response spectra was then obtained that best approximated the Ambraseys derived deterministic and probabilistic response spectra for rock. This was combined with the transfer functions to develop expected spectra for each local soil zone which were compared to the target spectrum for a local rock site. Spectral amplification factors for each zone were then developed by adjusting for the rock found in Barcelona. The amplification factors obtained for Barcelona for a range of structural periods are presented below (Figure 6.3).

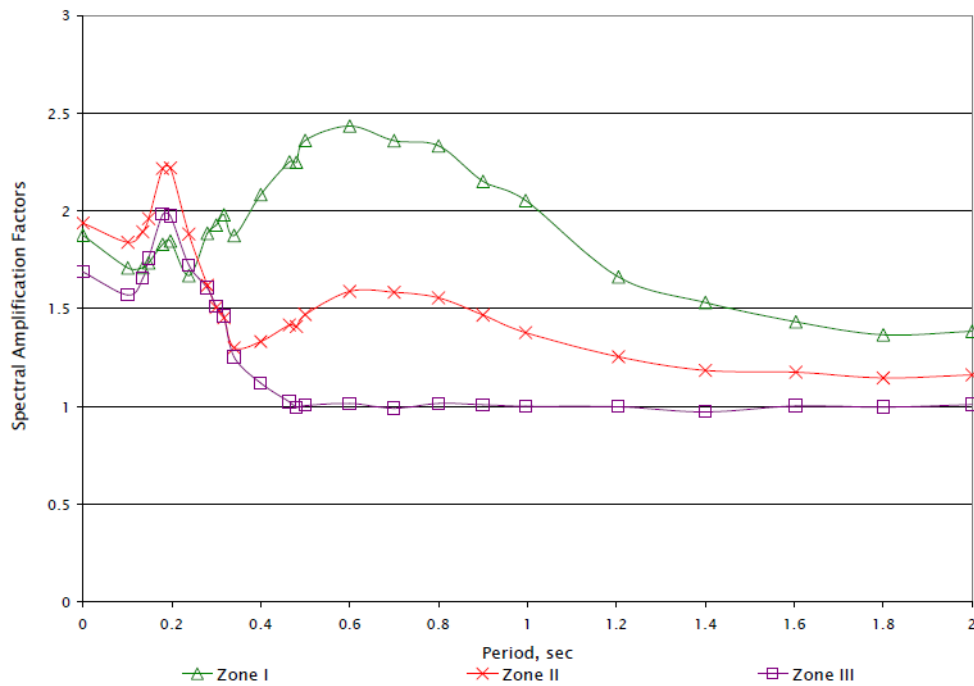


Figure 6.3: Soil amplification factors for Barcelona for Ambraseys relationship (Irizarry, 2004)

6.3 Smoothed Acceleration Response Spectra

As stated in Section 3.1, smoothed acceleration response spectra are required to support the comparison of the spectra to results of structural analysis and to define differences in spectra developed by various approaches. The typical form and parameters of a smoothed acceleration response spectrum are presented in Figure 3.2.

For this project, three approaches have been selected to develop acceleration spectra:

- Deterministic Approach.
- Probabilistic Approach.
- Code formulations (Eurocode 8 and NCSE-02).

The code formulations by their nature construct smoothed response spectra suitable for structural analysis and comparison. However, the deterministic and probabilistic approaches develop response spectra that are significantly more uneven and are more representative of spectra developed directly from records of seismic events. As such, to support structural analysis and comparison to code results, smoothed spectra must be defined.

The simplest method to develop a smoothed response spectrum is to define parametric functions for each segment of the spectra and to iteratively adjust the functions to most closely fit the shape of the initial response spectrum. A quantitative comparison can be made between the original and smoothed spectra by the root mean square of the acceleration values and by the total error percentage.

A number of sets of parametric functions have been developed to describe smoothed response spectra. In previous studies for Barcelona, two such sets of functions were used to develop smoothed response spectra, those from Eurocode 8 (2004) and those developed by Lagomarsino et al. (2002) (Irizarry, 2004). A comparison was made by Irizarry (2004) between the original and smoothed spectra for both the deterministic and the probabilistic approaches, and for all four subsoil classes. Following this comparison, it was found that the functions proposed by Lagomarsino et al. (2002), best approximate the initial spectra for both the deterministic and probabilistic approaches.

The modified parametric functions for each segment of the response spectrum can therefore be described as follows (Irizarry, 2004). Figure 6.4 provides a diagrammatic representation of these functions for the smoothed response spectrum.

$$0 \leq T \leq T_B \quad S_A(T) = PGA \cdot \left[1 + T/T_B (B_C - 1) \right] \quad (\text{Eqn. 6.1})$$

$$T_B \leq T \leq T_C \quad S_A(T) = PGA \cdot B_C \quad (\text{Eqn. 6.2})$$

$$T_C \leq T \leq T_D \quad S_A(T) = PGA \cdot \left[T_C/T \right]^d \cdot B_C \quad (\text{Eqn. 6.3})$$

$$T \geq T_D \quad S_A(T) = PGA \cdot \left[T_D/T \right]^2 \cdot B_D \quad (\text{Eqn. 6.4})$$

$$B_C = S_{A,max}/PGA; B_D = S_A(T_D)/PGA \quad (\text{Eqns. 6.5; 6.6})$$

$$d = - \frac{\log\left(\frac{B_D}{B_C}\right)}{\log\left(\frac{T_D}{T_C}\right)} \quad (\text{Eqn. 6.7})$$

Where:

- S_A : Spectral acceleration.
- T : Vibration period of a linear single degree of freedom system.
- PGA: Peak ground acceleration.
- T_B , T_C , T_D : Definition of ranges of the structural period to define the start values for the constant acceleration response (T_B), constant velocity response (T_C), and for constant displacement response (T_D).

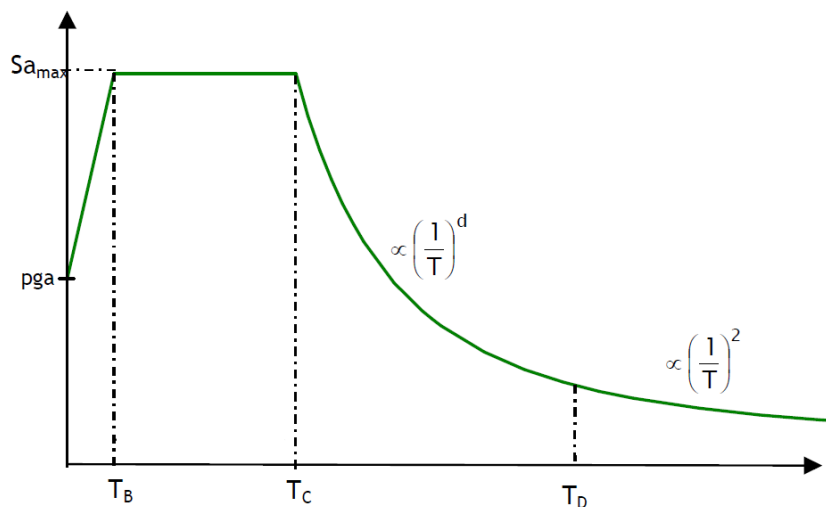


Figure 6.4: Diagrammatic smoothed response spectrum – functions after Lagomarsino (2002) (Irizarry, 2004)

The values of the abovementioned parameters are provided below for both the deterministic and probabilistic approaches for the four soil zones characterised by Cid et al. (2001) (Table 6.2).

Table 6.2: Values of parameters – functions developed by Lagomarsino (2002) (Irizarry, 2004)

	Deterministic				Probabilistic			
	Zone I	Zone II	Zone III	Rock	Zone I	Zone II	Zone III	Rock
PGA (cm/s²)	133.3	137.7	120.0	71.1	183.9	183.9	165.5	98.1
T_B (sec)	0.10	0.10	0.10	0.10	0.10	0.10	0.10	0.10
T_C (sec)	0.39	0.22	0.22	0.23	0.40	0.40	0.19	0.25
T_D (sec)	2.30	2.20	2.00	1.75	2.85	0.14	1.77	0.34
B_C	1.91	2.45	2.29	2.26	2.00	2.85	2.57	1.75
B_D	0.09	0.09	0.10	0.23	0.14	1.34	0.20	0.98
d	1.70	1.43	1.40	1.12	1.34	2.00	1.12	2.29

6.4 Deterministic Approach

As stated in Section 3.3, the deterministic approach involves the development of a hazard assessment from past earthquake events that have had the most pronounced effect at the subject site. For Barcelona, in previous studies two such events have been selected to more accurately assess the hazard for both short-period and longer-period ranges. The two seismic events are as follows, each event caused observed damage to structures in Barcelona (Irizarry et al., 2011), (Figure 6.5):

- An earthquake that occurred in 1448 in the Cardedeu region, with an epicentral distance of about 15km from the city. The earthquake had an approximate epicentral intensity of VIII (MSK), and a focal depth of about 7km.
- An earthquake in 1428, in the Eastern Pyrenees, with an epicentral distance to Barcelona of about 90km. The epicentral earthquake intensity was approximately IX (MSK), and the focal depth about 10km.

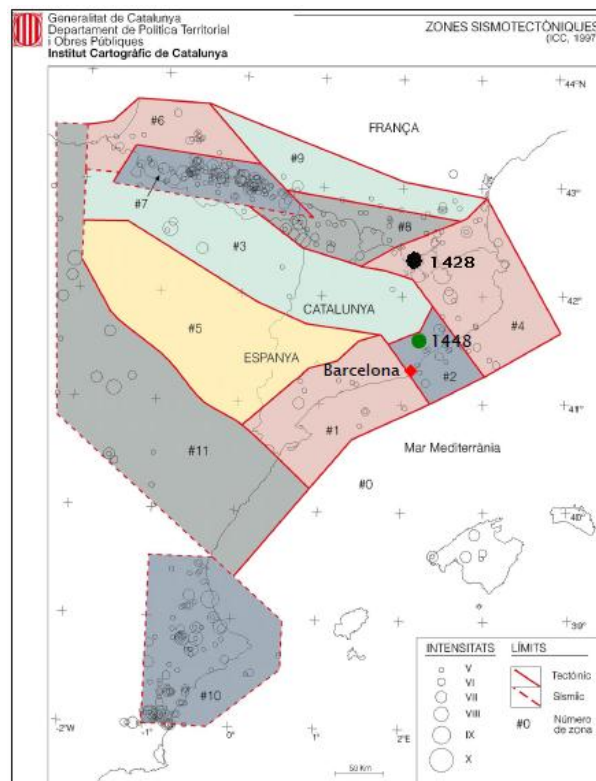


Figure 6.5: Location of reference earthquakes (Irizarry et al., 2004)

As recommended within the Risk-UE project (2004), a deterministic approach without zones was used, whereby locations of past earthquake events are analysed from their true epicentral locations and are not shifted within a 'source zone' to heighten the effect at the subject site (Faccioli, 2006).

An approximate surface wave magnitude (M_S) for each earthquake event was then developed by initially using the correlation relationship for macroscopic intensity developed by Gonzalez (2000)

(Figure 3.4), then the magnitude scale developed by Dufumier (2002) (Eqn.3.1). The developed M_s values are presented below (Table 6.3).

Table 6.3: Surface wave magnitude of reference earthquakes

Reference Earthquake	Intensity (MSK)	Local Magnitude (M_L)	Surface wave magnitude (M_s)
Cardedeu (1448)	VIII	5.4	5.1
Eastern Pyrenees (1428)	IX	6.2	6.5

A deterministic acceleration response spectrum was then developed using the Ambraseys et al. (1996) attenuation relationship, and adjusted for local soil conditions (Irizarry, 2004). Figure 6.6 presents the 5% damped elastic acceleration response spectra for a 475 year return period obtained for each soil zone of Barcelona, as characterised by Cid et al. (2001). Appropriate spectra for the analysis of the Eixample district are that of Zone I and Zone II.

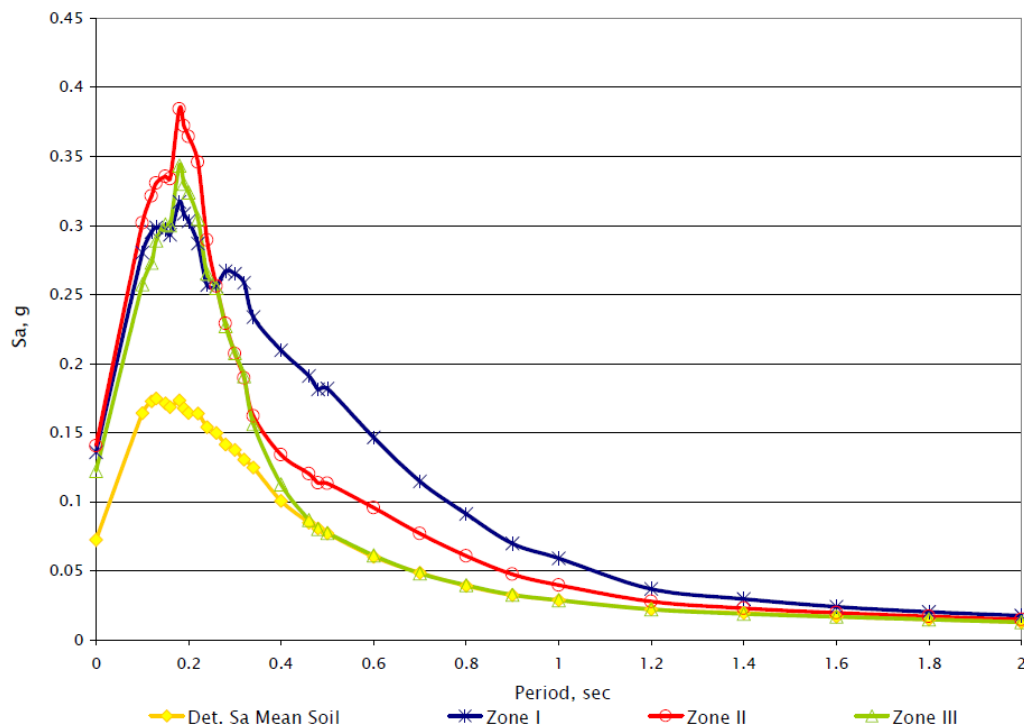


Figure 6.6: Deterministic acceleration response spectra for Barcelona – Ambraseys relationship (Irizarry, 2004)

As discussed in Section 6.3, following the development of the response spectra, it is necessary to obtain smoothed response spectra to support structural analysis and for the comparison of spectra obtained by different approaches. The smoothed response spectra for Barcelona are presented in Figure 6.7 using the functions of Lagomarsino (2002) and the parameters derived by Irizarry (2004), listed in Section 6.3. Demand spectra were also developed using equation 4.1 (Figure 6.8).

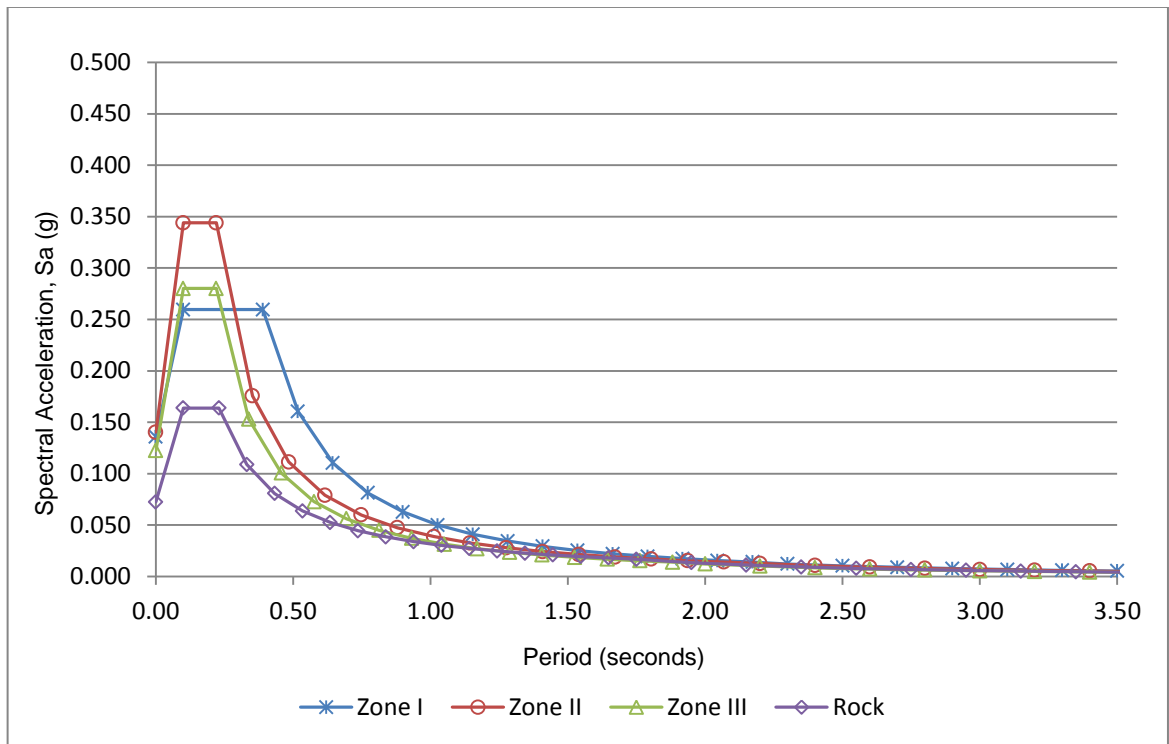


Figure 6.7: Deterministic smoothed acceleration response spectra for Barcelona

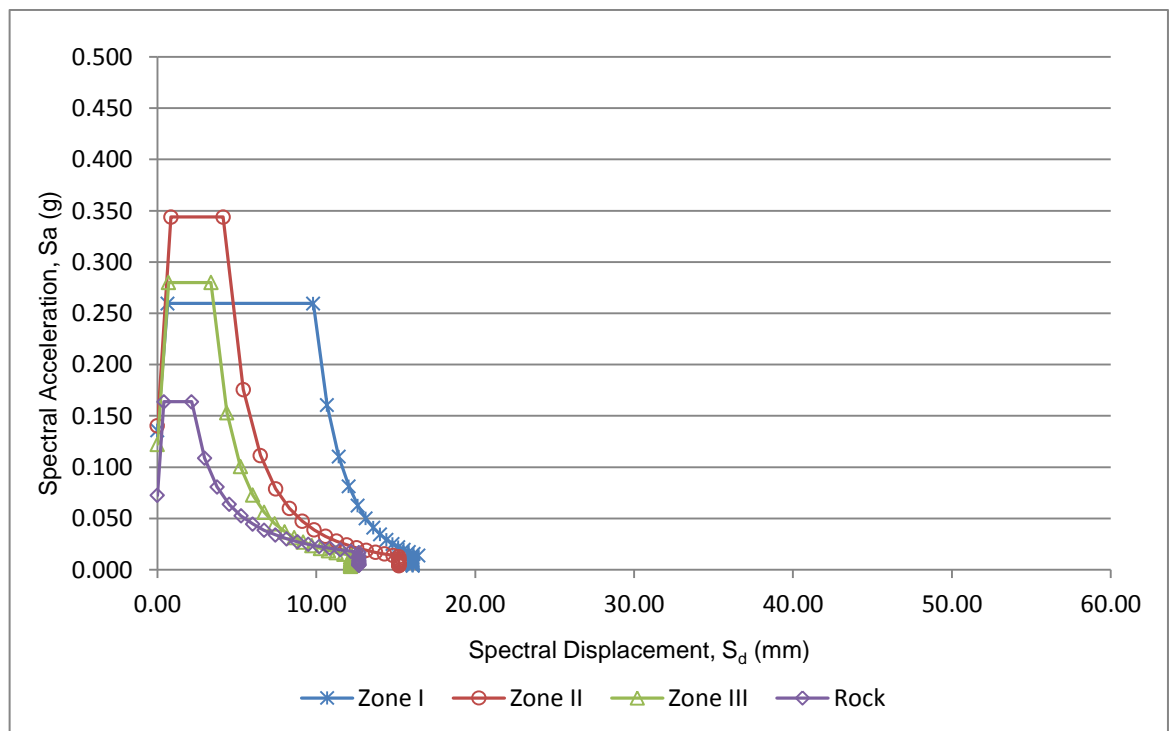


Figure 6.8: Deterministic ADRS demand spectra for Barcelona

6.5 Probabilistic Approach

As discussed in Section 3.4, the probabilistic approach develops a hazard assessment utilising the full range of possible seismic actions that could affect the subject site.

For Catalonia, the location of active faults is unknown. As such, the seismotectonic zonation was based upon the measured seismicity and tectonics of the region, combined with the heterogeneous nature of the continental crust in the north-east Iberian Peninsula (Irizarry et al., 2011). The resultant zonation, consisting of eleven source zones, is presented in Figure 6.9.

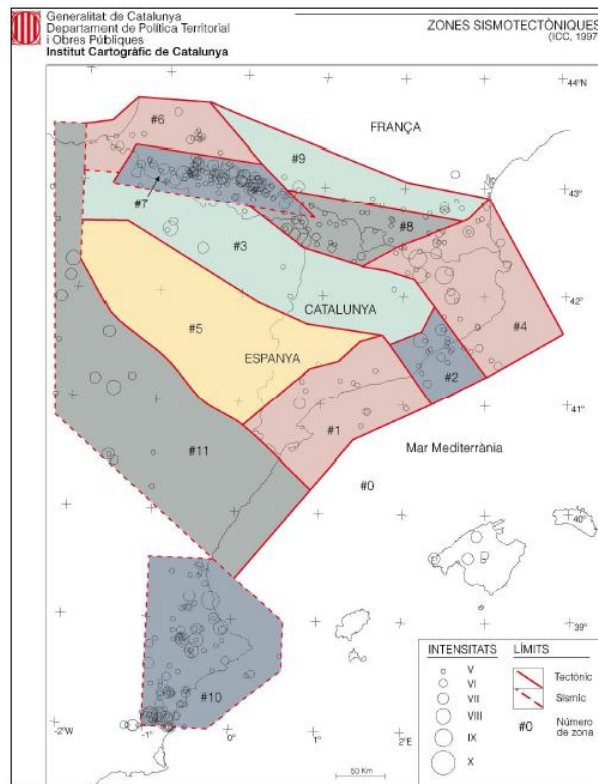


Figure 6.9: Seismotectonic zonation for Catalonia region (Irizarry, 2004)

Of the eleven source zones, it was found by Irizarry (2004) that only five impact the seismic vulnerability of Barcelona, zones 2, 4, 7, 8 and 10. Barcelona is located with source zone 2 and as such the seismicity of this zone has the greatest influence on the hazard assessment for the city, particularly for periods lower than one second. For greater periods, the higher levels of seismicity of the other source zones also influence the hazard assessment.

The CRISES-99 computer code together with the Ambraseys attenuation relationship were used by Irizarry (2004) to develop the probabilistic model for a rate of exceedance of 10% in 50 years, a return period of 475 years.

Given the relatively small size of Barcelona, it was found that the level of hazard does not vary appreciably across the city. As such, a single acceleration response spectrum could be developed.

The 5% damped elastic acceleration response spectra for Barcelona are presented below for each site subsoil zone as characterised by Cid et al. (2001) (Figure 6.10). Appropriate spectra for the analysis of the Eixample district are that of Zone I and Zone II.

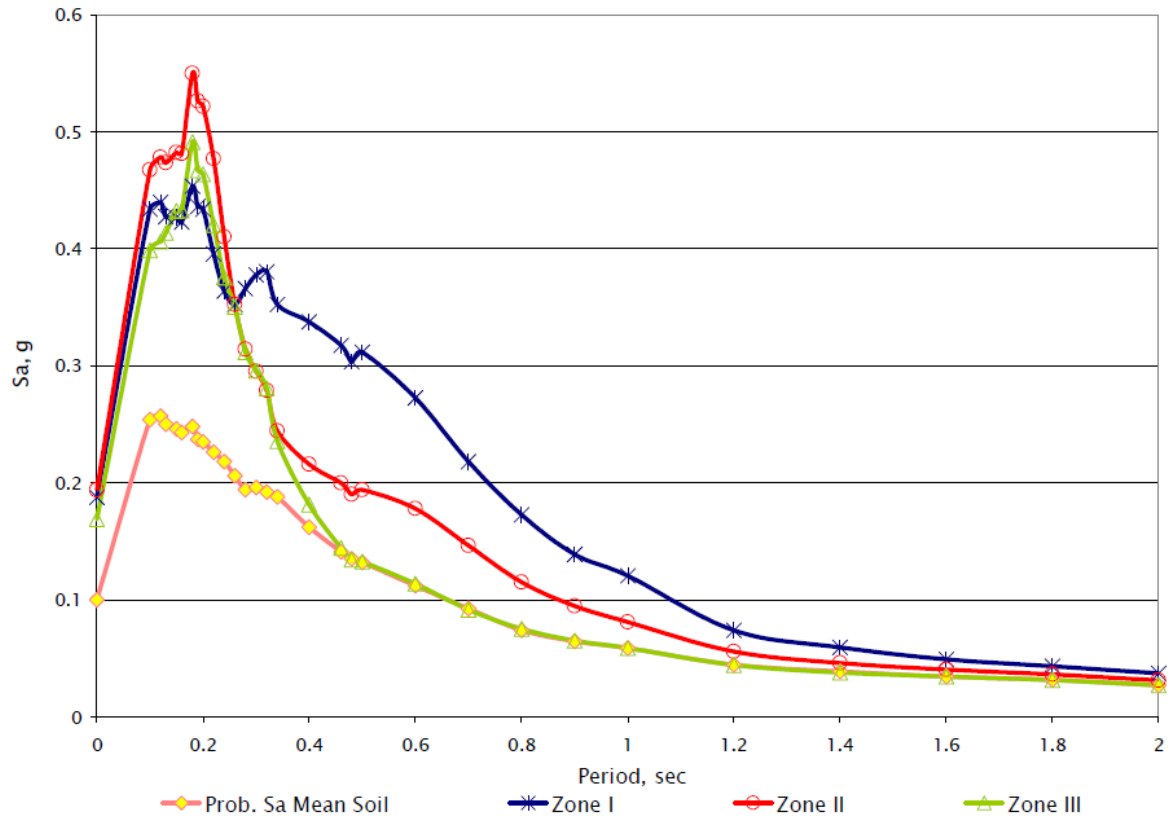


Figure 6.10: Probabilistic acceleration response spectra for each Barcelona soil zone (Irizarry, 2004)

The resultant smoothed acceleration response spectra are presented in Figure 6.11, using the functions by Lagomarsino (2002) and the parameters developed by Irizarry (2004). The demand spectra in ADRS format were also derived using equation 4.1, these are also provided below (Figure 6.12).

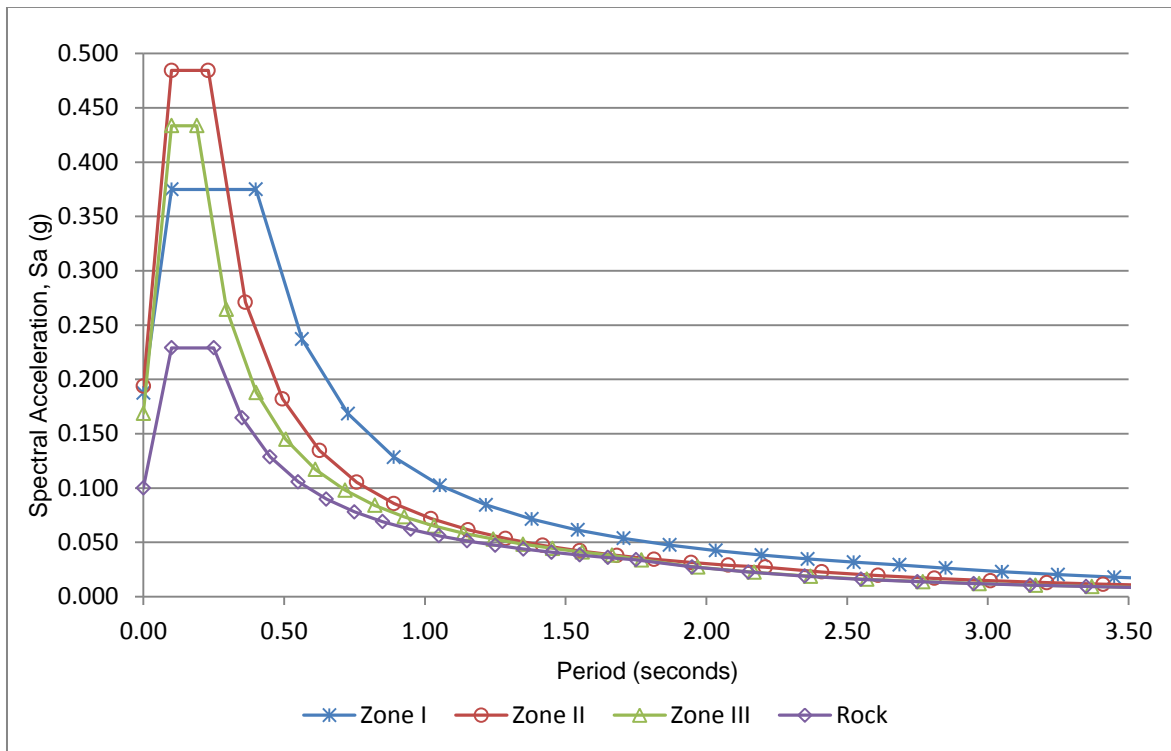


Figure 6.11: Probabilistic smoothed acceleration response spectra for Barcelona

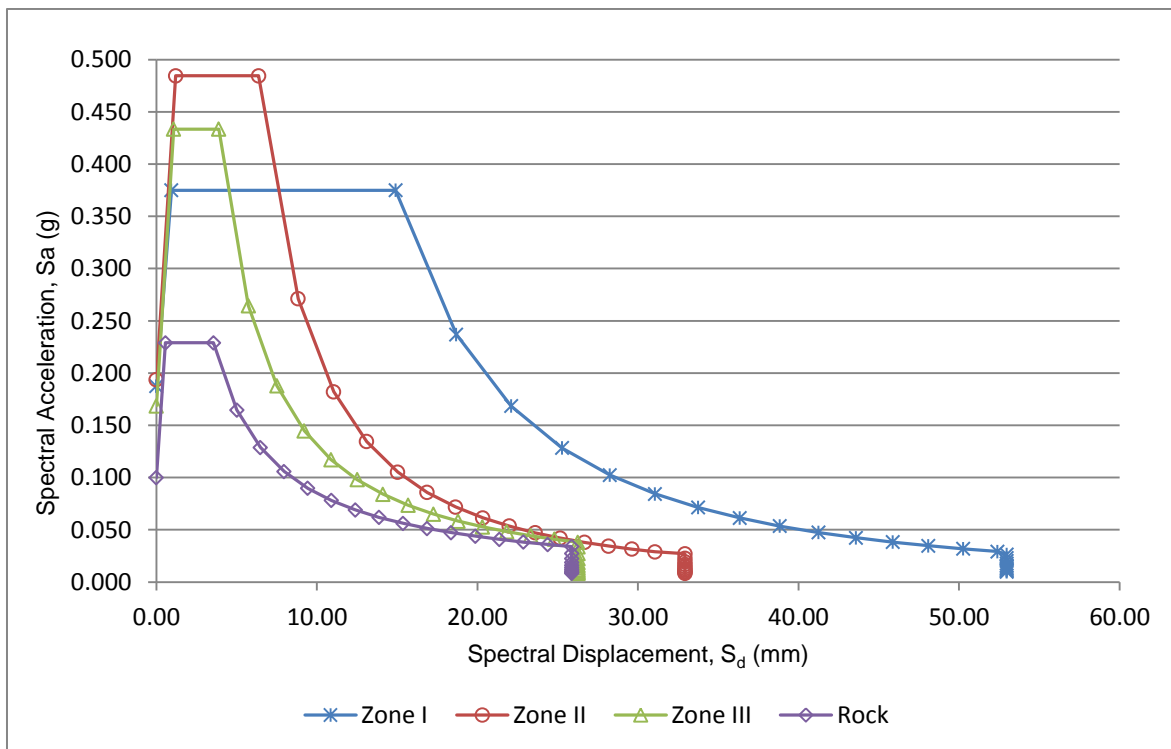


Figure 6.12: Probabilistic ADRS demand spectra for Barcelona

6.6 Code Recommendations

6.6.1 Eurocode 8

As discussed in Section 3.5.1, Eurocode 8 develops elastic response spectra based upon a set of parametric functions that are dependent on the level of damping, the reference ground acceleration and the local soil conditions. Values for the parameters are provided in the code for five soil classifications and for two types of spectra.

The initial task is to determine the most appropriate spectra type for Barcelona. To do so, Irizarry (2004) compared the normalised spectra for each spectra type for a rock soil classification to the normalised mean probabilistic response spectra for rock (Figure 6.13). This comparison clearly demonstrates that the Type II spectra more closely match the local seismicity of Barcelona. This is to be expected, as Eurocode 8 recommends the Type II spectra for sites where the majority of expected surface wave magnitudes (M_S) are less than 5.5, such as Barcelona.

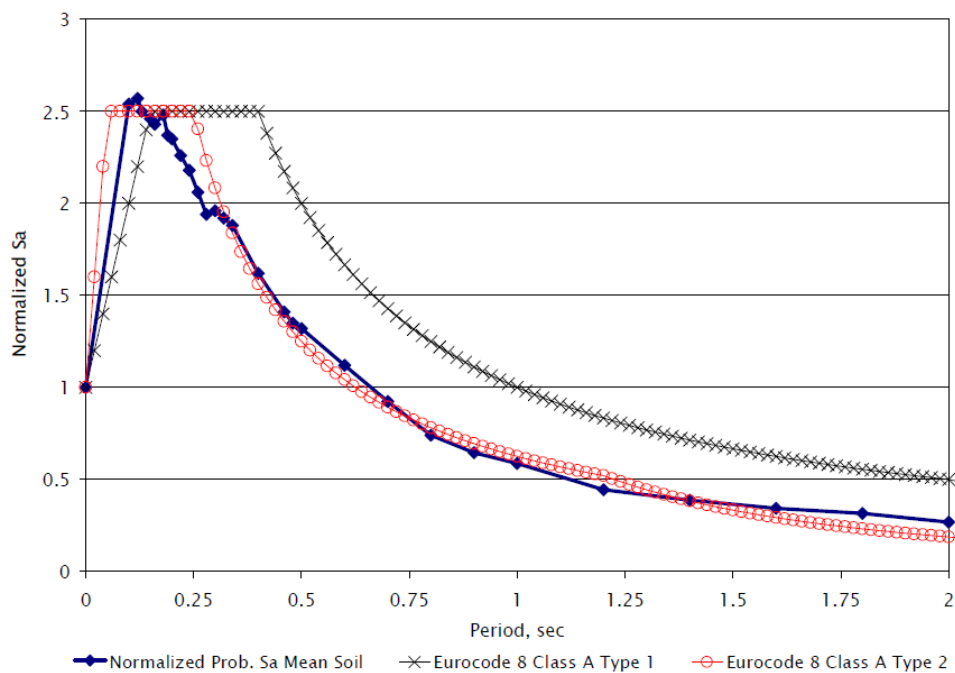


Figure 6.13: Comparison of probabilistic response spectra to Eurocode 8 Type I and Type II spectra for rock (Irizarry, 2004)

To develop response spectra for Barcelona, a comparison must be made between the soil classifications of Eurocode 8 and the soil zones defined for the city. This comparison is presented in Section 6.2, Table 6.1 which demonstrates that Eurocode 8 soil classification B is appropriate for much of the Eixample district. A comparison between the normalised Type II elastic spectrum for soil class B and the normalised probabilistic response spectra obtained for soils in Zone II and Zone III as characterised by Cid et al. (2001) is shown in Figure 6.14.

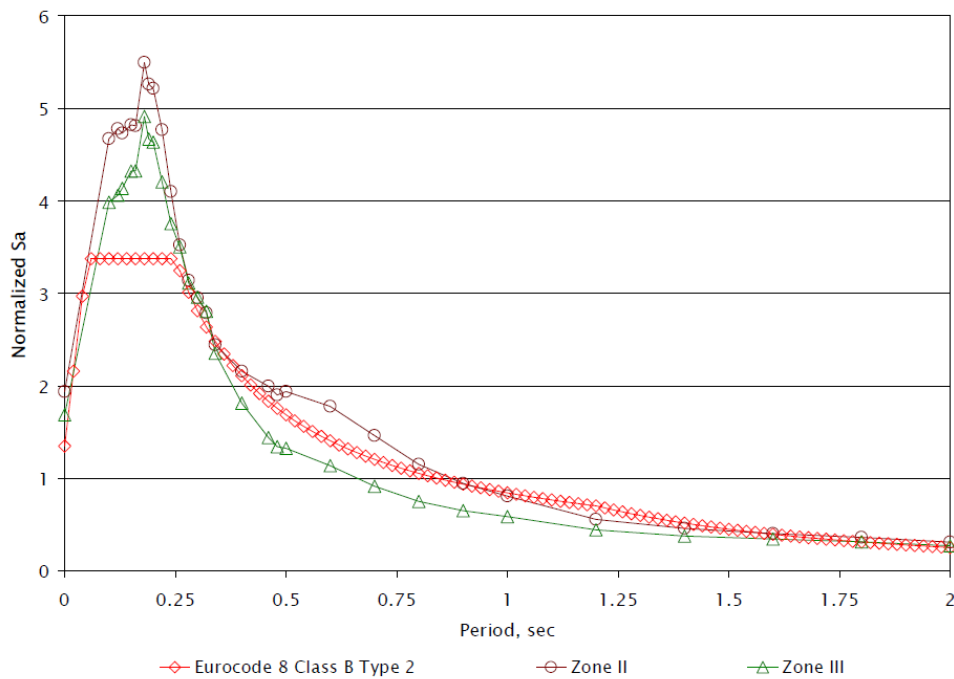


Figure 6.14: Comparison of probabilistic response spectra for Zones II and III to Eurocode 8 spectrum Type II, soil class B (Irizarry, 2004)

The above comparison shows that in general the Eurocode formulation is very similar to that of the probabilistic approach. In the region of constant acceleration, the accelerations predicted by the probabilistic approach are significantly greater than that of the Eurocode spectrum. If, as suggested by Irizarry (2004), in the shorter period range of the probabilistic spectrum the spectral acceleration is reduced by $2/3$, then the results are far more similar.

Hence, it can be seen that the Eurocode 8 formulations provide spectra that are suitable for the type of seismic actions expected in Barcelona and which are comparable to those of the probabilistic approach.

6.6.2 NCSE-02

As described in Section 3.5.2, the NCSE-02 code provides parametric functions to describe the form of an elastic acceleration response spectrum. The parameters are dependent on local soil conditions, the importance level of the structure, the base acceleration of the site, the expected type of earthquake and the local terrain.

For the buildings of the Eixample district of Barcelona, the importance level can be considered to be for structures of heritage significance and hence the value of ρ is 1.3. The base acceleration and the coefficient to describe the type of expected earthquake are provided in Annex 1 of the code, with values for Barcelona of $a_g=0.04$ and $K=1.0$. The NCSE-02 subsoil classifications appropriate to the Eixample district are Type III and Type IV (Table 6.1). Values for the soil classification factor, C , are provided in the code for each soil type.

The horizontal acceleration response spectra for each of Barcelona's soil types using the formulations and parameters of NCSE-02 are presented below (Figure 6.15).

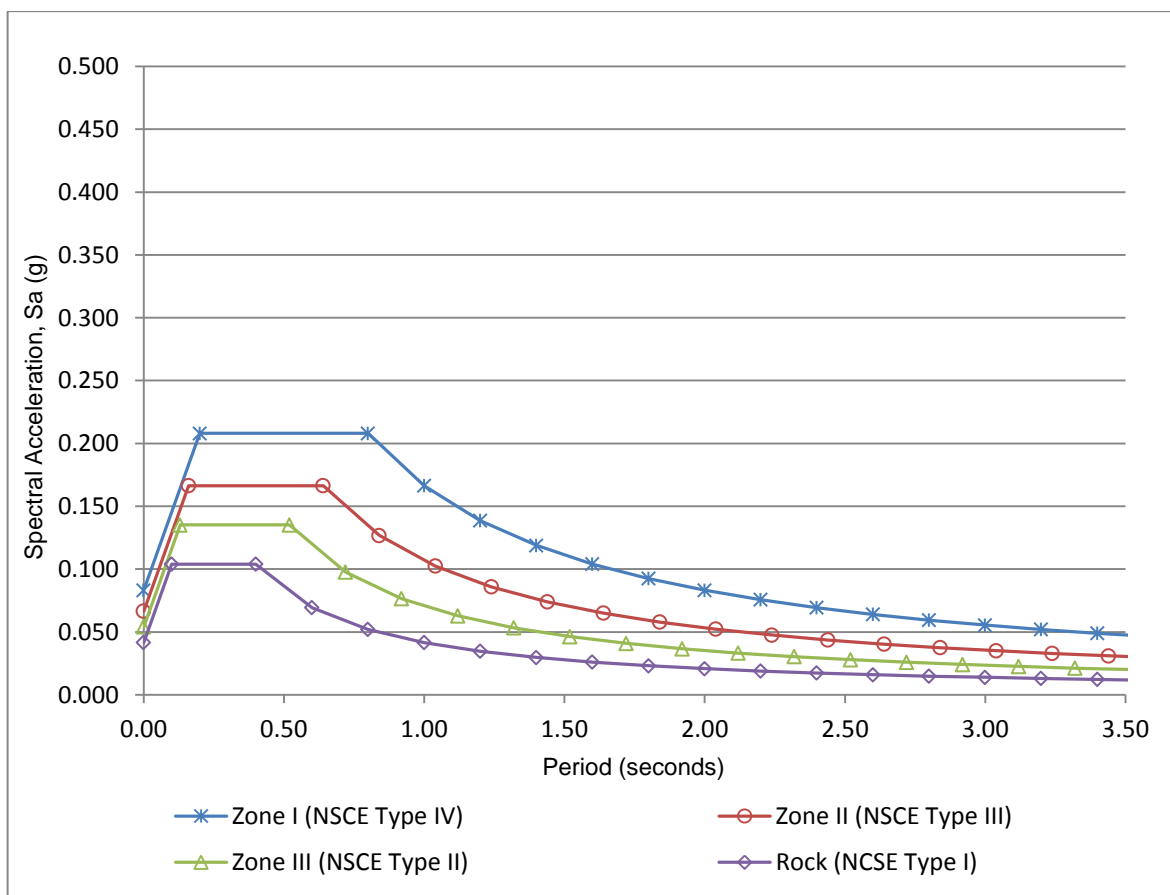


Figure 6.15: Elastic acceleration response spectra for Barcelona soil zones, to NCSE-02

The demand spectra in ADRS format were also derived using equation 4.1, these are shown in Figure 6.16.

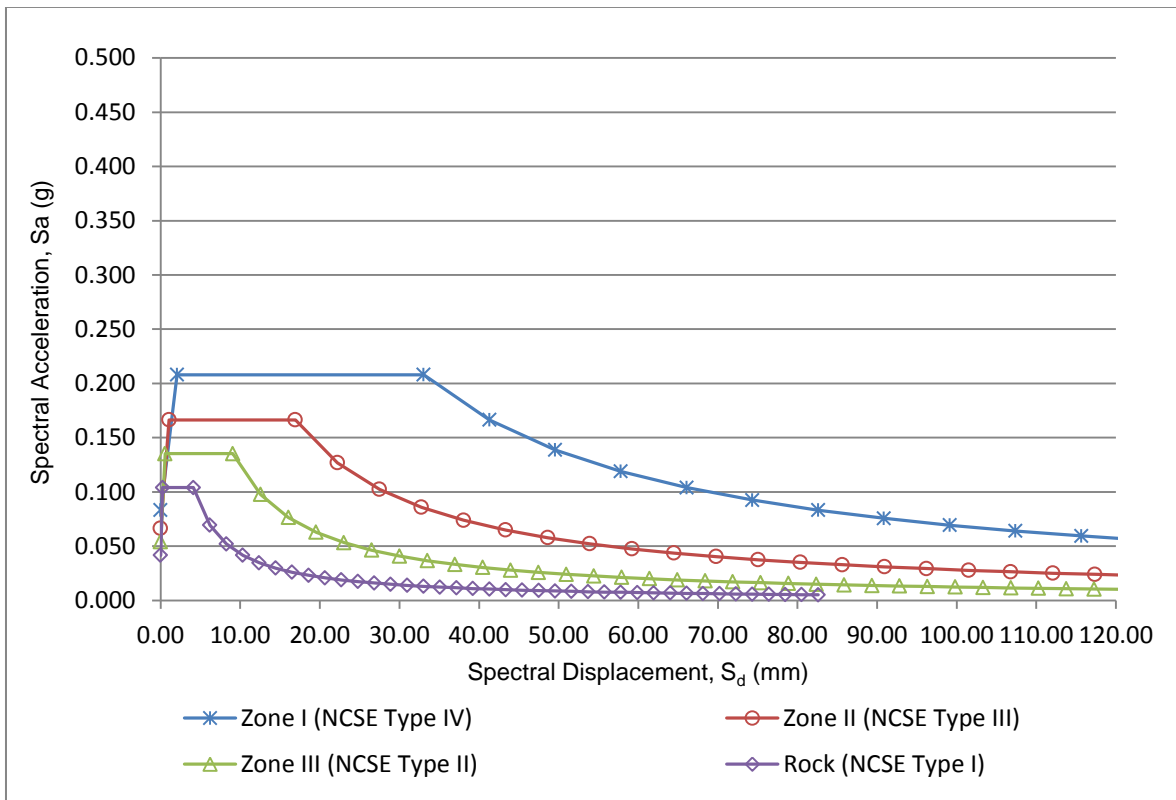


Figure 6.16: ADRS demand spectra for Barcelona soil zones, to NCSE-02

6.7 Discussion of Results

The following chart presents the demand spectra obtained for the Eixample district of Barcelona by the deterministic, probabilistic and NCSE-02 code approaches (Figure 6.17). As discussed in Section 6.6.1, the Eurocode 8 earthquake Type II demand spectra as are appropriate to Barcelona, were found to be well approximated by the probabilistic approach.

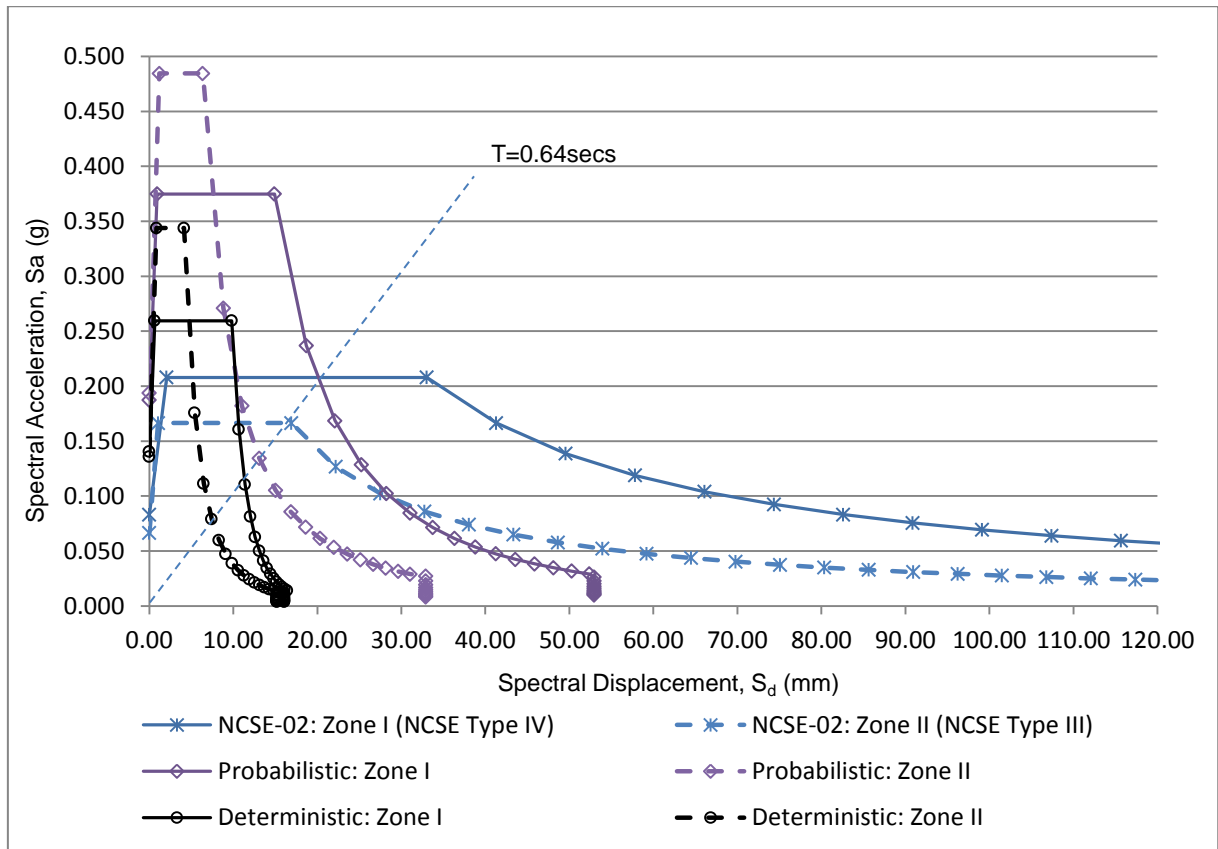


Figure 6.17: Comparison of demand spectra for the Eixample district, Barcelona by different approaches

The comparison illustrates that in general the probabilistic approach generates higher accelerations than the deterministic approach. This is the case for this study due to the intrinsic standard deviation of the results of the regional seismicity used to develop the spectra (Irizarry, 2004). For each soil type, the lowest spectral displacements are derived by the deterministic approach and the highest are by the NCSE-02 approach. The graph also indicates that the range of periods for constant acceleration is considerably longer for the NCSE approach for each soil zone. This suggests that the form of the NCSE spectra are more akin to the Type I earthquake spectra proposed by Eurocode 8, typically used to describe the response to larger scale seismic events of significant distance from the subject site.

For both the deterministic and probabilistic approaches, the maximum spectral acceleration is lower in the softer soils of Zone I than for Zone II. For the NCSE-02 approach, the maximum acceleration is higher for the Zone II soils.

For SDOF periods greater than 0.64 seconds (as shown in Figure 6.17), the spectrum governing the displacement demand will be the NCSE-02 spectrum for Zone I soils (NCSE soil Type IV). For lower values of the period, in the capacity spectrum method, the governing spectrum will depend on both the period and maximum acceleration of the capacity spectrum.

7. STRUCTURAL ANALYSIS – CASE STUDY

This chapter presents the procedure and results of a non-linear finite element structural analysis of a typical unreinforced masonry building of the Eixample district, Barcelona. Initially, the derivation of the model geometry and constraints is discussed. The values and behavioural models used to characterise the materials are then presented.

Following a description of the analysis procedure, the results of the analysis are presented and the displacement demand for the structure is determined. From this value, probabilities are calculated for various levels of seismic damage. Finally, the results are compared with those from a kinematic limit analysis and critical elements of the structure are identified that would require inspection and maintenance to limit the risk of seismic damage.

7.1 Introduction

As discussed in Section 2, the structural analysis forms only one part of an overall structural assessment and its results should be considered in the context of other qualitative and quantitative outcomes from other phases of the assessment.

In general, the aim of a structural analysis is to provide quantitative results of the structural response and capacity under possible loading conditions. In doing so, the analysis can provide an estimate of the serviceability and safety of the structure. In addition, an analysis can be made of the likely effectiveness and consequences of proposed interventions.

The aim of this structural analysis is to determine the displacement demand for a typical unreinforced masonry building of the Eixample district. As such, a detailed model of the structure has been developed to analyse the likely structural response to the imposed actions determined by the seismic hazard analysis (Section 6). The following sections describe the procedure and results of the seismic analysis.

7.2 Model Geometry and Constraints

The model geometry has been based upon the plans, sections and elevations of an unreinforced masonry building of the Eixample district. As discussed in Section 5.3, this building represents a typical building of the Eixample, as its geometry is in accordance with the planning bylaws of the development. The building plan is provided in Appendix A.

Two different models have been developed for this analysis, in the finite element program iDiana (Ver. 9.4). The principal characteristics of each model are presented below (Section 7.2.1). The simplifications and assumptions of each are then discussed in Section 7.2.2.

7.2.1 Model Descriptions

Two models have been developed for the structural analysis, the principal characteristics of each are as follows.

7.2.1.1 Model 1

- Only loadbearing walls are modelled. The mass of the floor, roof and stair structures and non-loadbearing walls are applied as concentrated or distributed loads to the walls.
- Dimensions of walls are in accordance with the plans, sections and elevations of the representative building, as discussed in Section 5.3 and presented in Appendix A.
- All perimeter loadbearing walls are continuous from ground to parapet level.
- All internal loadbearing walls are continuous from ground to roof level.
- Walls spandrels are removed, hence walls are modelled as individual wall segments.
- Rigid diaphragms in the horizontal plane at floor and roof levels approximate the stiffness of the masonry-steel composite slab systems.
- Walls are securely connected to the rigid diaphragm at floor and roof levels.
- Only half the building has been modelled, with an axis of symmetry along the central longitudinal axis. Appropriate restraints have been provided to all elements along this axis to replicate the effect of the entire structure.

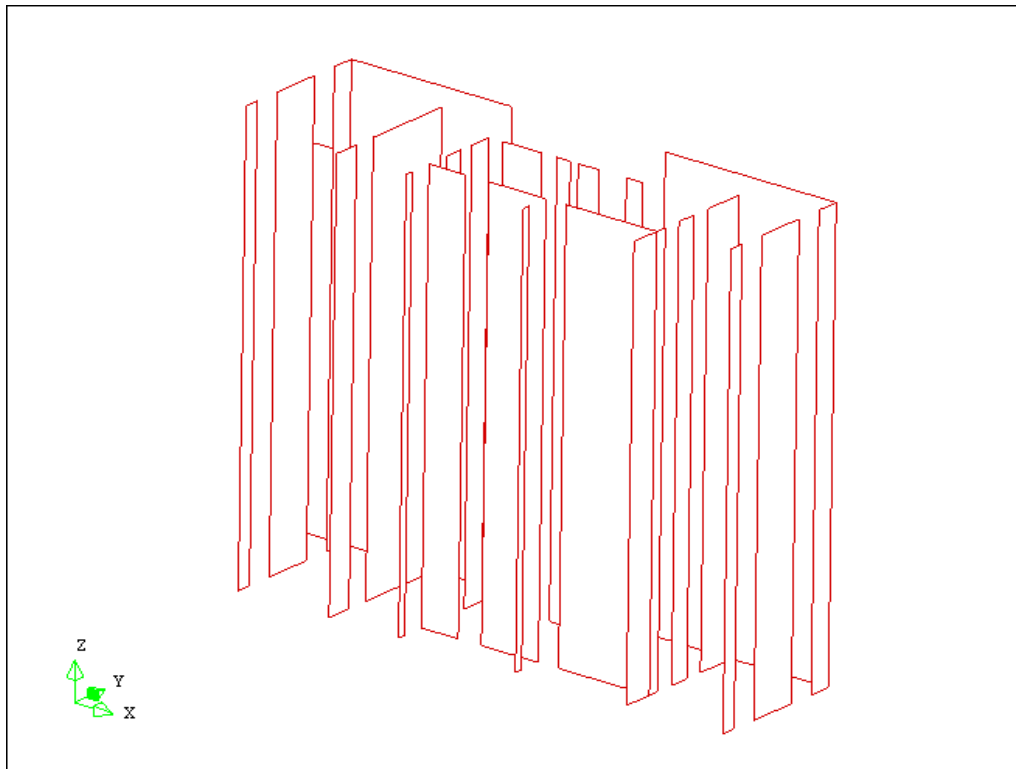


Figure 7.1: Model 1 wall panels

7.2.1.2 Model 2

Model 2 represents the condition where a number of transverse ground floor internal load-bearing walls are replaced with steel beams and column supports. In practice, this was done to enlarge the internal spaces at ground floor level and is commonly found in the buildings of the Eixample district. The majority of the geometry, loading and constraints are the same apart as for Model 1, apart from the following:

- Only the internal walls at the perimeter of voids and the staircase are continuous from ground to roof level. Other internal walls are continuous from first floor to roof level (Figure 7.2).
- Vertical constraints have been introduced at first floor level at the base of the reduced walls to approximate the support by steel beams and columns.

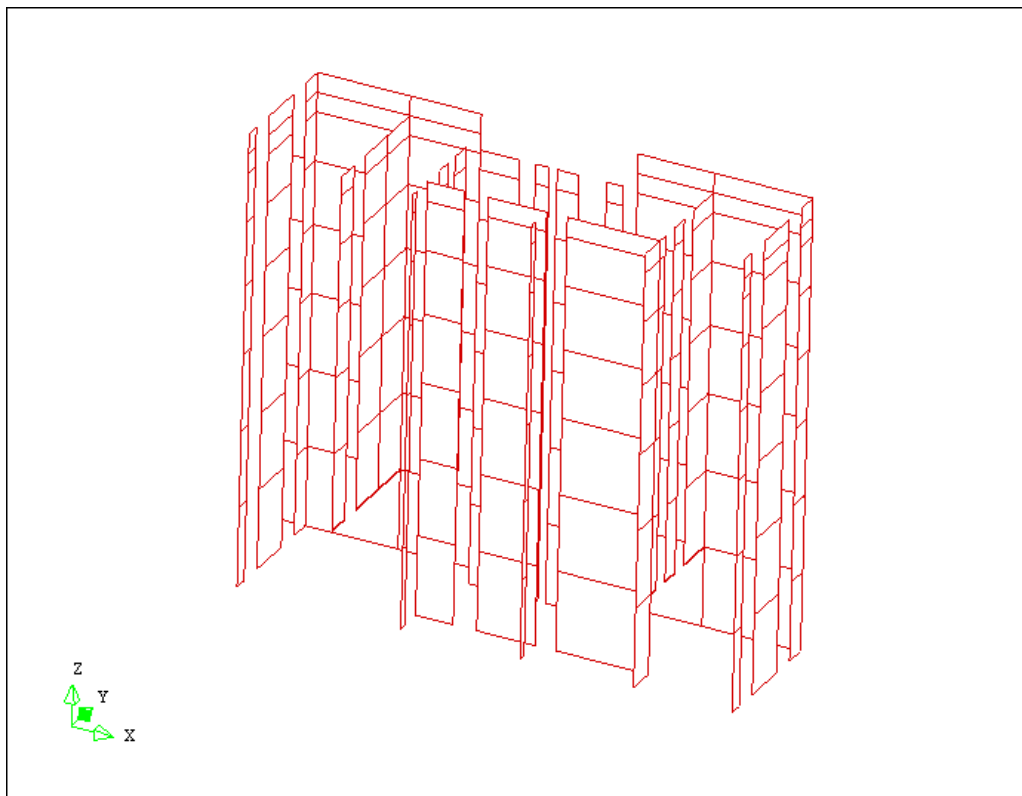


Figure 7.2: Model 2 wall panels

7.2.2 Model Simplifications and Assumptions

For each model, a number of simplifications have been made to approximate the form and characteristics of a typical building. The primary simplifications to the geometry and constraints are:

1. Wall spandrels removed above and below wall openings.
2. Floors are modelled as rigid diaphragms in the horizontal plane.
3. Floors are assumed to be securely attached to all loadbearing walls.
4. Walls are assumed to be undamaged and regular in plan.
5. Half the structure has been modelled, along the longitudinal axis of symmetry.
6. Removed ground floor walls are supported by vertical constraints at first floor level.

The assumptions and implications of each of these are discussed in the following sections.

7.2.2.1 Wall spandrels removed above and below wall openings

The walls are therefore modelled as vertical wall panels rather than continuous wall segments. The mass of the spandrels and load from any supported floor or roof elements has been applied to the wall segments at each side of all wall openings.

Removing the spandrels provides a slightly conservative estimation of the lateral load capacity for the following three reasons:

- At the junction of perpendicular walls, the spandrels provide lateral restraint to the adjacent wall between floor levels. By removing this restraint, the effective dimensions of the wall panels in these areas is increased.
- Deletion of the spandrels also increases the effective height of wall panels between openings.
- Stresses are no longer distributed within the spandrels and the walls, but are concentrated only within the continuous vertical wall panels. Although this would naturally occur at wall heights with both door and window openings, the removal of the spandrels develops this stress state for the full wall height. This may not significantly affect the capacity as the stress state at the wall mid-height, the critical location for lateral buckling, will not significantly change.

Removing the spandrels may improve the estimation of the capacity for the following reasons:

- Spandrels provide a connection between continuous sections of wall, in some cases of different wall thickness and each with different stress states. As such, there is a marked difference in the stress state at each side of every spandrel. In addition, there can be differential displacement (vertical or lateral) of two adjacent continuous panels. For these reasons, even for serviceability loading conditions, stresses can develop in the spandrels and cause minor cracking.

Practically, such cracking is usually of no structural significance. For a finite element model however, the non-linear response and ultimate capacity are dependent on the stress state calculated at individual finite elements. Hence if excessive stress levels are calculated at the spandrels, this will limit the calculated capacity to their failure, rather than to failure of the continuous wall elements. By removing the spandrels, this effect is prevented and the calculated capacity is more representative of that of the continuous wall elements.

- As stated above, it is likely that spandrels will exhibit cracking due to differential stress levels and displacements. As such, the capacity of spandrels to redistribute stresses from adjacent continuous wall elements is reduced by this cracking.

If the spandrels are included, they form an integral part of the wall and stresses can redistribute to them. This may prove unconservative given the likelihood for pre-existing cracking. By removing them from the model, this effect is prevented.

7.2.2.2 Floors are modelled as rigid diaphragms in the horizontal plane

The typical flooring of the Eixample unreinforced masonry buildings comprises the steel joists and masonry arch system described in Section 5.3. In contrast to a floor system of timber joists and boards, the typical floor system has a solid cross-section and hence exhibits significant stiffness in the horizontal plane. To represent this stiffness, the floors have been modelled as infinitely rigid diaphragms in the horizontal plane. Each floor will therefore displace horizontally as a rigid element. Differential vertical movements have been permitted.

Modelling the floors to have infinite in-plane rigidity is a simplification of the true floor stiffness. In practice, although the floors have a solid cross-section, they comprise isolated segments of masonry tiling, rubble and lime mortar between the steel floor joists. In most cases, there are no shear studs or ties to connect the joists to the rubble and mortar fill (Casademunt, 2009). The differences in thermal expansion and stiffness between the steel joists and mortar fill will cause cracking at their interface. As such, although the floor will be extremely stiff parallel to the joists, the cracking will render it less stiff perpendicular to the joists. In seismic actions, the cyclic nature of the movements is likely to exacerbate this cracking and further reduce the stiffness perpendicular to the joists.

It is not practical to estimate this difference in stiffness, as many factors can influence it including the specific material properties, floor morphology and loading history. Hence, in a similar approach to previous studies of the buildings by Pujades et al. (2010), it is assumed that infinite in-plane rigidity provides a reasonable approximation of the floor stiffness.

7.2.2.3 Floors are assumed to be securely attached to all loadbearing walls

A secure connection has been assumed from the floors to the loadbearing walls. No out-of-plane stiffness has been attributed to the floors, so there is no moment transfer between them and the walls.

In practice, the connection consists of the partial embedment of the steel floor joists and rubble fill to the masonry walls. For those walls perpendicular to the joists that support the majority of the vertical load, there are regular steel joist connections. For walls parallel to the joists that primarily support self-weight, the connection is limited to the arch springing and rubble fill. The typical floor system is presented in figures 5.9 and 5.10. No mechanical fixings have been observed at these connections (Casademunt, 2009).

The true capacity of the connection will be dependent on frictional resistance. At the steel joist connections there is likely to be cracking between the steel and the masonry due to the differences in thermal expansion and the ongoing movement of the joists with changes in floor loading. This cracking will slightly reduce the frictional resistance of the connections. Under seismic actions, the cyclical nature of the actions may develop additional cracking and further limit the shear capacity. At the rubble fill to wall connections, the section may be more consistent. However the rubble fill is brittle and a relatively weak material in tension, hence it is susceptible to cracking and a reduction in the connection capacity.

For these reasons it is extremely difficult to estimate the true strength of the wall to floor connections under seismic actions.

The assumption of a secure wall to floor connection has two primary consequences, as follows:

- a) Local out-of-plane movement of the walls is prevented.
- b) Lateral forces at floor level transfer to loadbearing walls in proportion to wall stiffness.

The suitability and implications of these are discussed below.

- a) Local out-of-plane wall movements are a common cause of seismic damage to unreinforced masonry structures (Augenti, 2010; Binda et al. 2011). Typically, such failure mechanisms are related to a loss of lateral wall restraint and commonly occur in buildings with significant lateral loading, such as those with concrete or masonry composite floor systems. The failures are also commonly observed where the floor system has been introduced to an existing building and where inadequate connections have been provided to the wall.

The present study is considering an unreinforced masonry structure where a masonry composite floor system has been introduced during the initial construction. As such, the connection is integrated to the construction of the wall.

As discussed above it is extremely difficult to quantify the strength of the floor to wall connections, especially when subjected to seismic actions. As such it is important for an analysis to consider two mutually independent conditions for the structure:

- o Adequate strength of the floor to wall connection.

In this case, local out-of-plane failure mechanisms are prevented and the model considers the global response of the building. This condition is represented by the present study.

- Separation of the wall to floor connections under seismic actions.

In this case, local out-of-plane failures are possible. This condition is best modelled by kinematic limit analysis and is the focus of a concurrent report. The outcomes of this report are discussed in Section 7.7.

Hence, although local out-of-plane movements are prevented, this will enable the analysis of the global response of the structure which can be compared to the results of the kinematic limit analysis.

- b) Lateral forces must be proportioned in some way to the loadbearing walls to represent the global building response. Although the connections of walls perpendicular to the joist direction may be slightly stronger than those parallel, the difference in strength is unknown. Hence, the assumption has been to ensure an equal strength along each wall, so that the loads proportion in accordance with the relative wall stiffness.

As stated above, this model considers the global response of the building to seismic actions. Seismic damage observations of unreinforced masonry buildings with significant lateral in-plane loading have also identified that local shear failure mechanisms can occur. As for the local out-of-plane mechanisms, these are best studied using a kinematic limit analysis approach, which is the focus of a concurrent study.

Although the secure restraint of the wall to floor connection prevents the development of local failure mechanisms, it provides the means to study the global response of the structure for the case where local failures do not govern the capacity.

A benefit of this approach is the ability to quantify the required shear capacity of the wall to floor connections. This capacity can then be verified by in-situ testing and may help guide intervention works to reduce the risk of seismic damage.

7.2.2.4 Walls are assumed to be undamaged and regular in plan

By assuming walls are uncracked and of regular dimensions, no local stress variations or out-of-plane moments are considered in the walls.

This is an appropriate assumption for a typological study, as it would be difficult to quantify suitable estimates for crack sizes and out-of-plane deformations and to select appropriate wall sections and locations on which to apply them.

For the seismic analysis of a particular structure, the cracking and deformations should be surveyed and applied to the model. By analysing with and without them, their influence on the seismic capacity of the structure can be established. It would then be possible to assess whether interventions are required to repair the structure and remove the deformations.

7.2.2.5 *Half the structure has been modelled, along the longitudinal axis of symmetry*

To limit computational requirements, only half of the structure has been modelled along the longitudinal axis of the building (perpendicular to the façade). The response of the entire structure has been represented by applying suitable boundary conditions to all elements along the axis of symmetry (Figure 7.3).

This simplification does not affect the results of either the gravity loading or the seismic actions along the longitudinal direction of the structure. This is because the gravity loads are evenly distributed at each side of the symmetry axis and the longitudinal lateral forces are applied at the centre of mass, which aligns with the symmetry axis.

By modelling in this way, it is not possible to assess the seismic response of the structure in the transverse direction. As discussed in Section 5.3, the typical unreinforced masonry buildings of the Eixample district were constructed as part of the development of each city block. They were constructed immediately adjacent to the neighbouring buildings and the form of each building was designed to complement those at either side. As such, each building must be considered part of a building aggregate rather than a separate structure.

Structures part of a building aggregate have significantly different responses to seismic actions than individual structures. For the buildings of the Eixample district, these differences will be concentrated in the transverse direction, parallel to the front façade. The variations in seismic response to that of individual structures arise from:

- The integrity of the connection between adjacent structures.
- The relative height and mass the walls of each structure.
- The relative levels and mass of floors and the roof.

The physical implications are:

- The transverse movement can be restricted by adjoining buildings, or can be free if the adjacent buildings are lower.
- Seismic hammering can occur due to lateral excitation of the mass. This can be particularly influential if there is a difference in the values or levels of the lateral forces between adjacent structures.

To effectively determine how the structure would perform in a building aggregate requires the precise modelling of the entire block. The analysis should also include the dynamic monitoring of numerous locations throughout the block to calibrate the model. Such an approach is beyond the means of the present study. As such, it is not possible to determine a reasonably accurate estimate of the transverse seismic response of the typical Eixample building from the analysis of an individual structure.

In addition, results of previous studies that modelled an entire individual structure using a 3D non-linear macroelement approach indicate maximum expected damage in the longitudinal direction (Pujades et al., 2010).

Hence, it was decided to focus the analysis of the present study to the longitudinal direction.

The implications of the axis of symmetry to the modal results are that only the global modal responses in the longitudinal direction have been calculated. A full building model would be required to determine the global transverse and torsional modal responses.

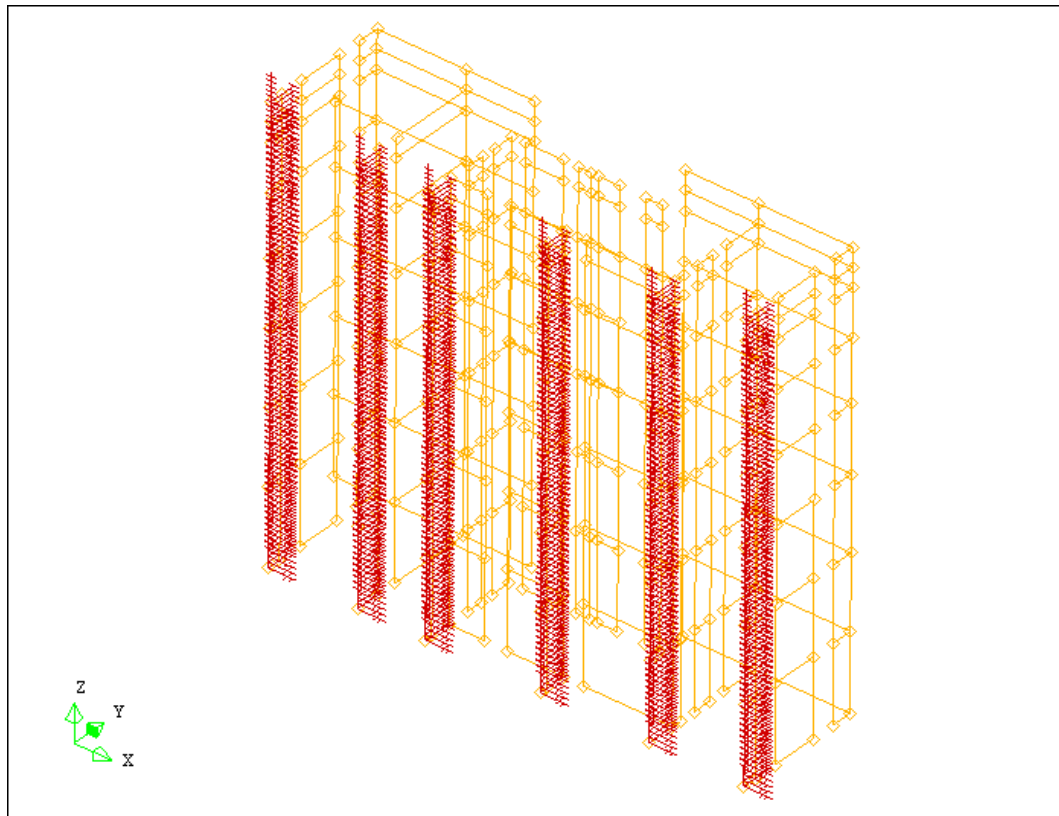


Figure 7.3: Model 1 – Axis of symmetry constraints

7.2.2.6 *Removed ground floor walls are supported by vertical constraints at first floor level*

Vertical constraints have been introduced at first floor level to simulate the support of steel beams and columns at ground floor level.

The seismic analysis of this building is focussed on the damage caused by the combination of gravity and seismic induced loadings. Hence when wall sections are removed, the redistribution of stresses to the remaining elements in the model must accurately represent those for the building.

When the ground floor sections of walls are removed, realistic force redistribution can be achieved by introducing vertical constraints at the base of the masonry at first floor level. These constraints will ensure an accurate calculation of the stress state within the masonry walls, and will permit a redistribution of the lateral components of force through the floor diaphragms.

There is no requirement to model the likely steel beams and columns, as the precise nature of the vertical support to the walls has no bearing on the lateral force transfer. In addition, the true size and location of beam and column elements is unknown.

It has been assumed that the steel beams and columns are of adequate strength and stiffness to support the walls with negligible deformations. As such, it is appropriate to model the wall supports as vertical constraints to approximate the vertical support of the steel beams and columns.

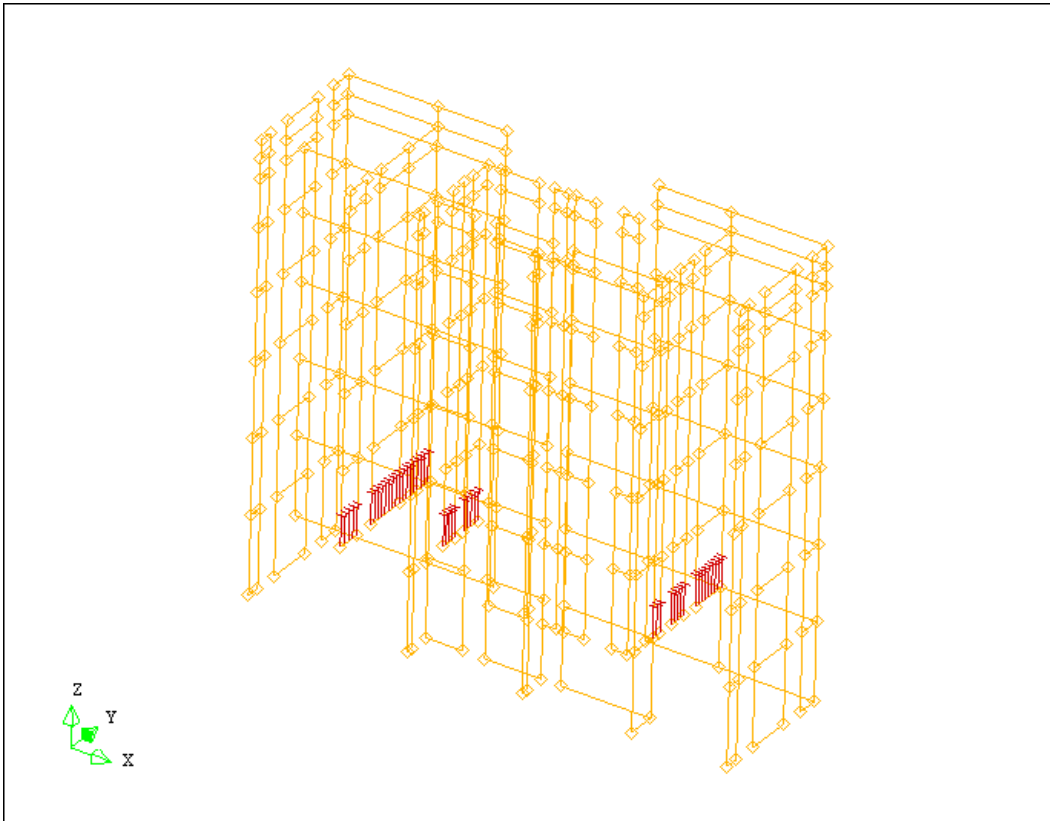


Figure 7.4: Model 2 – Vertical constraints at removed ground floor walls

7.2.3 Finite Element Discretisation

For each model, the structure has been discretised into a number of finite elements of either 300mm or 150mm size. Results have been obtained for each model with both sized elements and for varying load conditions. These are presented and discussed in Section 7.5.

The element type used for this analysis is a curved shell element. The primary characteristics of these elements are as follows, graphically represented in Figure 7.5 and Figure 7.6.

- Forces may act in any direction.
- Moments must act about an axis of the element.
- They have five degrees of freedom at each element node; three translations and two rotations.

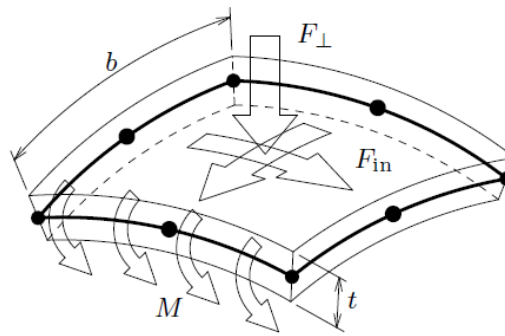


Figure 7.5: Characteristics of a curved shell element (DIANA Ver.9.4, 2009)

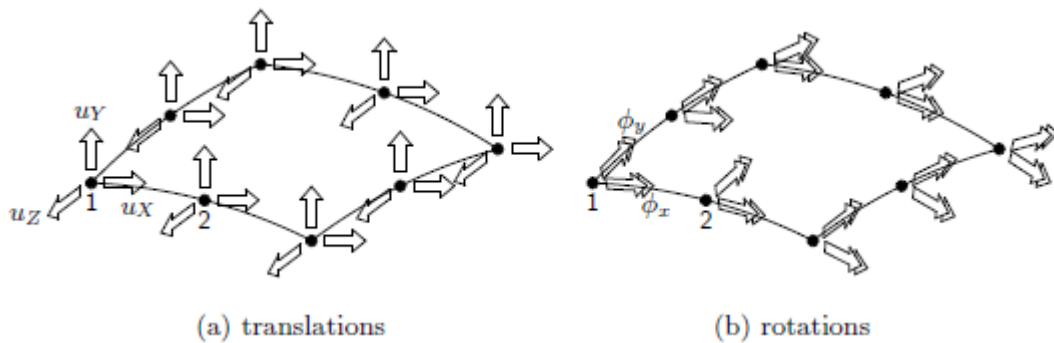


Figure 7.6: Nodal degrees of freedom for a curved shell element (DIANA Ver.9.4, 2009)

Curved shell elements are typically used in the modelling of heritage structures for masonry walls where the wall thickness is small compared to the overall wall dimensions.

The CQ40S quadrilateral curved shell element was selected for this analysis (Figure 7.7). This element has the following characteristics:

- It is isoparametric, so the same shape functions can be used for local and global coordinate systems.
- Based upon quadratic integration and Gauss integration. The integration scheme is 2x2 over the element area.
- In the element thickness, Simpson integration is used. This has three integration points, with one at each face of the element.
- Membrane and shear locking are prevented.

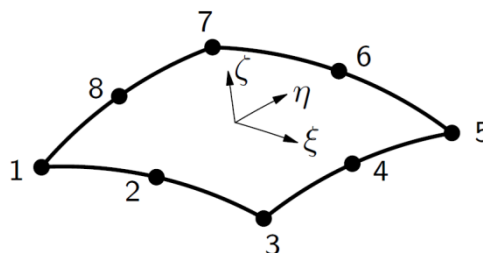


Figure 7.7: The CQ40S quadrilateral curved shell element (DIANA Ver.9.4, 2009)

7.3 Material Characteristics and Behavioural Models

The principal material characteristics for the masonry of the building were sourced from previous studies of the buildings (Pujades et al., 2010). These characteristics are the density, compressive strength, shear modulus and elastic modulus. The tensile strength was developed from a ratio of 5% of the compressive strength.

Table 7.1: Material characteristics

Material Characteristic		Value
ρ	Density	1800 kg/m ³
f_k	Masonry Compressive Strength	1.8 MPa
f_t	Masonry Tensile Strength	0.09 MPa
G	Shear Modulus	300 MPa
E	Elastic Modulus	1800 MPa

In addition to the primary material characteristics, the behavioural models for the masonry must be established. These identify the manner in which the finite element analysis models the behaviour of the materials under a given state of stress. For this analysis, a multi-directional fixed crack model was used that defines the development of orthogonally oriented cracking of the material that once cracked, remain in the same orientation regardless of the changing stress state.

Linear tension softening was also selected, with a constant stress cut-off. This gradually reduces the nominal tensile capacity of the material proportionally to the strain once a certain tensile stress is reached, regardless of the minimum principal stress condition in the material. This behaviour is represented in Figure 7.8, where g_f is the fracture energy over a given section of the material, G_f is the actual fracture energy of the material, and w is the crack spacing.

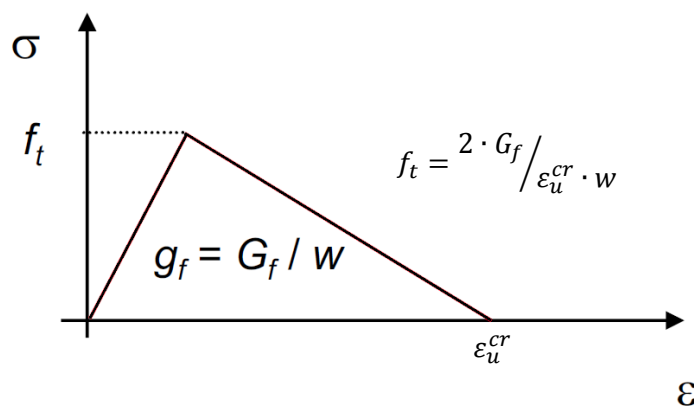


Figure 7.8: Linear tension softening (Lourenço, 2010)

The crack spacing is automatically defined by the finite element software depending on geometry and element size and layout. The fracture energy, G_f , is determined by multiplying the tensile stress, f_t , by a ductility index value, d_u . A value of the ductility index of 0.029mm was selected as a representative value for the masonry (Lourenço, 2010). Hence, the value of the fracture energy is 0.00261 N/mm.

Constant shear retention was selected, which reduces the shear strength of the masonry once the material has cracked. For this model, the reduced shear strength is approximately 0.02G.

The Drucker-Prager plasticity model was selected, which determines the maximum value of elastic energy required to induce plastic yielding. This model is an approximation of the Mohr Coulomb model and it similarly modifies the allowable energy value depending on the hydrostatic stress state in the material. It can be considered therefore as a conical yield surface (Figure 7.9). This relationship can well represent cohesive-friction materials and requires the definition of the internal friction angle, ϕ , and hence the cohesion, c . A value of the friction angle for the masonry was selected as 10° , therefore the cohesion for the material was calculated as 755 N/mm^2 (Equation 7.1).

$$c = f_k \cdot (1 - \sin \phi) / 2 \cos \phi \quad (\text{Eqn. 7.1})$$

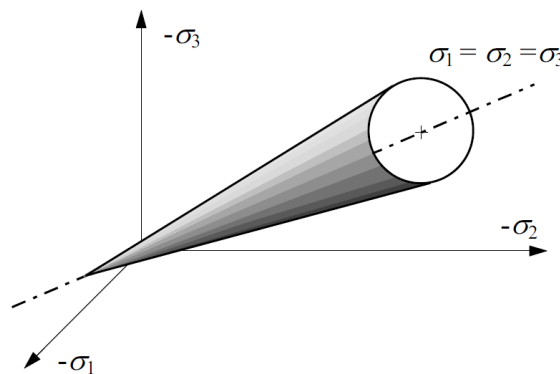


Figure 7.9: Drucker Prager yield surface (Lourenço, 2010)

7.4 Analysis Procedure

The displacement demand for the structure is determined by the capacity spectrum method, utilising the N2 approach. A detailed description of this approach is provided in Section 4. A summary of the procedure is as follows:

1. Determine the seismic demand for the site. Plot in acceleration-displacement (ADRS) format.
2. Apply lateral forces to non-linear modal and construct pushover curve, idealise as a bilinear capacity curve.
3. Modify capacity curve to ADRS format.
4. Determine location of intersection point. If in inelastic range, develop inelastic demand spectrum. Calculate single degree of freedom (SDOF) spectral displacement demand and convert to multi degree of freedom (MDOF) displacement demand.

The following sections detail the application and results of this procedure to the case study.

7.4.1 Step 1 – Seismic Demand

The seismic demand for the site has been developed from a seismic hazard analysis using the deterministic, probabilistic and code specified approaches. These approaches are defined in Section 3 and the results of the analysis are presented in Section 6.

The resultant demand spectra for the Eixample district of Barcelona have been derived (Figure 6.17). These spectra will be compared to the capacity spectra derived from the pushover analysis to determine the displacement demand.

7.4.2 Step 2 – Pushover Curve

7.4.2.1 Lateral Load Definition

The initial step for a pushover analysis is to determine an appropriate lateral force distribution to be applied to centre of mass of each floor level in the structure. The force distribution should be consistent with the inertial response of the building during a seismic event.

Two lateral load distributions are commonly used (Fajfar, 2000; FEMA 440, 2005):

- A distribution that corresponds to the first mode of vibration for the structure in the load direction.
- A linear increase in loading with building height.

To determine the lateral load distribution related to the first mode of vibration, first a modal analysis is required.

The modal analysis was completed using finite element analysis processing program Diana (Ver. 9.4) for both Model 1 and Model 2. The number of mode cases developed ensured that a total of 93% of

mass participation was accounted for. Hence any significant global modes of vibration would be observed in the results. As discussed in Section 7.2.2, the symmetry axis along the longitudinal direction prevents the determination of modal shapes in the transverse direction and torsional mode shapes. However, these results are not required for the pushover analysis in the longitudinal direction.

In both cases, one dominant global mode of vibration was identified in the loading direction. All others were local modes of vibration, involving the mobilisation of individual walls or groups of wall panels.

The deflected shape, period, frequency and mass participation of the first mode of vibration are presented below (Figure 7.10 and Table 7.2).

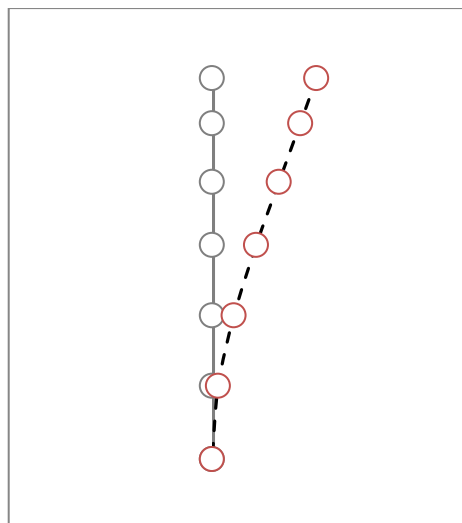


Figure 7.10: Model 1 – Deflected shape of first mode of vibration

Table 7.2: Results of first mode of vibration for each model

	Model 1	Model 2
Period (secs)	0.46	0.47
Frequency (Hz)	2.16	2.13
Total Mass Participation (%)	52.4	54.7

The deflected modal shape for each model was also compared. As expected, the shapes for each model are extremely similar as the differences between the two are limited to a slight change in the mass at ground floor level and the modified redistribution of lateral forces following the removal of the ground level walls. The removed walls in Model 2 were aligned with the transverse direction of the building, hence the global longitudinal stiffness is practically unchanged.

Following the modal analysis, the lateral load to be applied at each floor level was calculated (Equation 4.2). The shape factor was derived for both the modal and linear force distributions for each model. The resultant normalised lateral loads are presented in Table 7.3; these are also represented

in Figure 4.1. These forces were then applied to the structure in both the positive and negative longitudinal directions. The process of load application and the selected analysis methods are discussed below.

Table 7.3: Normalised lateral load distributions (kN) for each model

Floor Level	Model 1 (Modal distribution)	Model 2 (Modal distribution)	Model 1 (Linear distribution)	Model 2 (Linear distribution)
Roof	1000.000	1000.000	1000.000	1000.000
Fifth floor	779.769	779.229	813.679	813.679
Fourth floor	650.497	649.115	740.006	740.006
Third floor	450.909	448.580	600.513	600.513
Second floor	232.126	228.815	418.610	418.610
First floor	65.220	61.750	215.319	207.559
Ground	0.000	0.000	0.000	0.000

7.4.2.2 Model Load Cases

A total of eight cases were developed (Table 7.4). The differences in the cases derives from the loading type (modal or linear), the loading direction (positive or negative along the longitudinal direction), and whether 300mm or 150mm sized elements were used in the analysis. The reasons for selecting the parameters of each case are described in Section 7.5.

Table 7.4: Summary of analysis cases

Case Number	Model Number	Load Distribution	Load Direction	Element Size
Case 1	Model 1	Modal	Positive	300
Case 2	Model 1	Modal	Positive	150
Case 3	Model 1	Linear	Positive	300
Case 4	Model 1	Modal	Negative	300
Case 5	Model 1	Modal	Negative	150
Case 6	Model 1	Linear	Negative	300
Case 7	Model 2	Modal	Positive	150
Case 8	Model 2	Modal	Negative	150

7.4.2.3 Load Application and Analysis Techniques

The load application consists of initially applying the vertical loads to the structure (the dead load followed by 30% of the live load). Once these had been applied, the seismic action is modelled. It is represented by a monotonically increasing pattern of lateral loads corresponding to either a modal or linear force distribution.

Two methods of load application and analysis were used for each case, automatically generated load steps and explicitly defined load steps. The procedures and inputs for these methods are described below.

1. Automatically generated load steps

Initially, both the vertical loading (dead load and live load) and the lateral loading were analysed using adaptive load increments, sized automatically by the analysis program Diana (Ver. 9.4).

The inputs required for this analysis are:

- A maximum load step size. This value is the initial trial step value and should be selected so as to limit the number of step resizings required to achieve convergence. A value of 50% of the load was used for dead and live loads, as these are assumed to be within the linear range. A value of 1% was used for the lateral load application.

- A minimum size for each load step. The analysis will stop if the next step following re-sizing is less than the specified minimum value. A value of 25% was used for the vertical loads, whereas a value of 0.01% was used for the lateral loading.
- The convergence tolerance. The percentage difference between the applied load step and the final calculated load value for each step. The program will deem to have found convergence if the percentage difference is lower than the tolerance. A percentage of 2% was used for this analysis.

The automatic analysis procedure uses the Secant (or Quasi Newton-Raphson) iteration method, whereby the secant stiffness calculated at the beginning of each load step is used throughout the load step, rather than calculating a revised stiffness at each load increment within the step. This is represented graphically below (Figure 7.11).

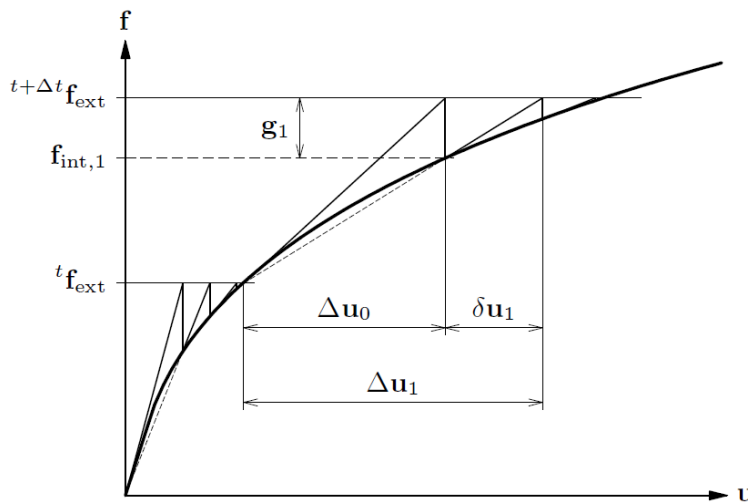


Figure 7.11: Secant (or Quasi Newton-Raphson) iteration method

The method also uses line search, which helps to find convergence by using the calculated change in displacement from the previous load step, multiplied by a factor, to define a range for a likely convergence point. This is particularly of use for masonry constructions where significant nonlinearity such as multiple cracking is likely to occur.

The benefit of this analysis is that the program automatically resizes the load step size if non-convergence is found until finding convergence or reaching a specified minimum load step. As such, it provides an excellent way to define an initial form for the pushover curve.

The drawbacks are that there is no provision for arc length control, so unloading conditions will result in non-convergence. The use of the Secant iteration method, while faster than Regular Newton-Raphson, is more approximate and may also lead to non-convergence. The process will also stop at the limiting minimum size. Hence, once the automatic analysis has been completed, the shape of the pushover curve and the percentage of load at non-convergence are used to define appropriate load steps for a more detailed analysis.

2. Explicitly defined load steps

Following the initial analysis, a secondary analysis was completed using DIANA (Ver. 9.4) for each case, using explicitly defined load steps.

Typically, the automatic analysis determined non-convergence at about 30% to 35% of the applied lateral loading. With this in mind, the approximate load step sizes used were:

- In the range of 1% to 0.5% of applied load for the first 15% or 20% of the total load.
- About 0.2% until about 30% of load.
- A gradual reduction from 0.1%, to 0.05% and finally to about 0.005%-0.0075% in the region where non-convergence was likely.

In each case, the number of load steps nominated for the final step size was made sufficient to ensure the analysis stopped due to non-convergence and not due to a lack of load steps.

In this analysis, arc length control was used to help ensure the analysis would continue regardless of minor unloading.

For most cases, the explicitly defined analysis determined ultimate deflections approximately three times larger than the automatic analysis. For the range of deflections calculated by the automatic analysis, both the shape of the pushover curves and the values of the loading were found to be very similar to the explicit analysis.

The pushover curves for each case are presented in force-displacement format in Section 7.5. Also presented on these graphs is the bilinear idealisation of the pushover curve, the methodology for which is discussed below.

The capacity spectra (in ADRS format), generated from the bilinear idealisations of the pushover curves, are then plotted together with demand spectra.

7.4.3 Step 3 – Capacity Spectrum

To determine the displacement demand, capacity spectra in ADRS format were derived from the pushover curves of each case. A detailed description of the standard procedure is contained in Section 4.4.

As part of this conversion, firstly an idealised bilinear pushover curve was developed. As discussed in Section 4.4, the shape of the idealised curve was determined as follows:

- The idealised curve intersects the pushover curve in the elastic range at a value of 60% of the idealised yield force.
- The total area below each curve is the same. This ensures that the total energy demand of both the calculated and idealised curves is equal.

The idealised bilinear pushover curves in force-displacement format are presented together with the original pushover curves in Section 7.5.

The next step was to convert the idealised pushover curve, from the original multi degree of freedom (MDOF) system, to an equivalent capacity spectrum which approximates a single degree of freedom (SDOF) system. This was achieved using the calculated modal participation factor for each case (Equations 4.4 to 4.7, Table 7.5) and then dividing the lateral force values of the SDOF curve by the equivalent mass (Equation 4.8). As expected, the modal participation factors are very similar for each model. The values are lower for each linear force distribution due to the larger equivalent modal mass calculated with this type of load distribution.

Table 7.5: Modal participation factors for each model and load distribution

Loading Type	Model 1		Model 2	
	Modal	Linear	Modal	Linear
Modal Participation Factor	1.372	1.357	1.371	1.355

The capacity spectrum for each case is presented in ADRS format in Section 7.5, in the graphical comparison to the demand spectra.

7.4.4 Step 4 – Displacement Demand

The demand and capacity spectra for each case were plotted on the same graph. For each case, it was determined whether the intersection point with the greatest spectral displacement value occurred within the elastic or the non-linear range. If in the elastic range, the spectral displacement was converted to an equivalent MDOF displacement demand using equation 4.5.

If the intersection point was in the non-linear range, then initially the value of the elastic period of the idealised bilinear system (T^*) was calculated (Equation 4.9). If T^* was greater than the characteristic period of the demand spectrum (T_C), then the seismic demand displacement was equal to the spectral displacement. If T^* was less than T_C , then the elastic demand spectra was modified to an equivalent inelastic spectra using the formulations presented in Section 4.5.3 and the spectral displacement calculated in accordance with equation 4.15.

In each case, the total displacement demand was then calculated by converting the spectral displacement to an equivalent MDOF displacement using equation 4.5.

7.5 Model Results and Damage Probability Assessment

The following section presents the results of the seismic analysis by the N2 capacity spectrum method with a non-linear pushover analysis using finite element software DIANA (Version 9.4).

The following results are displayed and discussed for a variety of model load distributions and geometries:

- The deflected shape of the structure.
- The original base shear force - roof displacement pushover curve from the finite element analysis.
- The idealised bilinear capacity curve derived from the pushover curve.
- A comparison in acceleration – displacement (ADRS) format of the calculated capacity spectrum to the demand spectra for the Eixample district of Barcelona.
- The displacement demand and its classification of damage level to the European Macroseismic Scale (EMS-98), obtained for the structure for each seismic scenario.
- The maximum and minimum principal strains and principal stresses at a damage level consistent with the 'substantial' level of damage to EMS-98. This level of damage was selected as it is within the inelastic range of the building's response and hence allows a review of the structure in a partially damaged condition. The damage level also correlates well with the calculated displacement demand for the critical seismic action.

As discussed in Section 7.2, two models were developed to represent the building geometry. In Model 1, the loadbearing walls are continuous from ground to roof level. In Model 2, transverse internal loadbearing walls at ground floor level are removed to replicate the common enlargement of internal ground floor areas.

For Model 1, a total of six cases were selected for the analysis to account for variations in the form of the load applied, load direction and element size. These cases are:

- Case 1: Modal load distribution in positive longitudinal direction, 300mm sized elements.
- Case 2: Modal load distribution in positive longitudinal direction, 150mm sized elements.
- Case 3: Linear load distribution in positive longitudinal direction, 300mm sized elements.
- Case 4: Modal load distribution in negative longitudinal direction, 300mm sized elements.
- Case 5: Modal load distribution in negative longitudinal direction, 150mm sized elements.
- Case 6: Linear load distribution in negative longitudinal direction, 300mm sized elements.

For Model 2, two different cases were analysed, as follows:

- Case 7: Modal load distribution in positive longitudinal direction, 150mm sized elements.
- Case 8: Modal load distribution in negative longitudinal direction, 150mm sized elements.

A comparison of the results of each case will enable a clearer determination of the seismic displacement demand and the response of the building to this action.

As discussed above, in this section representative principal strains and stresses are plotted for each case. For curved shell elements, it is possible to plot the strain and stress state at either the top, middle or bottom surface of the element. In this study, the values of the top, middle and bottom surfaces were compared for a number of cases and were consistently found to provide similar patterns of strains and stresses for the structure. Hence the description of the building's response to the imposed actions, the focus of the present study, was not affected by the selection of element surface level. As such, the results are presented for only one surface, the top surface of the element.

7.5.1 Gravity Analysis

Prior to analysing the cases for seismic demand, a review the structural condition under gravity loading conditions was completed. Model 1 was selected for this purpose as the stress state at the base of the internal transverse walls are more critical than for Model 2.

A load combination of 110% of dead load and 150% of live load was used for this analysis in accordance with the recommended values for the static equilibrium loading case in Table A1.2(A) of Annex A, Eurocode – Basis of Structural Design (EN 1990:2002).

The deflected shape, base reaction force – vertical roof displacement curve, and the maximum and minimum principal strains and stresses are shown below.

The deflected shape is as expected, with no discontinuities found in the model. The force displacement curve was developed from the total vertical base reaction and the vertical roof displacement (Figure 7.13). The load was applied in load steps, initially the dead load, and then the live loading. As can be seen from the curve, there is a slight non-linearity at the final load steps. As such, there is expected to be some minor localised cracking or crushing of the masonry at the ultimate loading condition. As this occurs only at the final load steps, it can be understood that the structure performs in the elastic range under serviceability loading conditions.

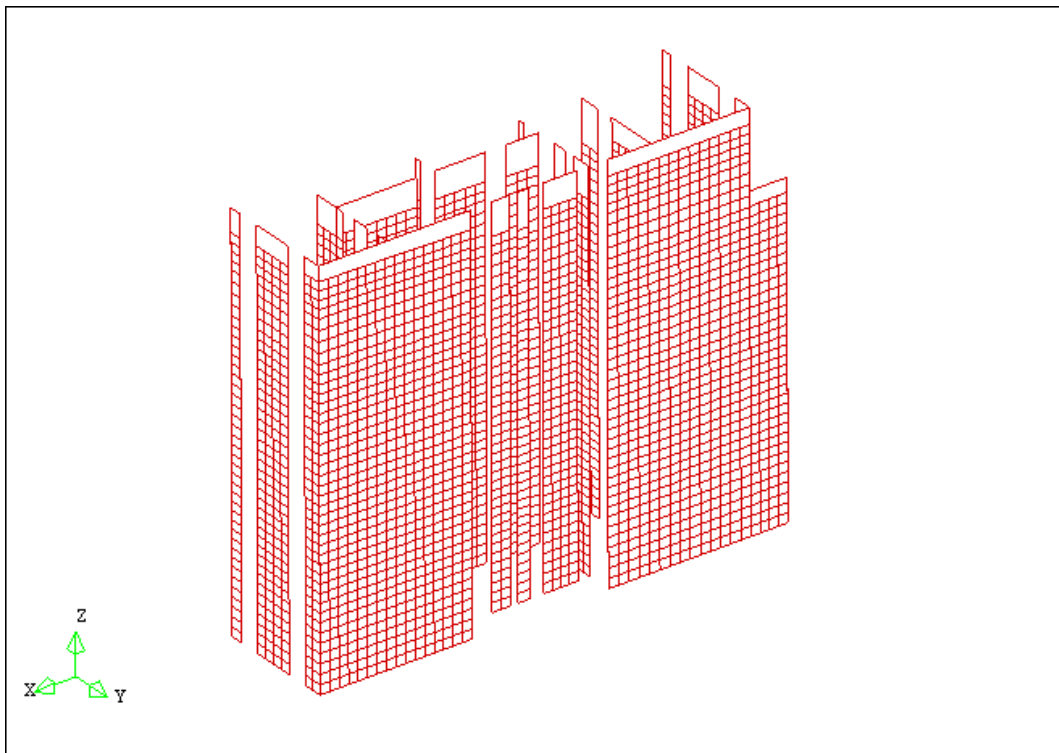


Figure 7.12: Deflected shape– Ultimate gravity loading

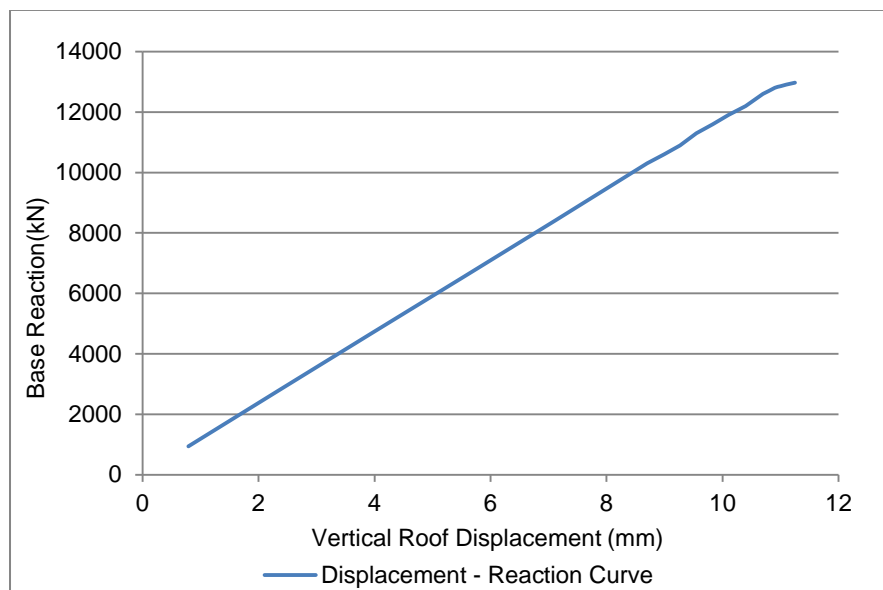


Figure 7.13: Base reaction – displacement curve, Ultimate gravity loading

The maximum principal strains indicate generally very low values, approximately 0.0005, which equates to about 1.7mm deformation over a floor level, which is a height to deformation ratio of 1:2000. Hence, there is likely to be no observed cracking in the majority of the structure at the ultimate loading condition. Higher values are recorded at the junction of walls that support floor loads and those that do not. This is likely due to the differential in total displacement due to the different compressive stress states of the walls. Changes in strain and stress state at the ground floor level are due to the increased thickness of the ground floor walls compared to those above.

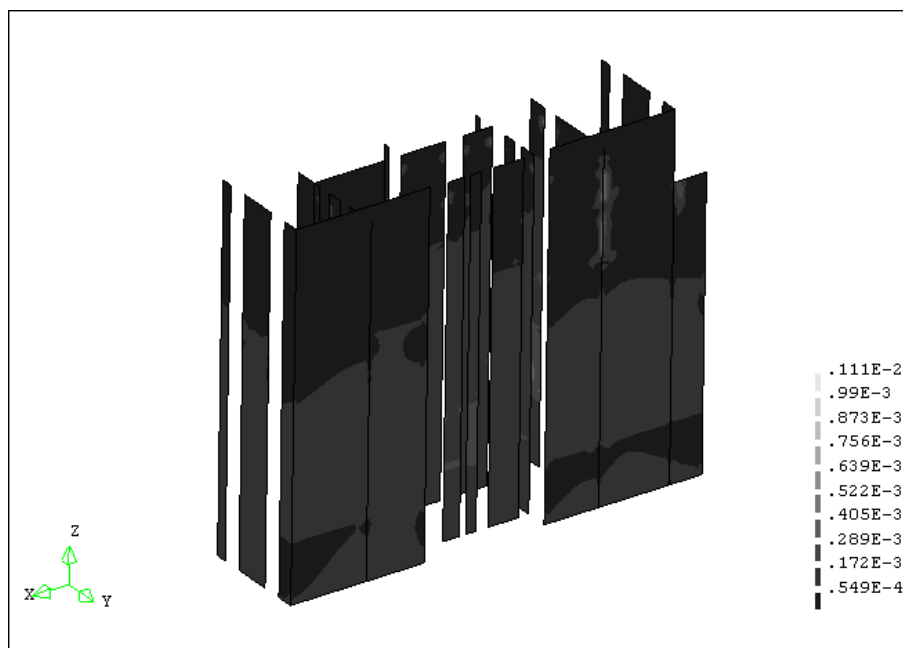


Figure 7.14: Maximum principal strains – Ultimate gravity loading

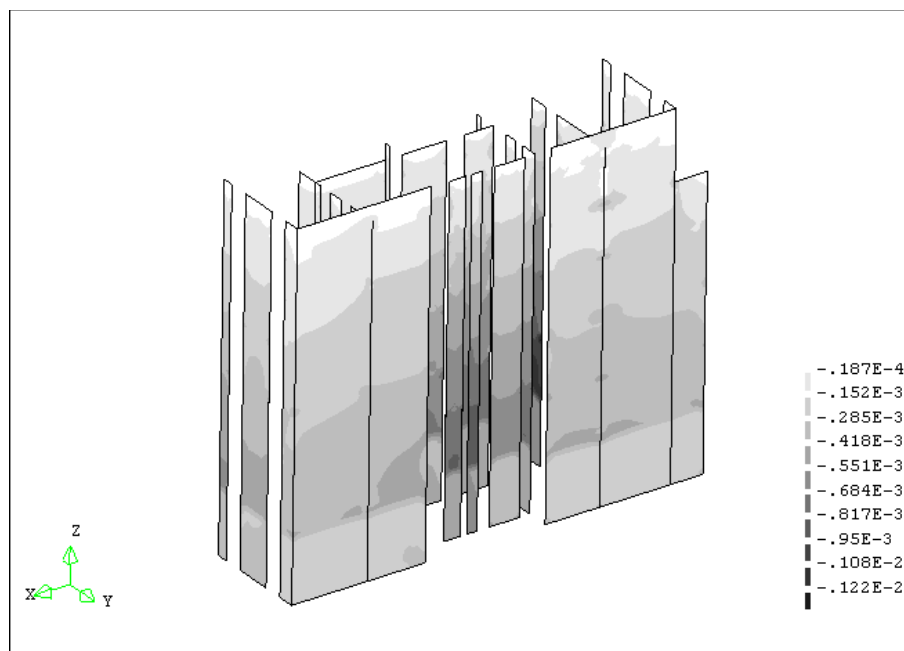


Figure 7.15: Minimum principal strains – Ultimate gravity loading

The minimum principal strains also generally indicate very low deformations. Slightly higher values are recorded with increased compression of the walls and within one thinner wall panel which has a higher load to cross-section ratio than the remainder of the walls.

Maximum principal stresses indicate very low tension values, as to be expected by the gravity loading condition (Figure 7.16).

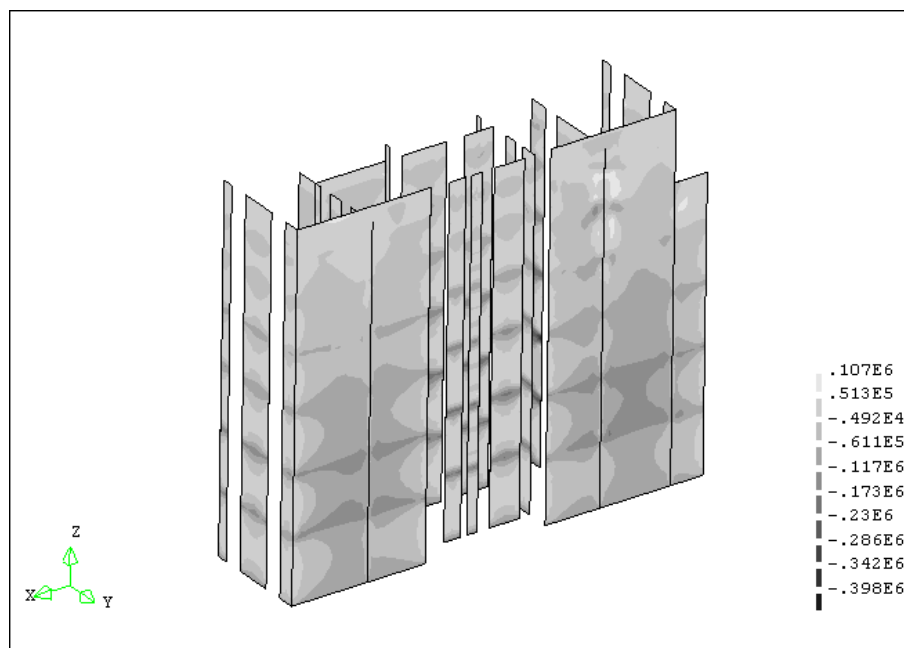


Figure 7.16: Maximum principal stresses – Ultimate gravity loading

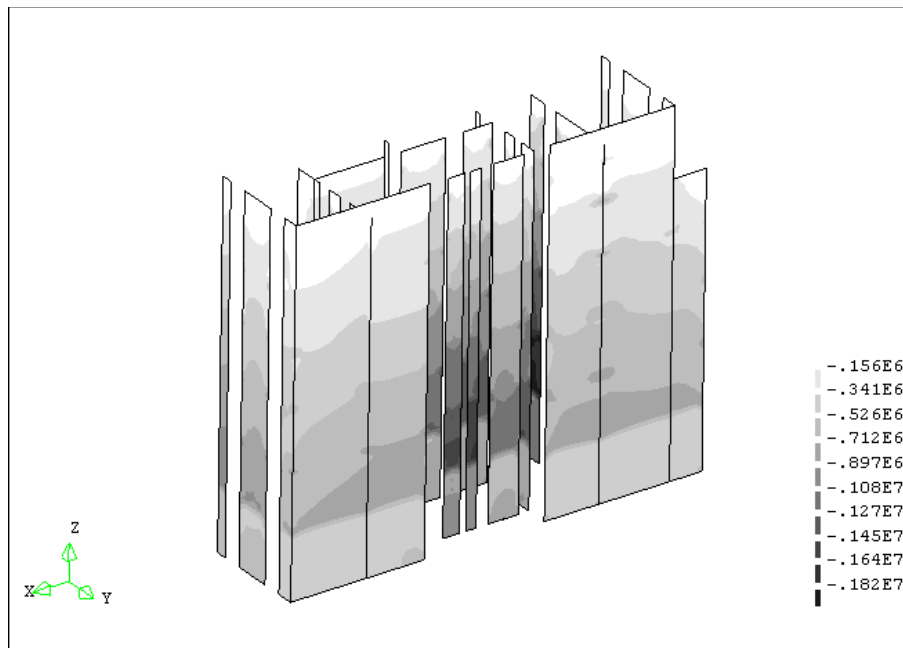


Figure 7.17: Minimum principal stresses – Ultimate gravity loading

Minimum principal stresses as expected indicate a gradual decrease in compression with height. Higher compressive stresses are experienced in the thinner wall panels and it is in these panels at first floor level (immediately above the thicker wall sections) that some minor crushing may be occurring in the ultimate load condition. The peak values of compression in the order of 1.8MPa are at the prescribed compressive capacity of the masonry, which support this hypothesis.

In summary, in serviceability loading conditions the structure is in the elastic range and is performing adequately. At the ultimate loading condition, minor damage may be expected at the junction of differentially loaded walls at the upper levels of the structure and at first floor level within thinner, more highly loaded wall panels.

7.5.2 Case 1 and Case 2

For Case 1 and Case 2, lateral loads approximating the seismic actions were applied with a modal distribution, in the positive longitudinal direction. The only difference between the two cases is the element size.

Following a review of the differences in the results, it was found that the patterns and levels of stresses and strains for each model were extremely similar. The only difference observed was that slightly higher peak stress values were obtained by Case 2, presumably due to the increased number of nodes. Given the similarity of the results, below are presented the results of only Case 1. Where notable variations were found between the cases, these are described.

The deflected shape at yield is shown so that a comparison can be made to the modal lateral force distribution based upon an elastic modal analysis (Figure 7.18).

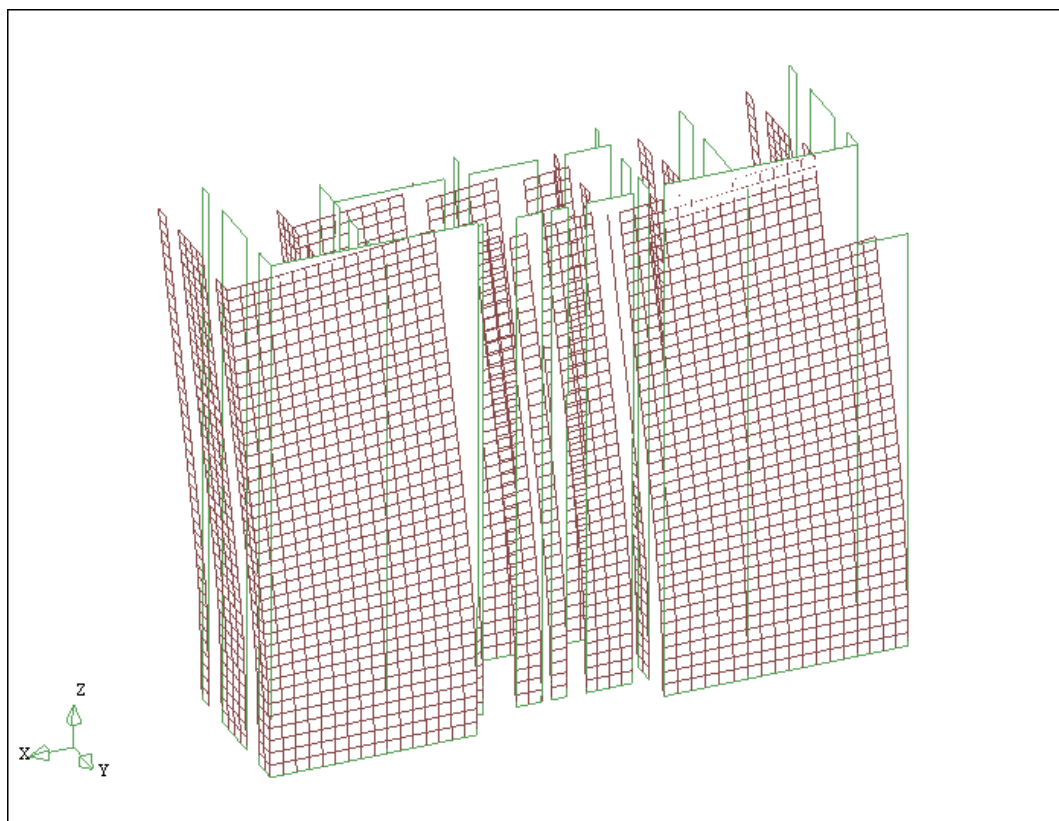


Figure 7.18: Deflected shape at yield – Case 1

The following table compares the normalised lateral deflections of the modal analysis and the non-linear pushover analysis at yield and at a level of 'substantial damage' as characterised by EMS-98 (Table 7.6). Two different load states were selected to highlight any differences in deflected shape due to the inelastic deformations.

The comparison shows that the deflected shape corresponds almost exactly to the modal shape in the elastic condition. For the inelastic condition, the deflected shape deviates no more than 3% from the

modal shape for all levels except at first floor. As such, the lateral force distribution using a modal shape approximates extremely well the inertial response of the structure for both the elastic and inelastic conditions.

Table 7.6: Comparison of normalised modal and non-linear analysis deflections – Case 1

Building Level	Building Height (m)	Normalised Modal Displacement	Normalised Yield Displacement	Normalised Displacement at 'Substantial' Damage Level (EMS-98)
Roof	21.105	1.000	1.000	1.000
Fifth floor	18.605	0.845	0.847	0.848
Fourth floor	15.355	0.640	0.642	0.646
Third floor	11.855	0.422	0.423	0.433
Second floor	7.955	0.209	0.210	0.214
First floor	4.055	0.058	0.058	0.047
Ground	0	0.000	0.000	0.000

The pushover curve obtained for Case 1 and the calculated idealised bilinear pushover curve are shown in Figure 7.19. The pushover curve is extremely regular, with only minor unloading occurring in the inelastic range. The ultimate displacement recorded was 372mm which was characterised by non-convergence of the analysis, the possible modes of failure are discussed below. The values for Case 2 are similar: $D_y=30\text{mm}$, $F_y=870\text{kN}$, $D_u=370\text{mm}$.

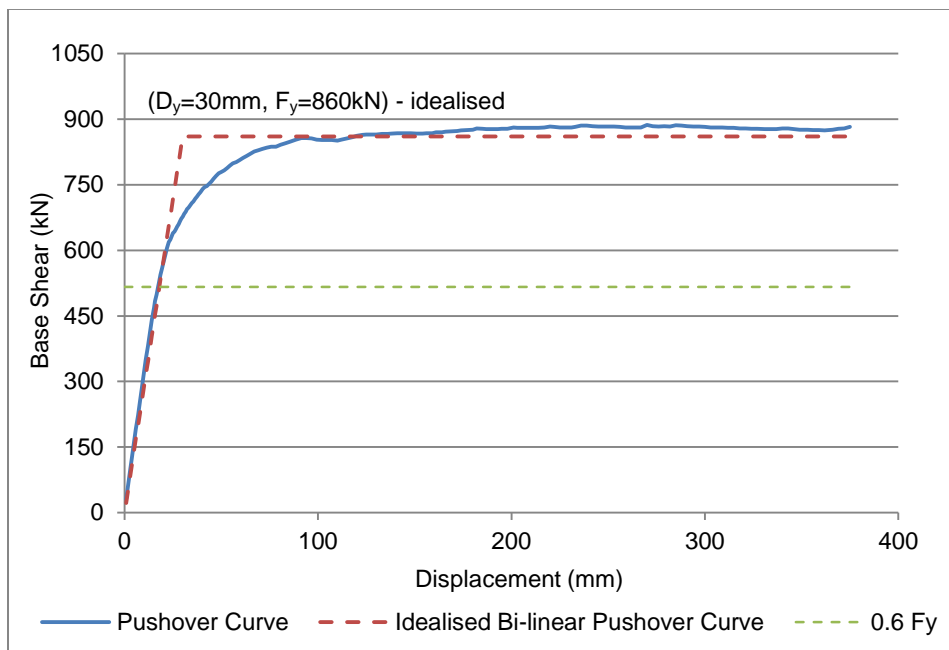


Figure 7.19: Pushover curve – Case 1

A capacity spectrum was developed using the bilinear curve and is plotted below in ADRS format in comparison with the seismic demand curves for the Eixample district (Figure 7.20). The displacement demand results for each seismic scenario are presented in Table 7.7.

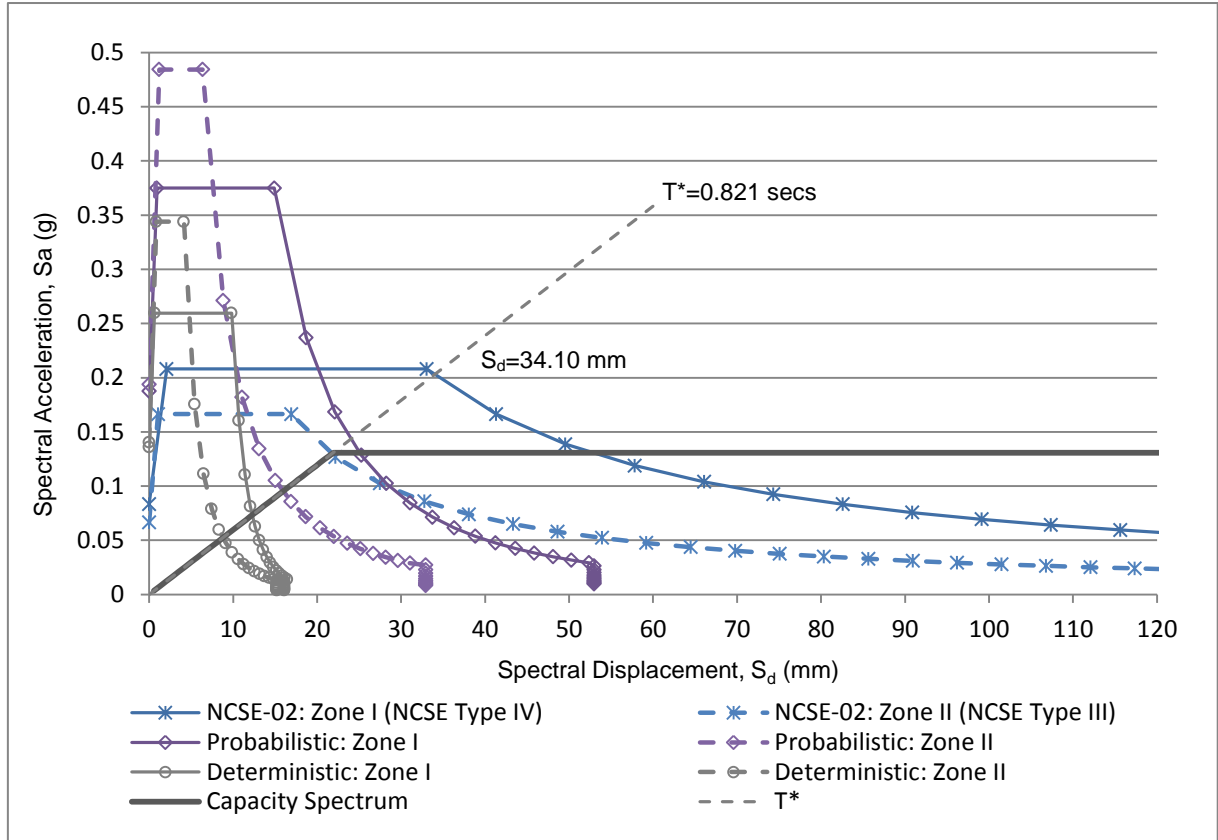


Figure 7.20: Comparison of capacity spectrum and demand spectra – Case 1

Table 7.7: Results of displacement demand – Case 1

Seismic Scenario	Spectral Displacement (mm)	Displacement Demand (mm)	Damage Classification to EMS98
Deterministic - Soil Zone II	8.86	12.15	Slight
Deterministic - Soil Zone I	12.42	17.03	Slight
Probabilistic - Soil Zone II	16.07	22.04	Slight
Probabilistic - Soil Zone I	24.34	33.38	Moderate
NCSE-02 - Soil Zone II (NCSE Soil Type III)	21.86	29.99	Moderate
NCSE-02 - Soil Zone I (NCSE Soil Type IV)	34.10	46.78	Substantial

The displacement demand is governed by the NCSE-02 seismic scenario in soil Zone I (NCSE soil Type IV), it occurs in the inelastic range of the building response. The displacement demand is 46.78mm and constitutes a substantial level of damage to EMS-98 gradings. A moderate level of damage is estimated from both the NCSE-02 scenario in soil Zone II (NCSE soil Type III), and the probabilistic scenario in soil Zone I. The elastic period (T^*) is greater than the characteristic periods of the demand spectra, hence the elastic and inelastic spectral displacement demands are equal. Reduced inelastic demand spectra have not been plotted for clarity of the figure.

To accurately represent the response of the structure to seismic loading, the maximum and minimum principal strains and principal stresses at the substantial damage state are presented below.

The maximum and minimum principal strains demonstrate the deformation of the masonry extremely well. At first floor level, a maximum principal strain of about 0.0015 is commonly seen at first floor level (Figure 7.21). For a floor height of approximately 3.5m, this equates to cracking in the order of 5mm between floor levels. At the upper levels, there is also cracking in the order of 2mm for the fourth floor level. From the maximum principal strains, similar magnitudes of masonry crushing can also be calculated for the first floor level for the critical wall panel (Figure 7.22). As such, it is clear that at this loading the structure is damaged. This therefore verifies the classification of substantial damage at this loading as characterised by EMS-98.

The magnitude of strains and stresses are lower at ground floor level as the ground floor walls are twice as thick as the walls above.

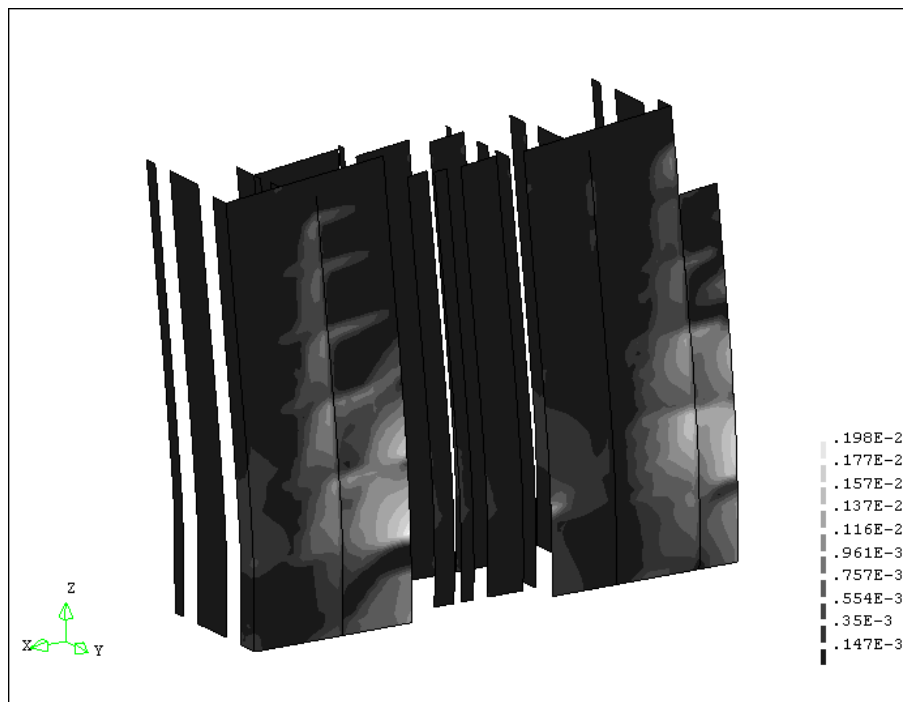


Figure 7.21: Maximum principal strains at substantial damage state – Case 1

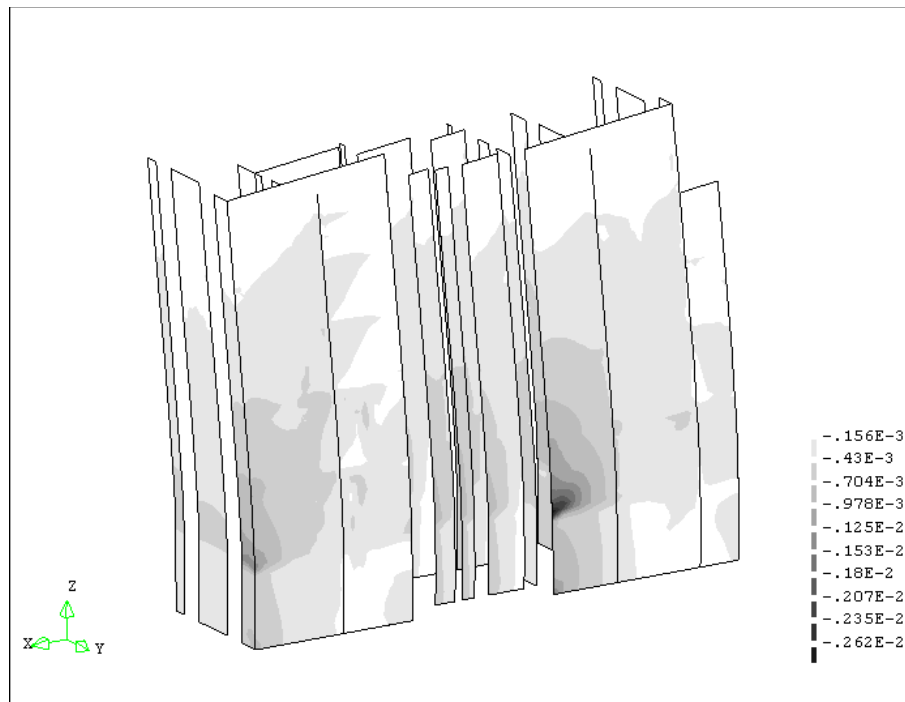


Figure 7.22: Minimum principal strains at substantial damage state – Case 1

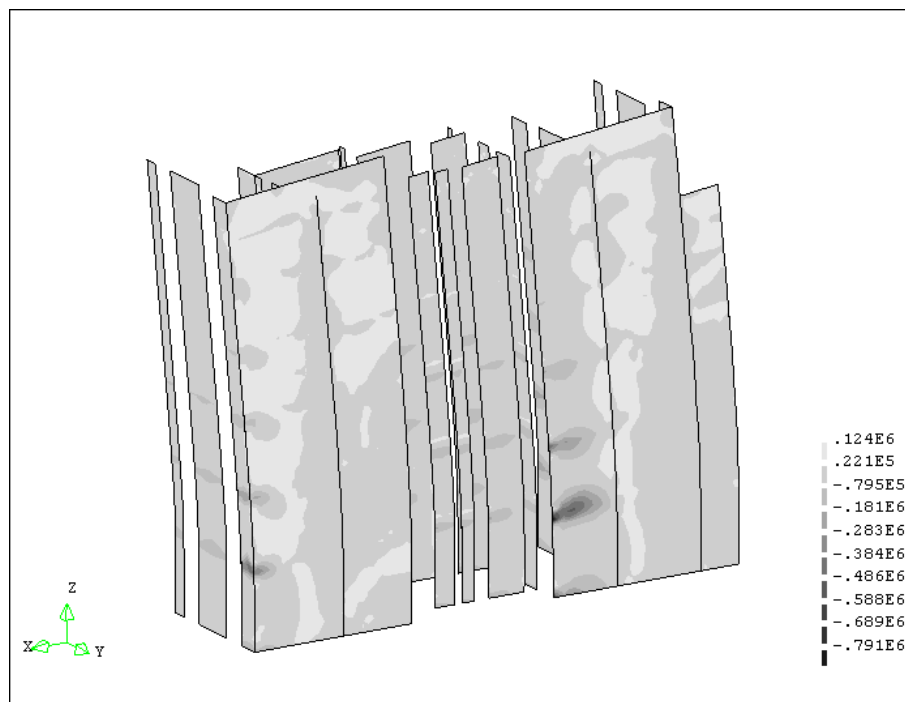


Figure 7.23: Maximum principal stresses at substantial damage state – Case 1

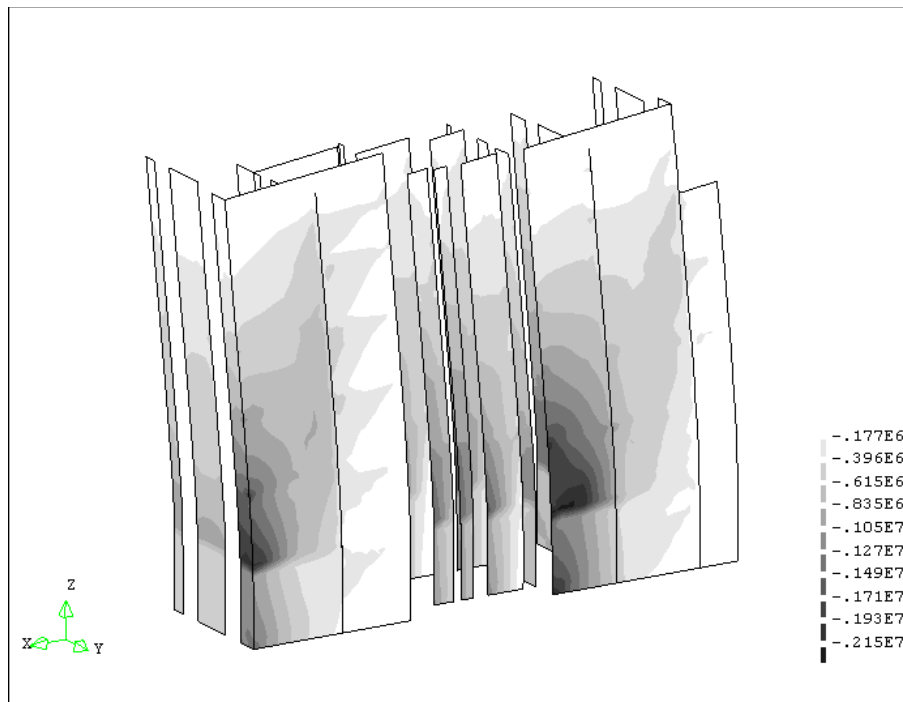


Figure 7.24: Minimum principal stresses at substantial damage state – Case 1

The maximum principal stresses indicate only isolated areas of tensile stresses in the masonry. This is primarily due to the low tensile strength and comparable fracture energy attributed to the masonry. Given these values, the masonry has cracked and no longer exhibits tensile stresses. The minimum principal stresses demonstrate the significant levels of compressive stresses within the critical wall panels. The compressive stresses are in the order of 2MPa which, similarly to the minimum principal strain diagram, indicates crushing of the masonry which has an attributed compressive strength of 1.8MPa.

The variation in stresses and strains through the structure shown above are similar throughout the inelastic response until non-convergence. In the elastic range, the masonry is uncracked and hence tensions are developed.

In summary, both Case 1 and Case 2 have a displacement demand of 47mm which equates to a substantial level of damage to EMS-98. The form of the displacements matches well the expected deformations and validates the use of a modal load distribution. The pattern of principal strains and stresses concurs with the expected building response. They indicate significant damage to wall panels at the demand displacement and justify the damage level classification.

7.5.3 Case 3

Case 3 involves applying seismic actions as a linear lateral load distribution to Model 1. In this case, the model uses 300mm sized elements.

The deflected shape of Case 3 is similar to that of Cases 1 and 2 (Figure 7.18). The load distribution for Case 3 is however linear, so it is of interest to compare how well the deflected shape corresponds to a modal distribution. A comparison of normalised deflections in the linear and non-linear ranges is presented below (Table 7.8). The results indicate a close relationship for each loading, with only slightly greater variation in the non-linear range. Hence the inertial response of the building is largely unaffected by the choice of load distribution and conforms well to a modal variation.

Table 7.8: Comparison of normalised modal and non-linear analysis deflections – Case 3

Building Level	Building Height (m)	Normalised Modal Displacement	Normalised Yield Displacement		Normalised Displacement at 'Substantial' Damage Level (EMS-98)	
			Displacement	Percentage	Displacement	Percentage
Roof	21.105	1.000	1.000	100.0%	1.000	100.0%
Fifth floor	18.605	0.845	0.851	100.7%	0.884	104.6%
Fourth floor	15.355	0.640	0.649	101.5%	0.680	106.3%
Third floor	11.855	0.422	0.433	102.6%	0.461	109.3%
Second floor	7.955	0.209	0.218	104.5%	0.235	112.4%
First floor	4.055	0.058	0.062	106.7%	0.063	108.0%
Ground	0	0.000	0.000	-	0.000	

The original and idealised bilinear pushover curves are presented below (Figure 7.25).

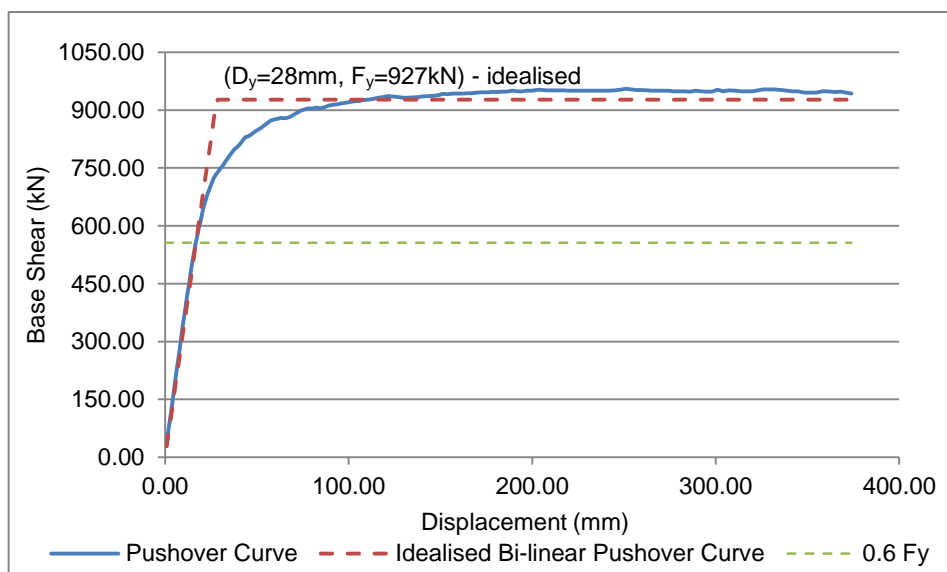


Figure 7.25: Pushover curve – Case 3

The curve is generally similar in form to that of Cases 1 and 2, with only minor unloading occurring in the inelastic range. The idealised elastic stiffness is however about 15% greater than for the previous cases, hence the elastic period of the structure (T^*) is about 8% lower. This may be attributed to a greater lateral loading near to the base of the structure due to the linear load distribution. The ultimate displacement of 374mm is comparable to the previous cases.

The capacity spectrum is compared below with the seismic demand curves for the Eixample district (Figure 7.26). Displacement demand results for each seismic scenario are presented in Table 7.9.

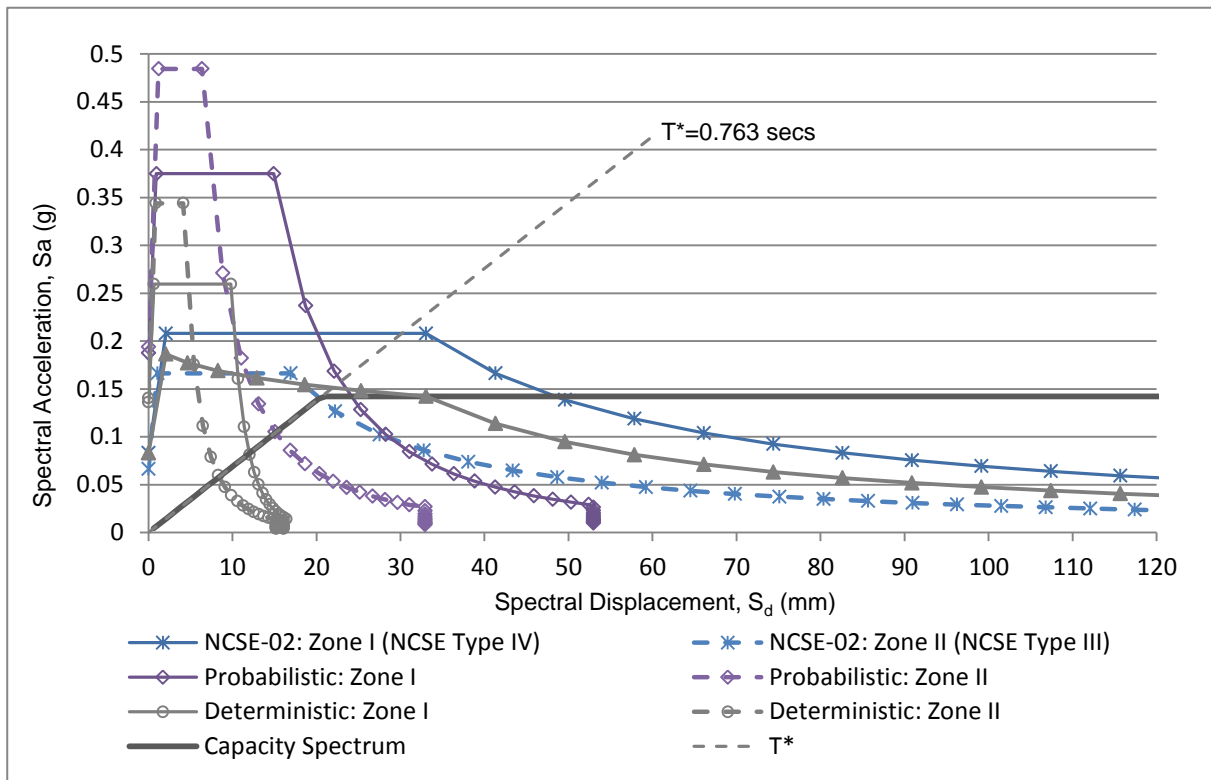


Figure 7.26: Comparison of capacity spectrum and demand spectra – Case 3

Table 7.9: Results of displacement demand – Case 3

Seismic Scenario	Spectral Displacement (mm)	Displacement Demand (mm)	Damage Classification to EMS98
Deterministic - Soil Zone II	8.45	11.46	Slight
Deterministic - Soil Zone I	12.06	16.36	Slight
Probabilistic - Soil Zone II	15.14	20.54	Slight
Probabilistic - Soil Zone I	23.10	31.34	Moderate
NCSE-02 - Soil Zone II (NCSE Soil Type III)	20.57	27.91	Moderate
NCSE-02 - Soil Zone I (NCSE Soil Type IV)	30.61	41.53	Substantial

Similarly to the previous cases, the displacement demand is governed by the NCSE-02 seismic scenario in soil Zone I (NCSE soil Type IV). The intersection occurs in the inelastic range and contrary to the previous cases, the elastic period is less than the characteristic period of the demand spectrum. As such, the inelastic spectral displacement demand is not equal to the elastic spectral displacement demand and must be calculated using equation 4.15. The inelastic NCSE-02 demand spectrum has been plotted on Figure 7.26. The resultant maximum displacement demand is 41.5mm and relates to a substantial level of damage to EMS-98 classification.

The maximum and minimum principal strains and principal stresses at a substantial damage level were compared to the results of Cases 1 and 2, which have the same load direction. The patterns were consistently similar, with negligible variation in values. As such, the loading type has had little effect on the manner of damage to the structure.

One aspect of the damage not yet discussed is the seismic effect on the smaller longitudinal wall panels adjacent to the internal void and stairs. The following figures show the minimum and maximum principal strains and the minimum principal stresses in these walls at a substantial damage level. The results show that cracking of these walls is not as critical as the perimeter walls with significantly lower levels of maximum principal strains (Figure 7.27). However, both the minimum principal strain and minimum principal stress diagrams indicate some likely crushing and high levels of compressive stress comparable to parts of the perimeter wall (Figure 7.28, Figure 7.29). This effect may be attributed to the higher relative gravity loading to these walls from the floor framing, compared to the end sections of the perimeter longitudinal walls which have no floor loading.

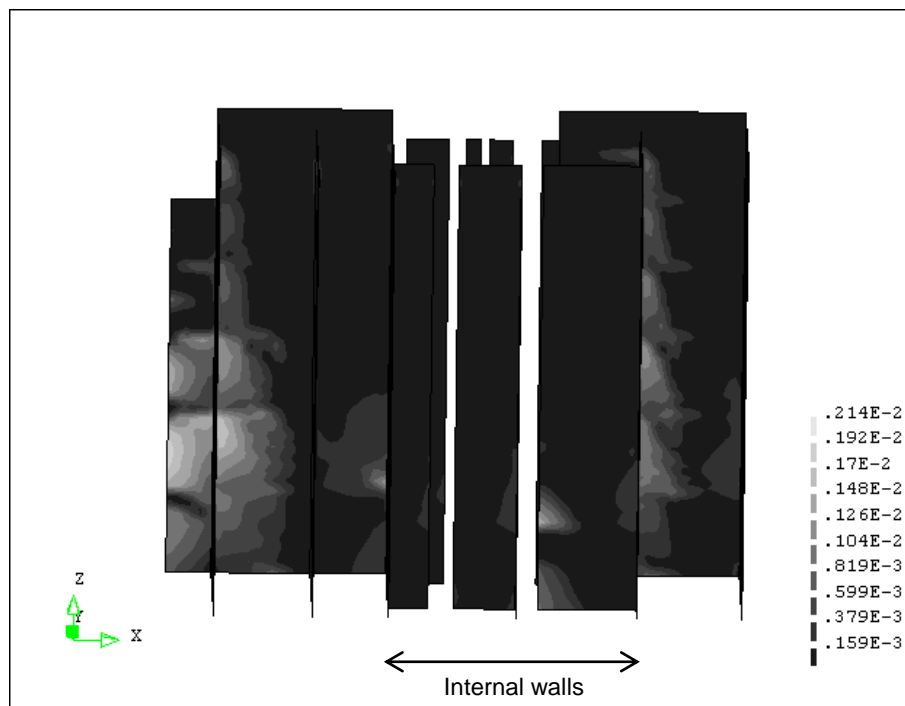


Figure 7.27: Maximum principal strains at substantial damage state, internal view – Case 3

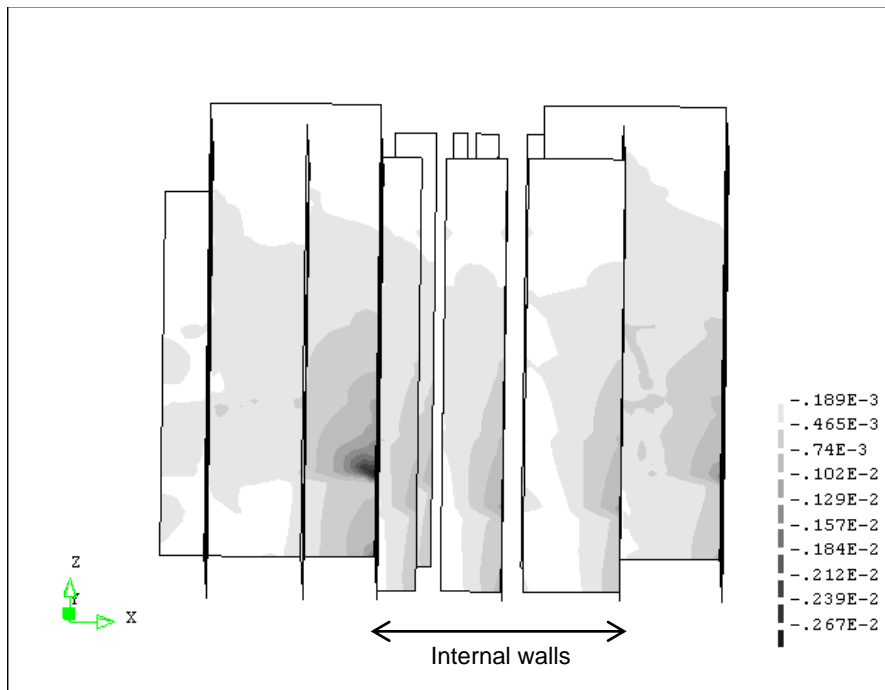


Figure 7.28: Minimum principal strains at substantial damage state, internal view – Case 3

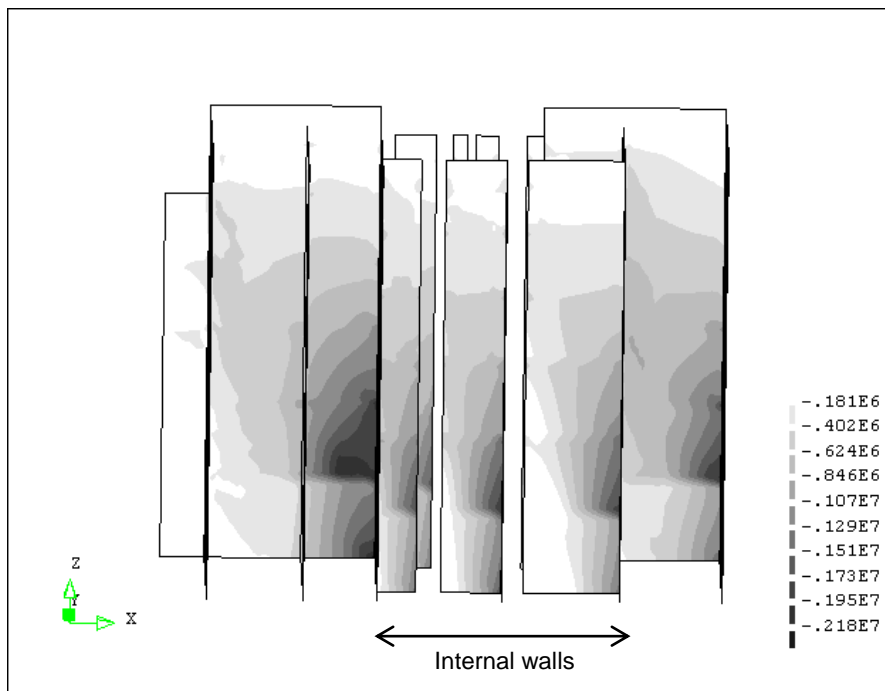


Figure 7.29: Minimum principal stresses at substantial damage state, internal view – Case 3

In summary, the modified load pattern had little effect on the overall building response. The effects on the base shear force and hence the elastic period are caused by a greater concentration of loading at lower levels with a linear load distribution and have little effect on building performance. Strain and stress patterns concur with the substantial damage level to be expected by the demand displacement.

7.5.4 Case 4 and Case 5

Case 4 and Case 5 were analysed with modal load distributions in the negative longitudinal direction, the only difference between the cases in the element size.

As was found for Cases 1 and 2, there was very little difference in the calculated response of the structure. The only difference was a slight increase in total base shear and compressive stresses, presumably due to an increased number of nodes in the analysis. Given the similarities, the results for Case 4 have been presented below.

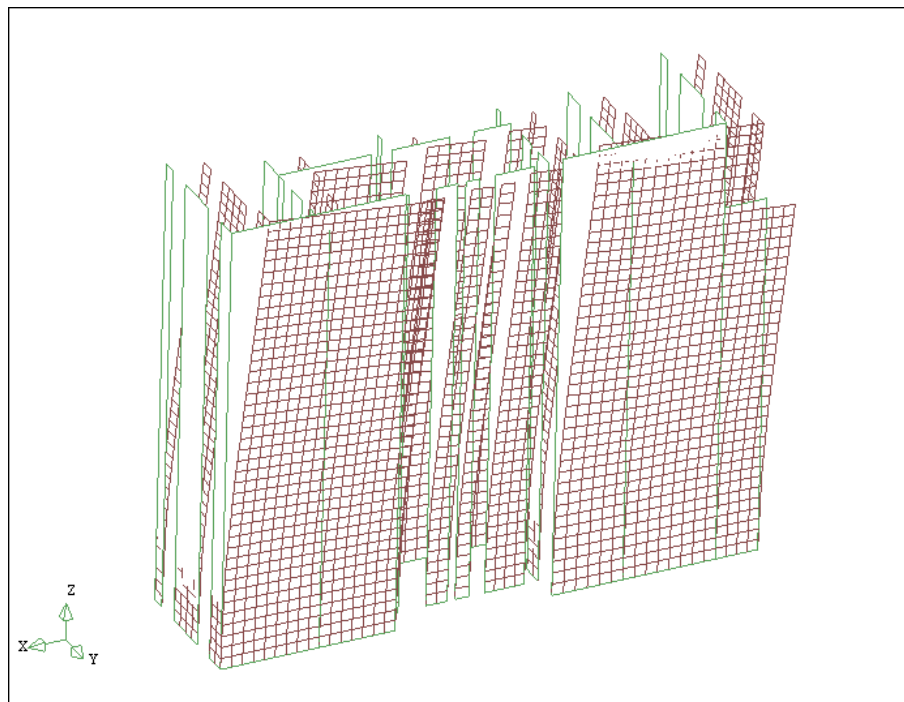


Figure 7.30: Deflected shape at yield – Case 4

As for Cases 1 and 2, the shape of the deflections was reviewed both at yield and within the inelastic range. Similarly to previous results, the deflections correspond well to the modal shape.

The pushover curve obtained for Case 4 and the calculated idealised bilinear pushover curve are shown in Figure 7.31. The curve is extremely similar in form to that of previous cases, with only minor unloading occurring in the inelastic range. The maximum lateral force and displacement at yield are approximately 5% greater than for loading in the positive longitudinal direction. Non-convergence of Case 4 occurred at an ultimate displacement of 365mm. For Case 5, non-convergence occurred at a displacement of 417mm, presumably due to the better distribution of stresses with the larger number of nodes.

The capacity spectrum was developed using the idealised bilinear curve and is plotted below in ADRS format in comparison with the seismic demand curves for the Eixample district (Figure 7.32). The displacement demand results for each seismic scenario are presented in Table 7.10.

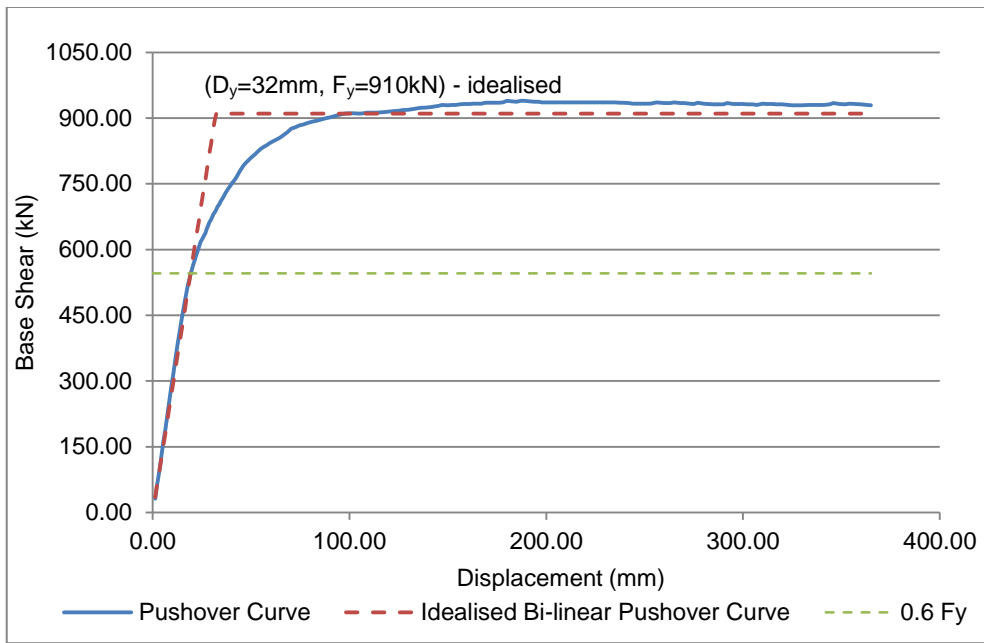


Figure 7.31: Pushover curve – Case 4

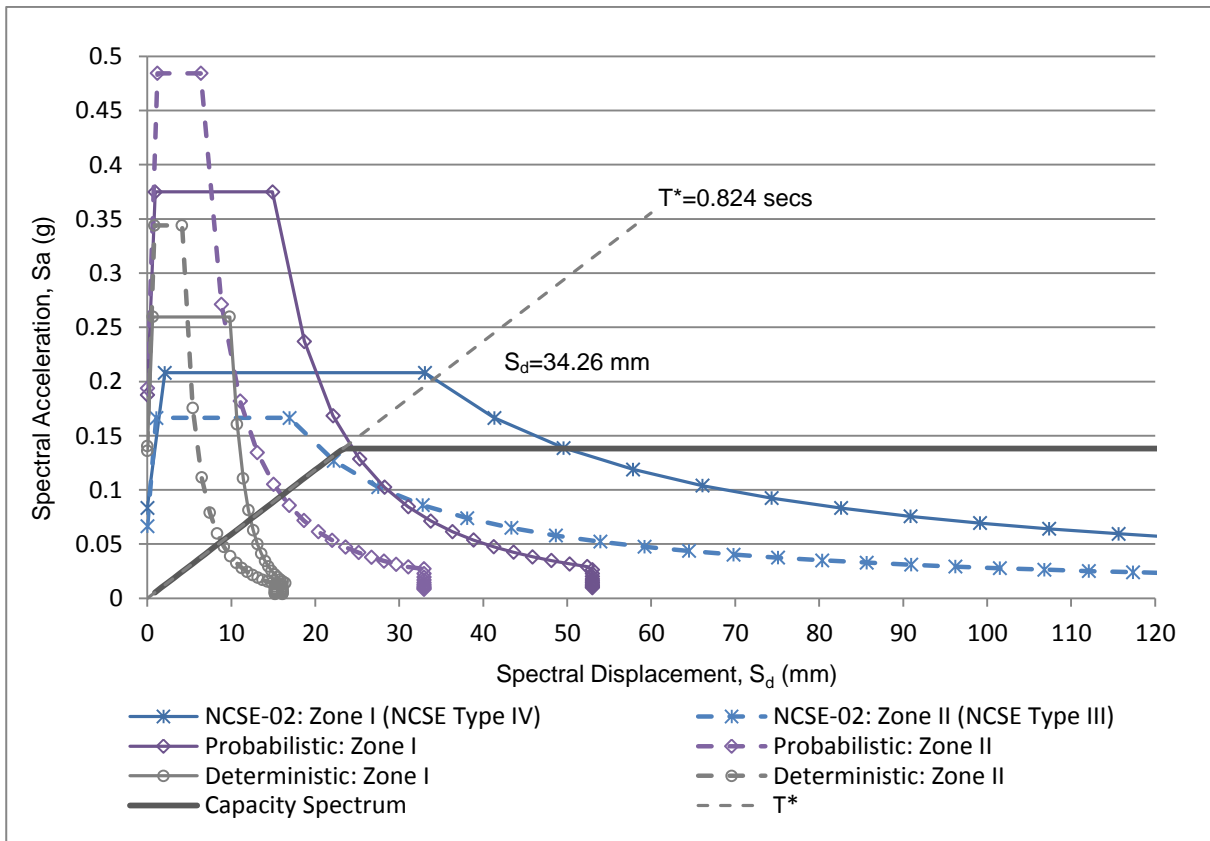


Figure 7.32: Comparison of capacity spectrum and demand spectra – Case 4

Table 7.10: Results of displacement demand – Case 4

Seismic Scenario	Spectral Displacement (mm)	Displacement Demand (mm)	Damage Classification to EMS98
Deterministic - Soil Zone II	8.88	12.18	Slight
Deterministic - Soil Zone I	12.44	17.06	Slight
Probabilistic - Soil Zone II	16.11	22.10	Slight
Probabilistic - Soil Zone I	24.40	33.47	Moderate
NCSE-02 - Soil Zone II (NCSE Soil Type III)	21.93	30.08	Moderate
NCSE-02 - Soil Zone I (NCSE Soil Type IV)	34.26	46.99	Substantial

Similarly to previous cases, the displacement demand is governed by the NCSE-02 seismic scenario in soil Zone I (NCSE soil Type IV), it occurs in the inelastic range of the building response. Displacement demand is 47.0mm for Case 4 and 47.3mm for Case 5. These values relate to a substantial level of damage to EMS-98 gradings. Moderate damage is again estimated from both the NCSE-02 scenario in soil Zone II (NCSE soil Type III), and the probabilistic scenario in soil Zone I. The elastic period (T^*) is greater than the characteristic periods of the demand spectra, so the elastic and inelastic spectral displacement demands are equal.

The maximum and minimum principal strains and principal stresses at the substantial damage state are presented below.

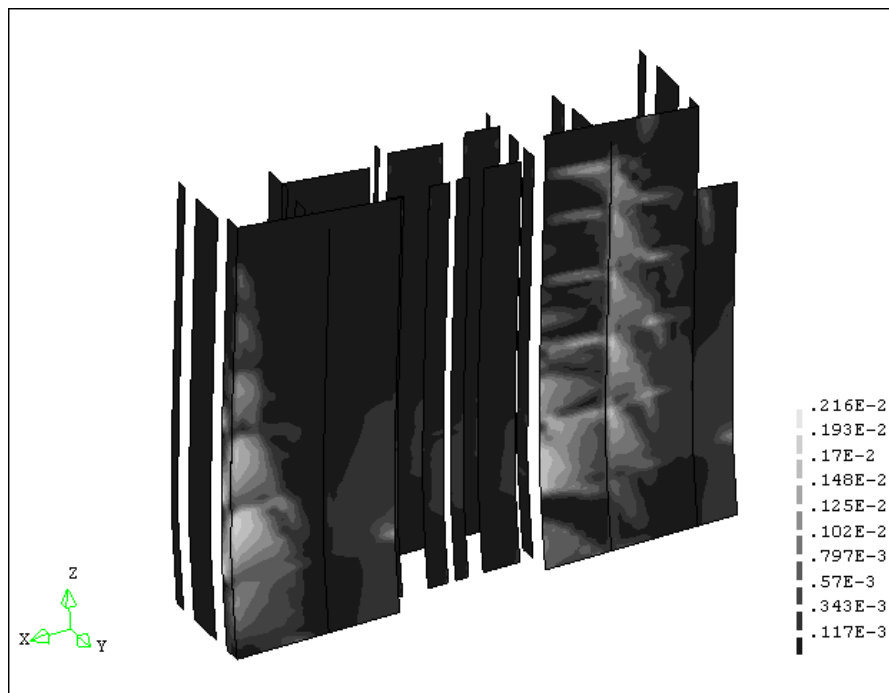


Figure 7.33: Maximum principal strains at substantial damage state – Case 4

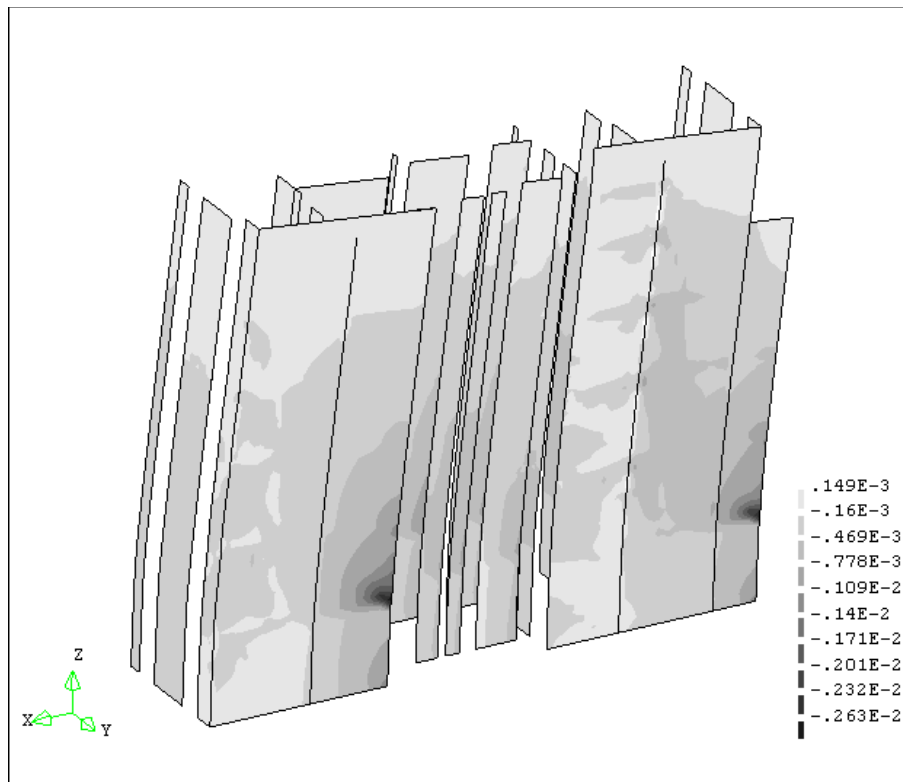


Figure 7.34: Minimum principal strains at substantial damage state – Case 4

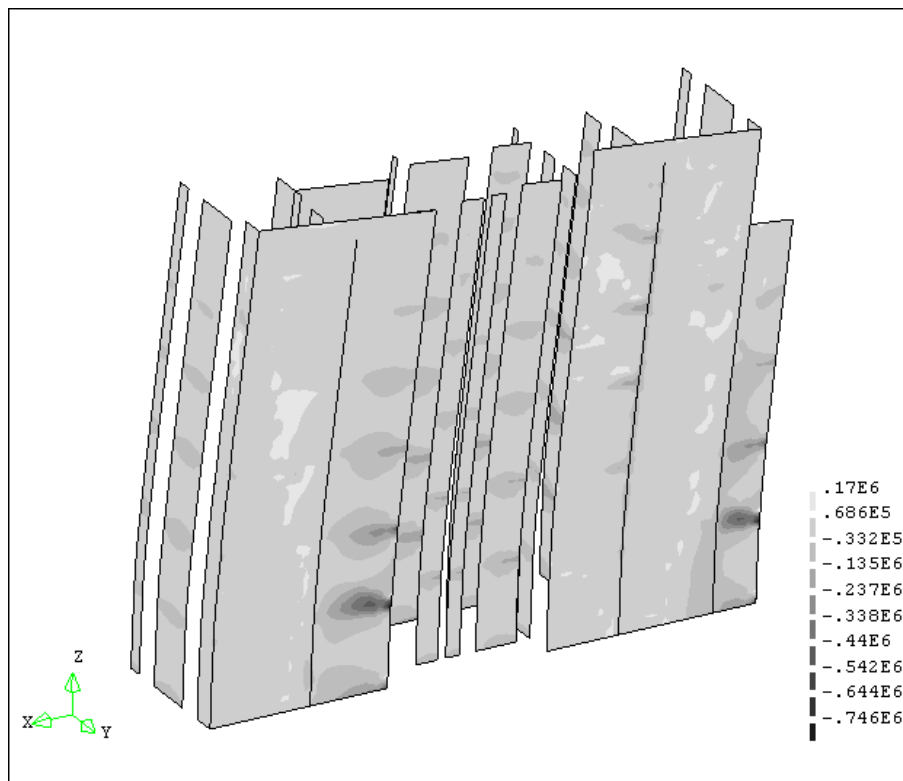


Figure 7.35: Maximum principal stresses at substantial damage state – Case 4

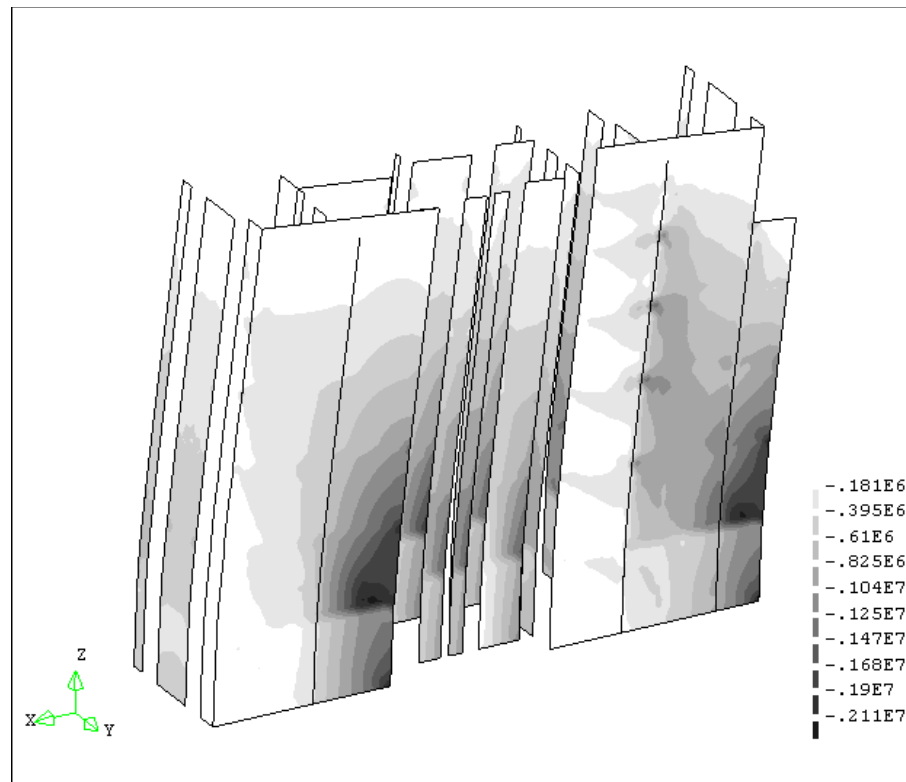


Figure 7.36: Minimum principal stresses at substantial damage state – Case 4

The patterns of maximum and minimum principal strains describe well the state of damage for these loading cases. Maximum principal strains in the order of 0.0017 are common at both first and second floor levels indicating cracking at one side of each critical longitudinal wall panel (Figure 7.33). This strain equates to a deformation of about 6mm between floor levels which correlates to the classification of substantial damage to EMS-98 at this loading. Crushing of a similar magnitude can be determined from the minimum principal strains in Figure 7.34.

The strains and stresses at ground level are lower as the ground floor walls are double the thickness of the walls above.

The cracked condition determined by the pattern of maximum principal strains is confirmed by few areas of tensile stresses in the pattern of maximum principal stresses (Figure 7.35). Similar to previous cases, this is due to tension stresses being relieved by the cracked state of the masonry. Compressive stresses are about 2MPa, which describes a significant compressive state for the masonry which has a nominated compressive strength of 1.8MPa.

In summary, although the load direction of Cases 4 and 5 is opposite that of Cases 1 and 2, the displacement demand and damage classifications for each seismic scenario are almost identical. The patterns of strains and stresses in the inelastic range correspond well to the expected damage condition.

7.5.5 Case 6

Case 6 is for a linear load distribution to Model 1 in the negative longitudinal direction.

The deformed shape is comparable to that of Cases 4 and 5, with loading in the same direction, and as expected it describes an inertial response in accordance with modal deformation. The original and bilinear pushover curves are shown below (Figure 7.37). The base shear force is higher than for the modal load distribution, due to the increased loads at the lower levels from the linear distribution. Hence the idealised elastic stiffness is higher than for Cases 4 and 5, and the elastic period (T^*) is lower. The form of the pushover curve is similar to those of the previous cases. An ultimate displacement of 400mm was calculated at non-convergence of the analysis.

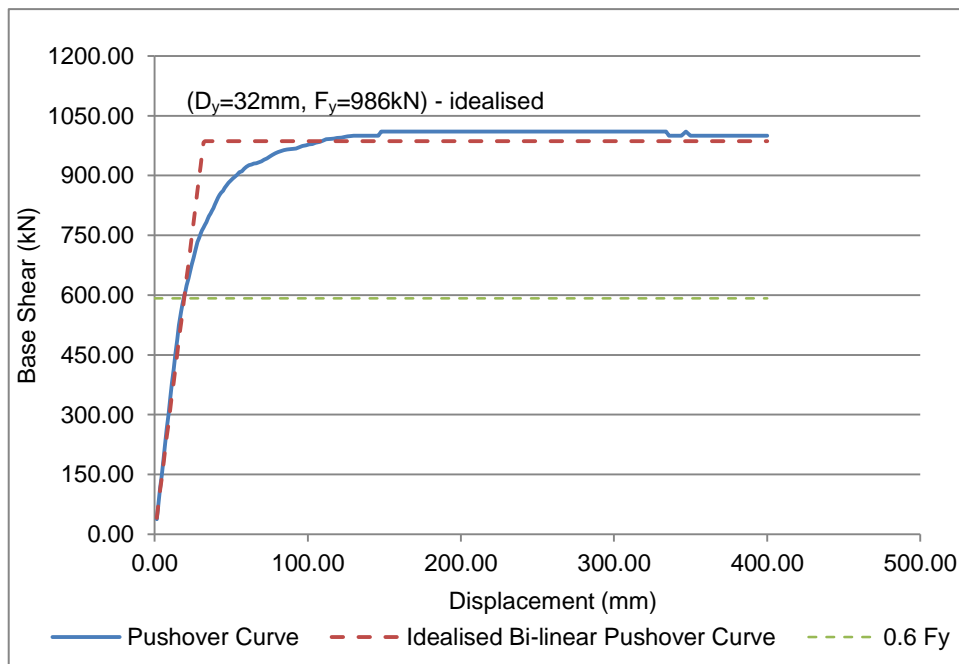


Figure 7.37: Pushover curve – Case 6

A comparison of the capacity spectrum to the seismic hazard is presented below (Figure 7.38). Similarly to the previous cases, the NCSE-02 scenario in soil Zone I (NCSE soil Type IV) governs the displacement demand. This demand corresponds to a moderate-substantial damage level in accordance with EMS-98.

Similarly to Case 3, the lower elastic period results in an intersection with the NCSE-02 demand curve in the region of constant acceleration. As such, calculation of the spectral displacement requires transformation of the demand spectrum from elastic to inelastic. The resultant inelastic spectrum is also presented on Figure 7.38.

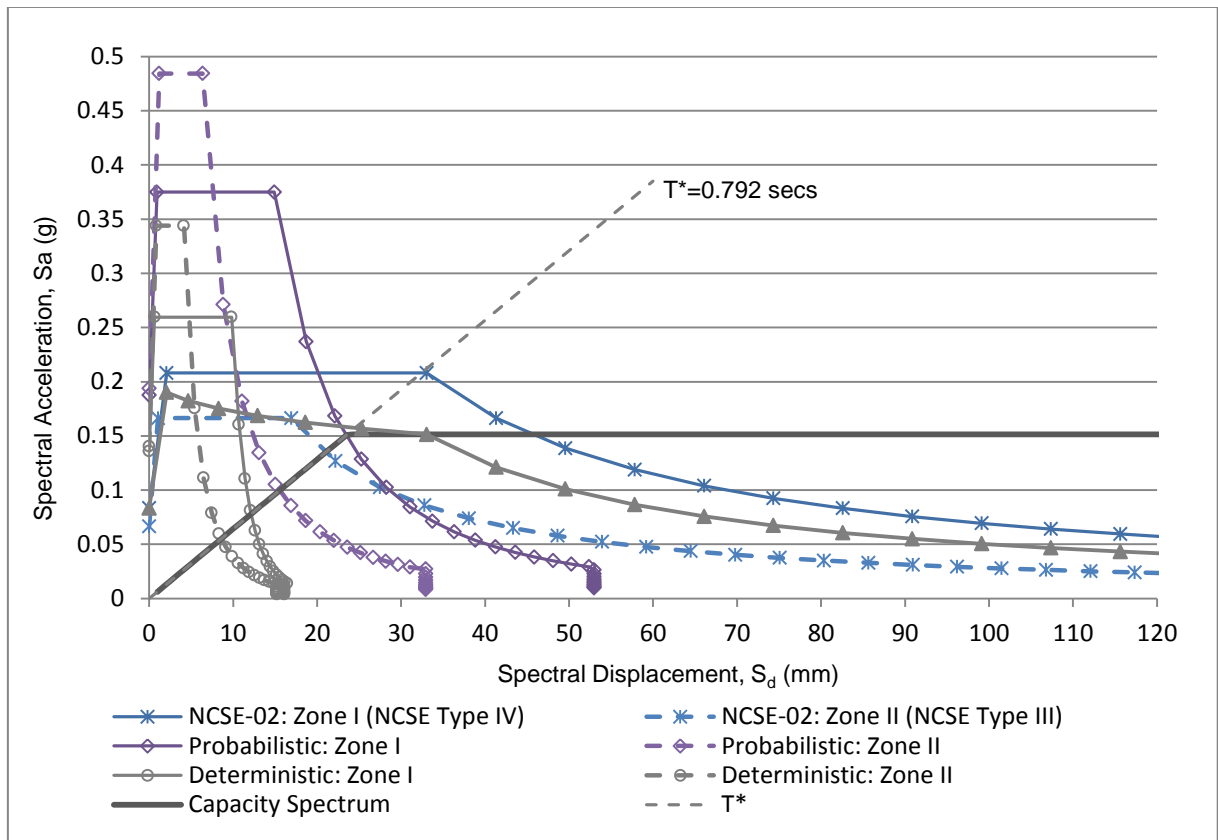


Figure 7.38: Comparison of capacity spectrum and demand spectra – Case 6

Table 7.11: Results of displacement demand – Case 6

Seismic Scenario	Spectral Displacement (mm)	Displacement Demand (mm)	Damage Classification to EMS98
Deterministic - Soil Zone II	8.67	11.76	Slight
Deterministic - Soil Zone I	12.21	16.57	Slight
Probabilistic - Soil Zone II	15.62	21.19	Slight
Probabilistic - Soil Zone I	23.76	32.23	Moderate
NCSE-02 - Soil Zone II (NCSE Soil Type III)	21.24	28.81	Moderate
NCSE-02 - Soil Zone I (NCSE Soil Type IV)	32.50	44.09	Moderate - Substantial

The maximum and minimum principal strains and principal stresses were derived and found to be of the same form and magnitude to those of Cases 4 and 5. Hence, as for lateral loading in the positive direction, the lateral loading in the negative direction has no measurable effect on building response compared to modal load distribution. In summary, the displacement demand level and building response of Case 4 are comparable to those calculated for a modal load distribution.

7.5.6 Case 7

Case 7 considers a modal load distribution in the positive longitudinal direction to Model 2, the model without internal transverse ground floor walls. A modal load distribution was used, as it was found in previous cases that this best approximates the inertial response of the structure.

The deflected shape is shown below (Figure 7.39). As expected, the shape conforms well to a modal distribution.

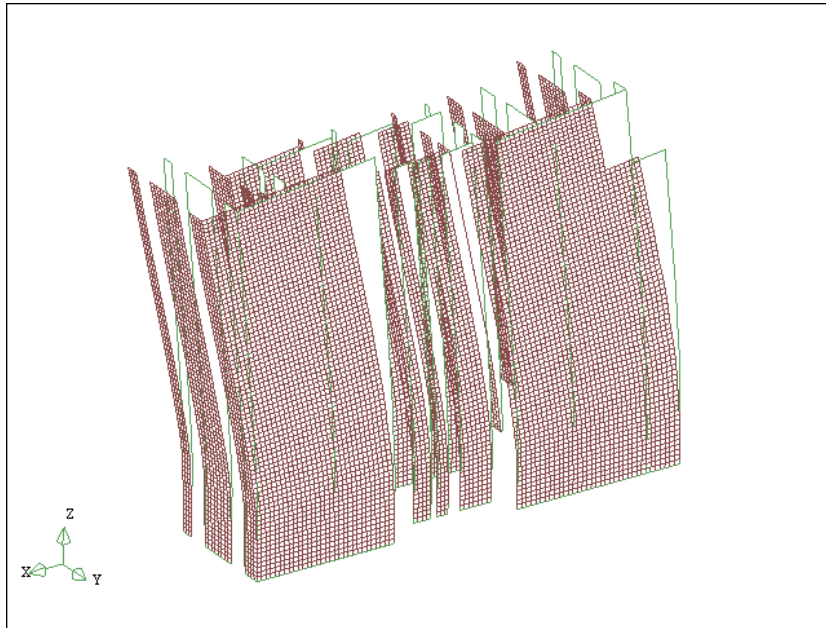


Figure 7.39: Deflected shape – Case 7

The pushover curve obtained for Case 7 and the calculated idealised bilinear pushover curve are shown in Figure 7.40. The pushover curve is extremely regular, with only minor unloading occurring in the inelastic range. The ultimate displacement recorded was 351mm which was characterised by non-convergence of the analysis. The maximum base shear force is lower than for Case 1 and Case 2, presumably because the force is concentrated within fewer walls at ground level. This has slightly reduced the elastic period in comparison to Cases 1 and 2.

The comparison of the capacity spectrum to the seismic demand for the Eixample district is presented in Figure 7.41. Displacement demand results for each seismic scenario are presented in Table 7.12. As the elastic period is slightly lower than for Cases 1 and 2, the demands are also slightly lower, however the damage levels remain the same.

The results indicate that the governing seismic scenario is the same as for all previous cases, the NCSE-02 seismic scenario in soil Zone I (NCSE soil Type IV). This demand occurs in the inelastic range of the building response. The displacement demand is 46.08mm and constitutes a substantial level of damage to EMS-98 gradings. A moderate level of damage is estimated from both the NCSE-02 scenario in soil Zone II (NCSE soil Type III), and the probabilistic scenario in soil Zone I.

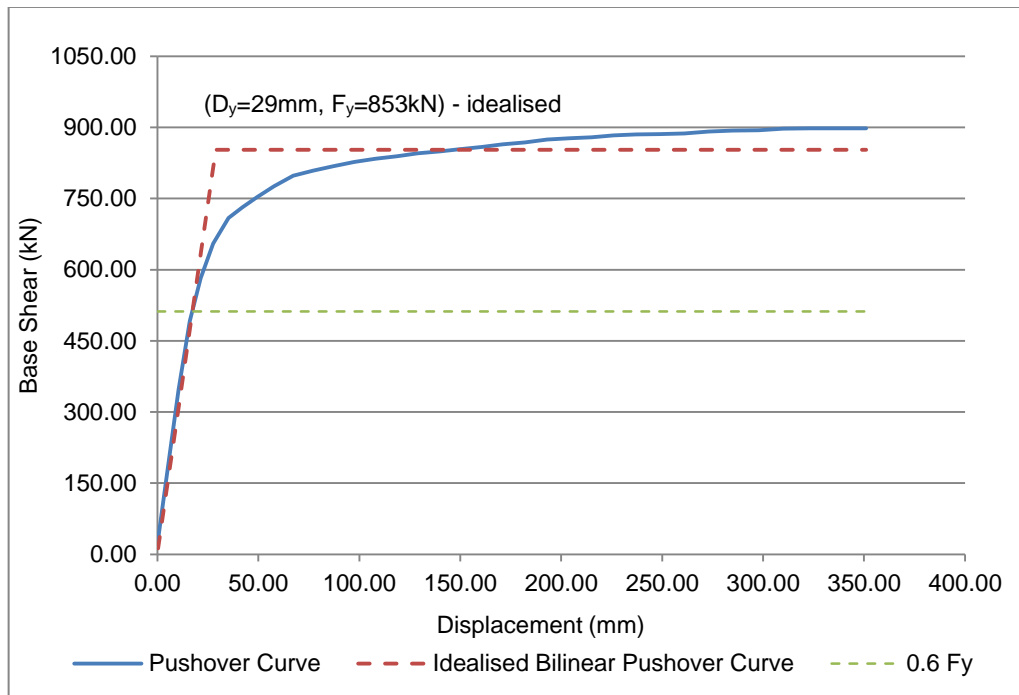


Figure 7.40: Pushover curve – Case 7

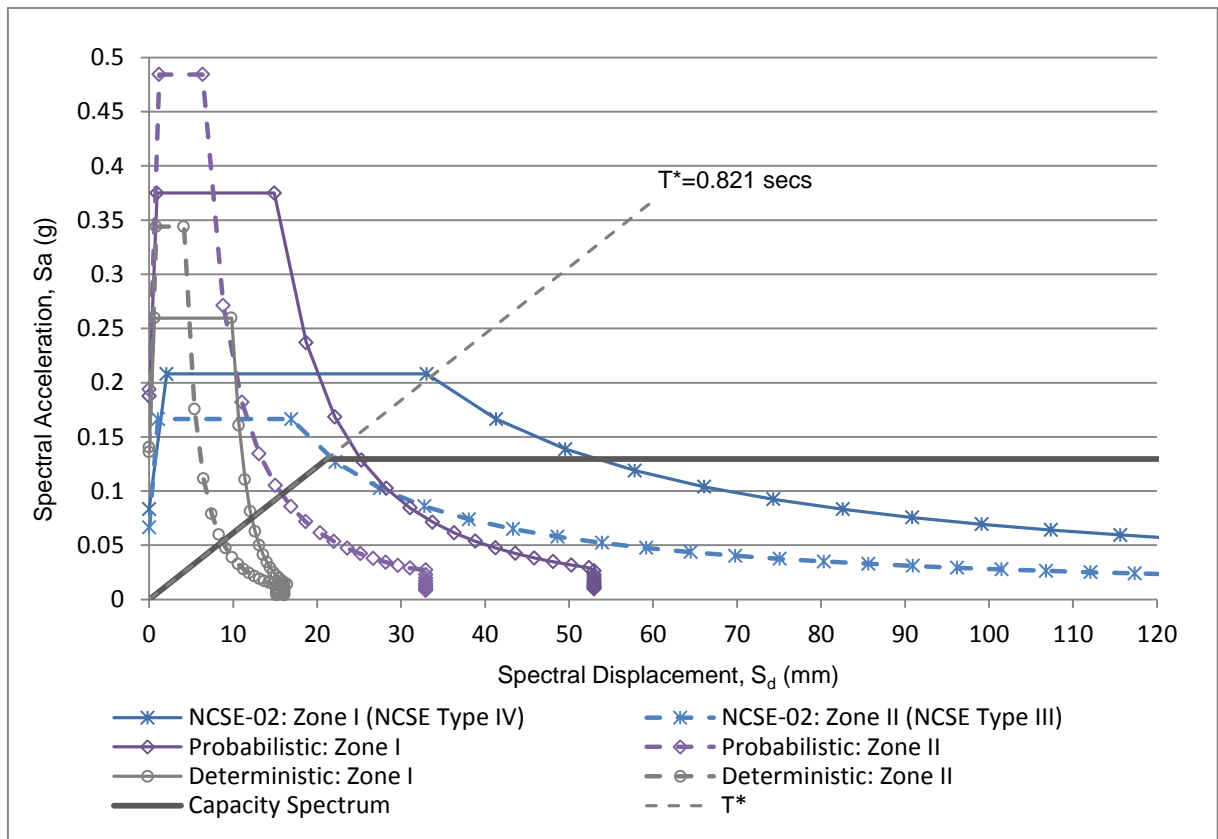


Figure 7.41: Comparison of capacity spectrum and demand spectra – Case 7

Table 7.12: Results of displacement demand – Case 7

Seismic Scenario	Spectral Displacement (mm)	Displacement Demand (mm)	Damage Classification to EMS98
Deterministic - Soil Zone II	8.80	12.07	Slight
Deterministic - Soil Zone I	12.35	16.94	Slight
Probabilistic - Soil Zone II	15.91	21.83	Slight
Probabilistic - Soil Zone I	24.14	33.11	Moderate
NCSE-02 - Soil Zone II (NCSE Soil Type III)	21.65	29.69	Moderate
NCSE-02 - Soil Zone I (NCSE Soil Type IV)	33.59	46.08	Substantial

The following figures present the maximum and minimum principal strains and principal stresses in the structure corresponding to the substantial damage state level. The pattern and magnitude of the strains and stresses are similar to that for Cases 1, 2 and 3, with loading in the same direction. This is to be expected, as the removed walls were perpendicular to the loading, hence the building stiffness in the load direction is practically unchanged with their removal.

As for the previous cases, maximum and minimum principal strains in the order of ± 0.0015 are clear at first floor level. These strains equate to cracking and crushing in the order of 5mm between floor levels which verifies the classification of substantial damage at this displacement demand.

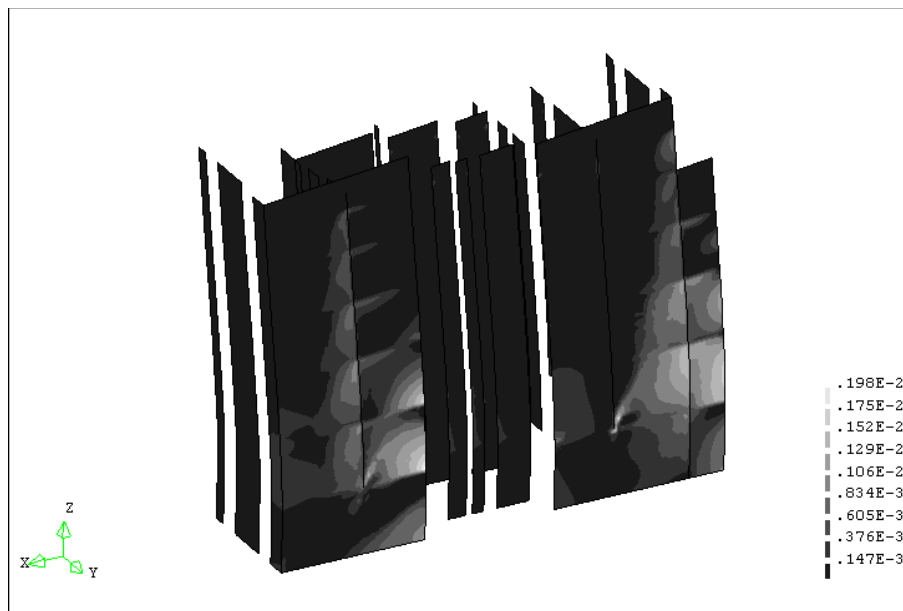


Figure 7.42: Maximum principal strains at substantial damage state – Case 7

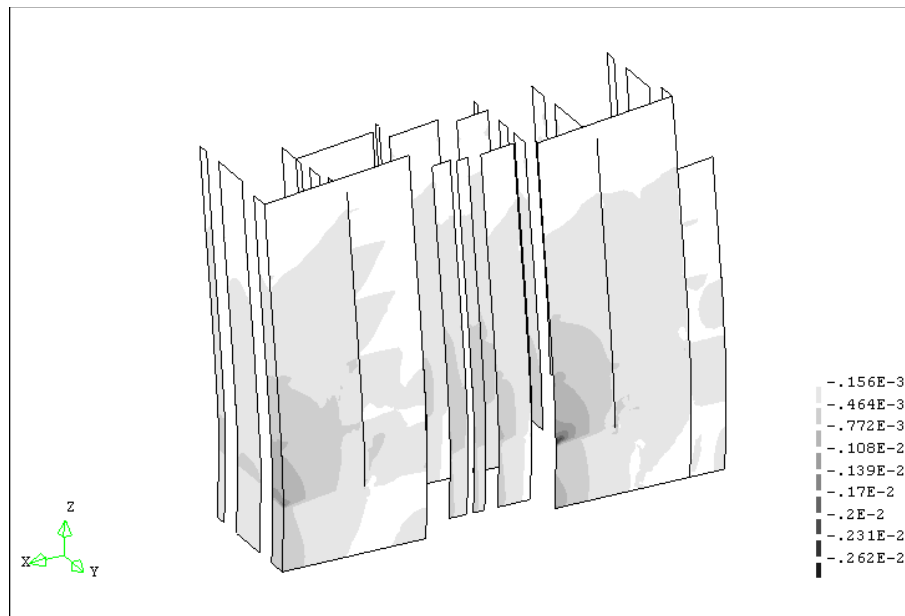


Figure 7.43: Minimum principal strains at substantial damage state – Case 7

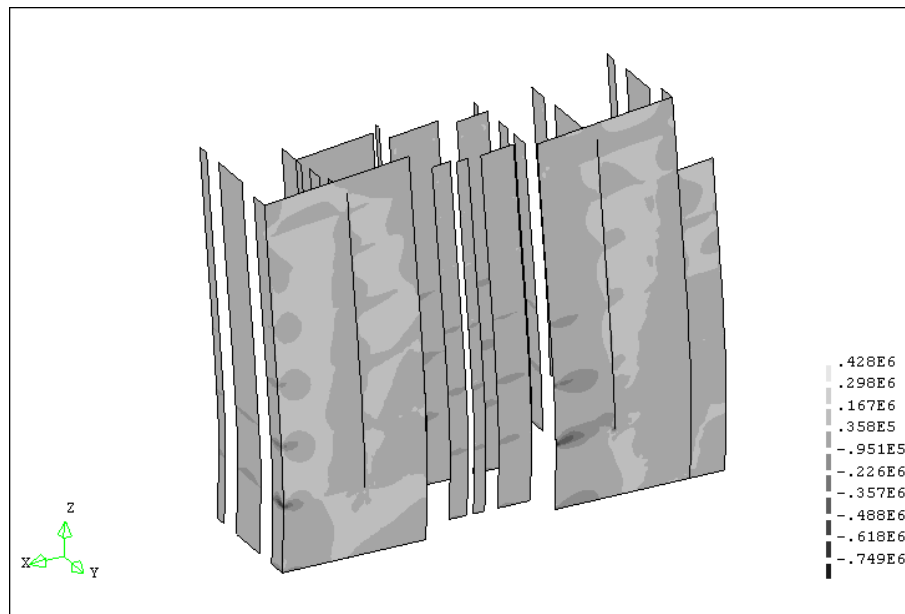


Figure 7.44: Maximum principal stresses at substantial damage state – Case 7

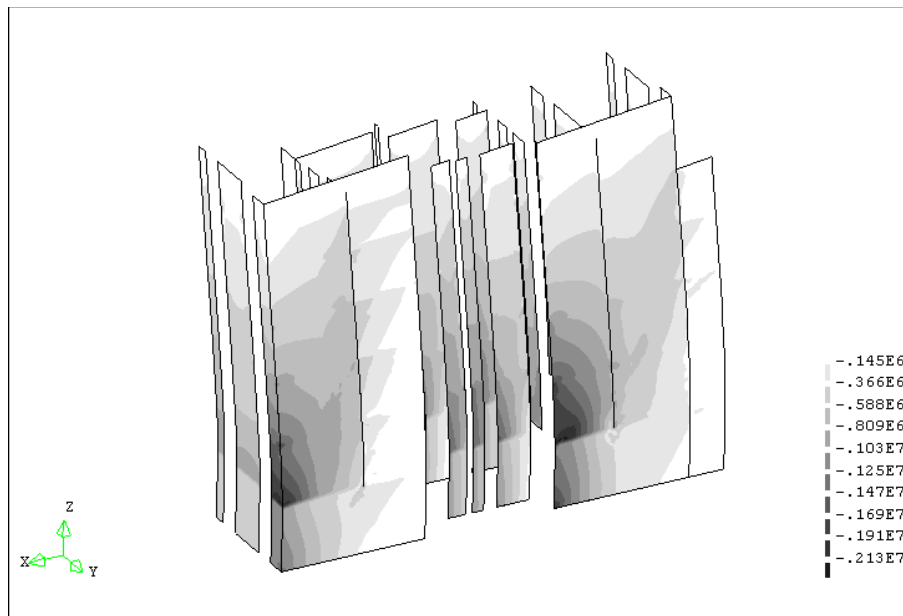


Figure 7.45: Minimum principal stresses at substantial damage state – Case 7

Similar to Cases 1, 2 and 3, the maximum principal stresses highlight only isolated sections of masonry that remain in tension at this damage level. This is likely to be due to the cracked nature of the wall, as illustrated by the maximum principal strain diagram, which has released the tensile stresses. The maximum compressive stresses at first floor level are in the order of 1.5MPa to 2MPa which, similarly to the minimum principal strain diagram, indicates crushing of the masonry which has an attributed compressive strength of 1.8MPa.

In summary, the removal of the transverse walls at ground floor level has had no significant effect on the longitudinal building response to seismic actions. The displacement demand is therefore comparable to that of Cases 1 and 2, with a value of 46mm which equates to a substantial level of damage to EMS-98. As for previous cases, the patterns of principal strains and stresses concur with the expected building response. They indicate significant damage to wall panels at the demand displacement and justify the damage level classification.

7.5.7 Case 8

Case 8 considers a modal load distribution in the negative longitudinal direction to Model 2, the model without internal transverse ground floor walls. The deflected shape is shown below (Figure 7.46), which conforms well to a modal distribution.

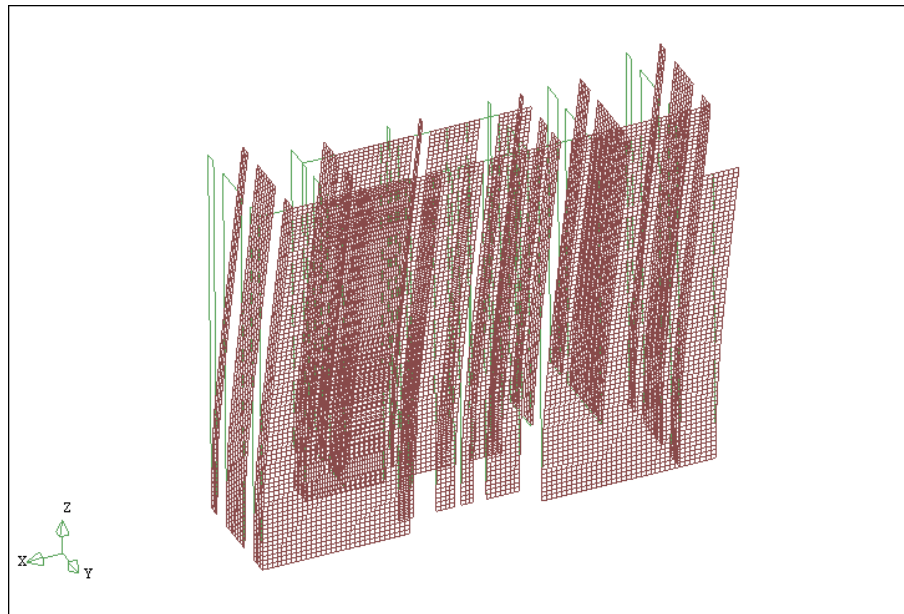


Figure 7.46: Deflected shape – Case 8

The pushover and idealised bilinear pushover curves obtained for Case 8 are shown in Figure 7.47. Similar to previous cases, the pushover curve is extremely regular, with only minor unloading occurring in the inelastic range. The ultimate displacement recorded was 340mm which was characterised by non-convergence of the analysis. The maximum base shear force is lower than for Cases 4 and 5 which have the same loading characteristics. Similar to Case 7, this is presumably because the force is concentrated within fewer walls at ground level. This reduction has slightly reduced the elastic period in comparison to Cases 4 and 5.

Comparison of the capacity spectrum to the seismic demand for the Eixample district is presented in Figure 7.48. Displacement demand results for each seismic scenario are presented in Table 7.13. As the elastic period is slightly lower than for Cases 4 and 5, the demands are also slightly lower, however the damage levels remain the same.

Similar to previous cases, the governing seismic scenario is the NCSE-02 seismic scenario in soil Zone I (NCSE soil Type IV). This demand occurs in the inelastic range of the building response. The displacement demand is 47.96mm and constitutes a substantial level of damage to EMS-98 damage classification. A moderate level of damage is estimated from both the NCSE-02 scenario in soil Zone II (NCSE soil Type III), and the probabilistic scenario in soil Zone I.

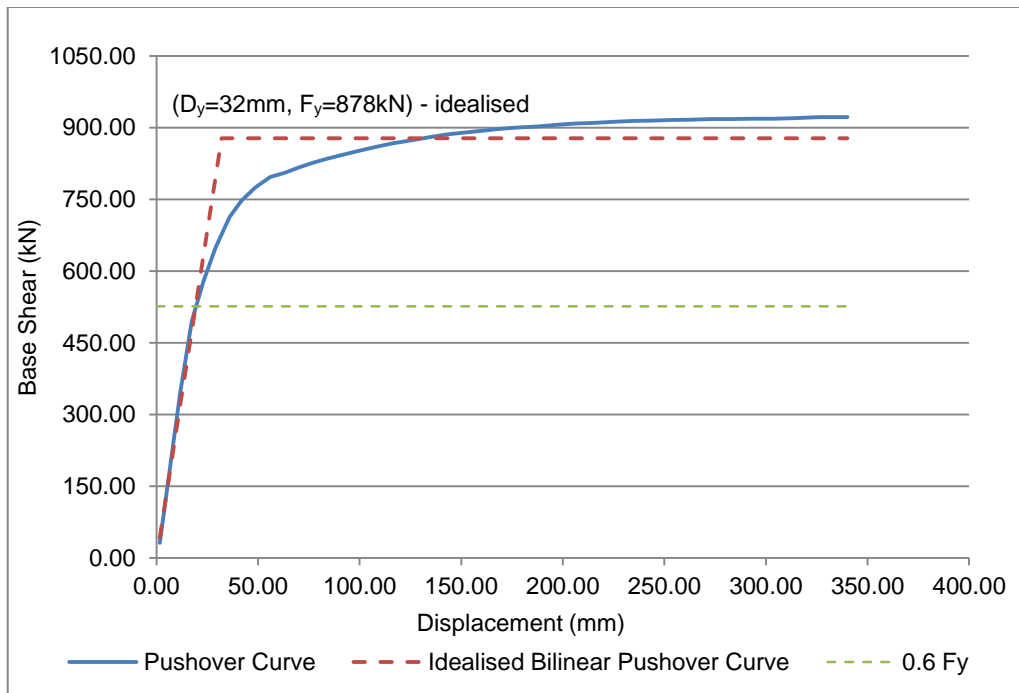


Figure 7.47: Pushover curve – Case 8

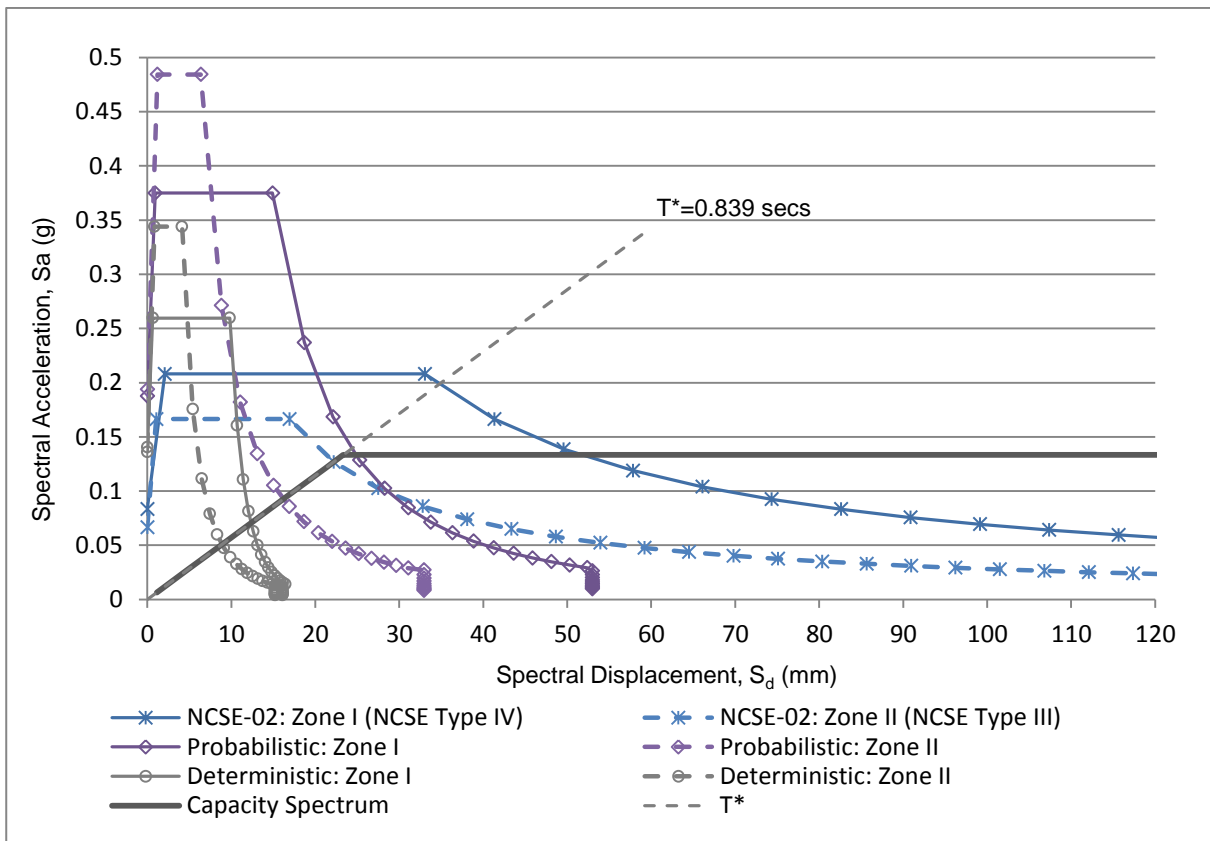


Figure 7.48: Comparison of capacity spectrum and demand spectra – Case 8

Table 7.13: Results of displacement demand – Case 8

Seismic Scenario	Spectral Displacement (mm)	Displacement Demand (mm)	Damage Classification to EMS98
Deterministic - Soil Zone II	8.96	12.29	Slight
Deterministic - Soil Zone I	12.51	17.16	Slight
Probabilistic - Soil Zone II	16.32	22.38	Slight
Probabilistic - Soil Zone I	24.65	33.81	Moderate
NCSE-02 - Soil Zone II (NCSE Soil Type III)	22.21	30.47	Moderate
NCSE-02 - Soil Zone I (NCSE Soil Type IV)	34.97	47.96	Substantial

The maximum and minimum principal strains and stresses were reviewed and compared to the results of Cases 4 and 5 with the same loading conditions. The patterns of both the strains and stresses were in principle the same. This is reasonably expected, as the stiffness in the load direction has not altered with removal of the transverse walls. For a discussion of these results, refer to Section 7.5.4.

Similarly to Case 7, the removal of the transverse walls at ground floor level has had no significant effect on the building's longitudinal response to seismic actions. The displacement demand is therefore comparable to that of Cases 4 and 5, with a value of 48mm which equates to a substantial level of damage to EMS-98.

7.6 Discussion of Results

A number of general conclusions can be made from the results of the seismic analysis, as follows:

- For both modal and linear lateral load distributions, the deflected shape of the structure approximated that of the primary mode shape. Hence, a modal distribution better describes the inertial response of the structure.
- Displacement demand derived for linear load distributions was consistently lower than for modal load distributions. This is caused by an increased base shear reaction which lowers the calculated elastic period (T^*). Hence they provide a less conservative estimate of the displacement demand than for a modal distribution.
- The overall building response to seismic actions and the resultant damage level classification were not affected by the selected variations in lateral load distribution and element size.
- Building response to positive and negative longitudinal directions of load was similar. This is due to the regular, almost symmetrical, layout of the building in the longitudinal direction.
- Longitudinal building response was not significantly affected by removal of ground floor transverse walls, as the building stiffness in the load direction is largely unchanged.

As each analysis case provided reasonably consistent results, the following conclusions can be made with respect to the seismic demand at the site.

- For a typical unreinforced masonry building in soil Zone I (NCSE-02 soil Type IV), the critical seismic scenario is that of the Spanish code (NCSE-02, 2002). The displacement demand for this scenario is for approximately 45mm longitudinal deflection at roof level. The damage level classification is substantial, according to the European Macroseismic Scale (EMS-98). The probabilistic scenario estimates a moderate level of damage with a displacement demand of approximately 33mm, whilst the deterministic scenario estimates slight damage and is in the elastic range of the capacity spectrum. These damage level classifications are the same as those of previous studies on these buildings (Pujades et al., 2010).
- For a typical construction in soil Zone II (NCSE-02 soil Type III), the critical seismic scenario is also derived from the Spanish code (NCSE-02, 2002). For this scenario, the displacement demand is approximately 30mm and the EMS-98 classification is for a moderate level of damage. Both probabilistic and deterministic scenarios estimate slight damage in the elastic range.
- The results support the vulnerability of these buildings to seismic damage identified by previous assessments. The variations in seismic demand are also in accordance with previous studies of seismic actions in Barcelona (Barbat et al., 2006; Irizarry et al., 2011).
- In all analysis cases, the patterns and magnitudes of principal strains and stresses concur with the expected building response and the damage level at the displacement demand.

The critical locations of the structure are at each end of the perimeter longitudinal wall panels and particularly at levels one and two. It is in these locations that the greatest strains and stresses were observed and hence are the areas that would experience the most damage. To minimise the risk of seismic damage, these critical elements should be regularly inspected to identify existing damages and alterations. Remedial works can then be completed as required to ensure their integrity.

7.7 Results of Kinematic Limit Analysis

The kinematic limit analysis on the building was completed as part of a concurrent study (Silva, 2011). As discussed in Section 2.9.1, the results are based upon linear and geometrically non-linear analysis of a set of possible local failure mechanisms for the structure. Results are then presented in terms of a relative capacity coefficient, either as a percentage of the ground acceleration to instigate failure (in a linear analysis), or as a percentage of displacement demand (for a geometrically non-linear analysis).

The kinematic analysis identified out-of-plane collapse mechanisms for two of the seismic scenarios. In-plane collapse mechanisms were found to be satisfactory for all scenarios.

1. The earthquake scenario derived from NCSE-02 in soil Zone I (NCSE-02 soil Type IV) resulted in overturning of two types of mechanisms:
 - Out-of-plane rotation of the façade walls and vertical separation of the walls within the width of the façade.
 - Out-of-plane rotation of a triangular shaped macro-element at the façade walls.
2. The probabilistic seismic scenario in Zone I instigated one out-of-plane failure:
 - Out-of-plane rotation of a triangular shaped macro-element at the upper level of the façade walls.

These results suggest that out-of-plane failure of local mechanisms for these seismic scenarios may occur concurrently with the significant damage calculated by the non-linear pushover analysis. Hence partial local collapse may be expected before the structure obtains the displacements calculated by the non-linear pushover analysis.

It should be noted that the kinematic limit analysis has assumed no restraint action at the floor or roof levels. Hence, the results may represent a conservative estimate of the possibility of developing local failures.

This page is left blank on purpose.

8. CONCLUSIONS

In this study, a seismic analysis was successfully completed for a typical unreinforced masonry building of the Eixample district, Barcelona. The analysis used a non-linear pushover approach and a capacity spectrum methodology. By doing so, it considered the global response of the building to a range of seismic scenarios. The results indicate that the building typology is at risk of significant damage during a seismic event.

Displacement demands were calculated for seismic scenarios based upon deterministic, probabilistic and current European code approaches. These demands were then correlated to an estimated level of damage as classified by the European Macroseismic Scale (EMS-98).

Results indicated that displacement demands from the Spanish seismic code (NCSE-02, 2002) corresponded to a substantial damage level in Zone I soils (NCSE-02 soil Type IV) and a moderate damage level in soil Zone II (NCSE-02 soil Type III). These results support the vulnerability of the buildings to seismic damage identified by previous studies (Pujades et al., 2010).

Seismic scenarios by other approaches returned lower estimates of damage. The probabilistic approach estimated moderate damage for Zone I and slight damage for Zone II, while a deterministic approach estimated slight damage for each soil zone. This variation in seismic demand is in accordance with previous studies of seismic actions in Barcelona (Barbat et al., 2006; Irizarry et al., 2011).

The seismic analysis formed only one part of a broader structural assessment completed for the buildings in the Eixample district. The assessment methodology was based upon the recommendations and guidelines for structural assessment by ISCARSAH (2005). For this study, key components of the assessment methodology were the following:

- A historical investigation which provided the understanding of the development of the Eixample district, and the influence of its planning on the building typologies.
- A geometrical, structural systems and materials survey. From this survey, a mathematical model was created that accurately represented the typical buildings of the district.
- Definition of actions and likely damages. As part of this task, a seismic hazard analysis was applied following the recommendations of the RISK-UE project (2004) and data from previous assessments (Irizarry, 2004). As a result, demand spectra for a range of seismic scenarios were obtained for the district.

A number of primary conclusions can also be drawn from the pushover analysis procedure, as follows:

- The deflected shape of the structure approximated that of the primary mode shape. Hence, a modal load distribution better describes the inertial response of the structure. The modal

lateral load distribution returned slightly larger displacement demands in comparison to a linear lateral load distribution.

- The non-linear model described well the expected building response of the damage level at the demand deflection.
- Removal of ground floor transverse walls did not significantly affect the longitudinal building response, as the building stiffness in the load direction is largely unchanged.

Limitations and uncertainties of the non-linear finite element modelling should also be considered. There were a number of assumptions in the geometrical representation of the building. In particular, the floors were assumed to act as horizontal rigid diaphragms and to be securely attached to the walls. In reality, there is likely to be a degree of deformation within the floor structure during a seismic event, both between the walls and at the wall connections. These deformations will dissipate energy but will concurrently cause damage to the structure. Limited lateral restraint to the walls also suggests the possibility of increased damage to the wall elements due to out-of-plane deformations.

Another inherent limitation of the analysis is the estimation of ultimate capacity which was determined by non-convergence. Although the majority of ultimate displacements obtained were similar, it is possible that alternate load stepping may provide different results.

Critical structural elements were identified during the review of the pushover analysis results. These elements are the façade and internal void ends of the perimeter longitudinal walls, particularly at first and second floor levels. It is recommended that these elements be regularly inspected for damage and alterations, and maintained in good condition to limit the risk of seismic damage.

Following a review of the results from a concurrent kinematic limit analysis, it was concluded that the failure of local macro-elements may precede development of the NCSE-02 displacement demands estimated by the global pushover analysis. Hence failure of local mechanisms may occur concurrently with the significant damage calculated by the non-linear pushover analysis.

This study highlights the risk of significant seismic damage to the typical unreinforced masonry buildings of the Eixample district of Barcelona. A suitable maintenance strategy to limit this risk has been identified. The results also reinforce the need for seismic response planning to manage the significant social and infrastructure demands should such a devastating event ever occur.

9. REFERENCES

- Ambraseys, N.N., Simpson, K.A., Bommer, J.J. (1996) Prediction of horizontal response spectra in Europe. *Earthquake Engineering & Structural Dynamics*, Vol. 25(4), pp. 371-400.
- Antonio, S., Pinho, R. (2004) Development and verification of a displacementbased adaptive pushover procedure. *Journal of Earthquake Engineering*. Vol 8(5) pp.643–661.
- ATC 40 (1996) Seismic Evaluation and Retrofit of Concrete Buildings, Applied Technology Council, Redwood City, California.
- Augenti, N., Parisi, F. (2010) Learning from Construction Failures due to the 2009 L'Aquila, Italy, Earthquake, *Journal of Performance of Constructed Facilities*, Vol. 24(6), pp. 536-555.
- Aydinoglu, M.N., Onem, G. (2010) Evaluation of analysis procedures for seismic assessment and retrofit design. *Earthquake Engineering in Europe (Geotechnical, Geological, and Earthquake Engineering)*. Vol. 17, London, United Kingdom, Chapter 8.
- Barbat, A.H., Pujades, L.G., Lantada, N. (2006) Performance of buildings under earthquakes in Barcelona, Spain. *Computer Aided Civil and Infrastructure Engineering*, Vol. 21 pp.573-593.
- Barbat, A.H., Pujades, L.G., Lantada, N. (2008) Seismic damage evaluation in urban areas using the capacity spectrum method: Application to Barcelona. *Soil Dynamics and Earthquake Engineering, Urban earthquake risk and damage assessment*, Vol. 28 (10-11), pp. 851-865.
- Barbat, A.H., Yépez, F., Canas, J.A. (1996) Damage scenarios simulation for seismic risk assessment in urban zones. *Earthquake Spectra*, Vol. 12(3), pp. 371-394.
- Binda, L., Gambarotta, L., Lagomarsino, S., Modena, C. (1999) A multilevel approach to the damage assessment and seismic improvement of masonry buildings in Italy. *Seismic Damage to Masonry Buildings*, Bernardini Ed., Rotterdam: Balkema.
- Binda, L., Modena, C., Casarin, F., Lorenzoni, F., Cantini, L., Munda, S. (2011) Emergency actions and investigations on cultural heritage after the L'Aquila earthquake: the case of the Spanish Fortress, *Bulletin of Earthquake Engineering*, Vol. 9 pp.105–138.
- Borcherdt, R.D. (1994) Estimates of site-dependent response spectra for design (methodology and justification). *Earthquake Spectra*, Vol. 10, pp. 617-653.
- BS EN 1998-1:2004 (E) (2004) Eurocode 8: Design of structures for earthquake resistance – Part 1: General rules, seismic actions and rules for buildings. *British Standards Institution*. Approved by European Committee for Standardization (CEN), 23 April 2004.

Casademunt, A.P. (2009) *Secrets D'Un Sistema Constructiu. L'Eixample*, Edicions Universitat Politecnica de Catalunya SL, Barcelona, Spain.

CCCB (2009) *Cerda and the Barcelona of the Future – Reality Versus Project*. Centre de Cultura Contemporània de Barcelona, Barcelona, Spain.

Chopra, A.K. (1981) *Dynamics of structures, A Primer*. Earthquake Engineering Research Institute, Berkeley, CA, 126 pp.

Chopra, A.K., Chintanapakdee, C. (2004) Inelastic Deformation Ratios for Design and Evaluation of Structures: Single-Degree-of-Freedom Bilinear Systems. *Journal of Structural Engineering*, September 2004, pp. 1309-1319.

Cid, J., Susagna, T., Goula, X., Chavarria, L., Figueras, S., Fleta, J., Casas, A., Roca, A. (2001) Seismic zonation of Barcelona based on numerical simulation of site effects. *Pure and Applied Geophysics*, Vol. 158, pp.2559-2577.

CTE-DB-SE-AE (2007) *Acciones en la Edificación. Documento Basico: Acciones en Edificacion*. Ministerio de Formento, Madrid, Spain.

DDPC – Modello B-DP (2006) *Scheda per il rilievo del danno ai beni culturali – Palazzi*, Dipartimento Della Protezione Civile.

EN 1990:2002 (E) (2002) *Eurocode: Basis for Structural Design*. Approved by European Committee for Standardization (CEN), 29 November 2001.

Faccioli, E. (2006) Seismic hazard assessment for derivation of earthquake scenarios in Risk-UE. *Bulletin of Earthquake Engineering*, Vol. 4(4), pp. 341-364.

Fajfar P. (2000) A nonlinear analysis method for performance-based seismic design. *Earthquake Spectra*, Vol. 16 (3), pp. 573-92.

FEMA 440 (2005) *Improvement of non-linear static seismic analysis procedures*. Federal Emergency Management Agency, Washington, D.C., United States of America.

Goel, R.K., Chopra, A.K. (2004) Evaluation of modal and FEMA pushover analyses: SAC buildings. *Earthquake Spectra*, Vol, 20 (1), pp. 225–254.

Grunthal G., Musson, R.M.W., Schwarz, J., Stucchi, M. (1998) *European Macroseismic Scale 1998 (EMS-98)*. European Seismological Commission, Working Group Macroseismic Scales, Luxembourg.

Gutierrez Alfonso, L., Gutierrez Diaz, J. (2010) *Rehabilitacio i canvi d'us d'un edifici situat al Carrer Consell de Cent, 435, Barcelona*. Final Architectural Report, Universitat Politecnica de Catalunya.

Irizarry, J. (2004) An advanced approach to seismic risk assessment. Application to the cultural heritage and the urban system of Barcelona, *PhD Thesis*, Universitat Politècnica de Catalunya, Spain, 406 pp.

Irizarry, J., Goula, X., Susagna, T., Roca, A., Mana, F. (2004) Earthquake risk scenarios for monuments in Barcelona, Spain, *Proceedings of the 13th World Conference on Earthquake Engineering*, Vancouver, B.C., Canada, Paper No. 2162.

Irizarry, J., Lantada N., Pujades L.G., Barbat A.H., Goula X., et al. (2011) Ground-shaking scenarios and urban risk evaluation of Barcelona using the Risk-UE capacity spectrum based method, *Bulletin of Earthquake Engineering*, Vol. 9(2), pp. 441-466.

ISCARSAH (2005) Recommendations for the Analysis and Restoration of Historical Structures. International Scientific Committee on Analysis and Restoration of Structures of Architectural Heritage, ICOMOS.

ISO 13822 (2010) Bases for design of structures Assessment of existing structures. International Organization for Standardization, Geneva, Switzerland.

Kalkan, E., Kunnath, S.K. (2006) Adaptive Modal Combination Procedure for Nonlinear Static Analysis of Building Structures. *Journal of Structural Engineering*, November 2006, pp. 1721-1731.

Kalkan, E., Kunnath, S.K. (2007) Assessment of current nonlinear static procedures for seismic evaluation of buildings. *Engineering Structures*, Vol. 29, pp. 305-316.

Lagomarsino, S. (1998) A new methodology for the post-earthquake investigation of ancient churches. *Proceedings of the XI European Conference on Earthquake Engineering*, Paris.

Lagomarsino, S., Giovinazzi, S., Podestà, S., Resemini, S. (2002). WP4 -Vulnerability assessment of current buildings: I level methodology for the vulnerability assessment of current buildings and guidelines for the implementation. RISK-UE project: An advanced approach to earthquake risk scenarios with applications to different European towns. Contract No. EVK4-CT-2000-00014. pp. 28.

Lantada, N., Pujades, L.G., Barbat A.H. (2009) Vulnerability index and capacity spectrum based methods for urban seismic risk evaluation. A comparison. *Natural Hazards*, Vol. 51, pp. 501-524.

Lourenco, P.B. (2010) SA2 - Structural Analysis Techniques, Course Notes – Advanced Masters on the Structural Analysis of Historical Constructions.

Molin, D. (1995) Considerations on the assessment of macroseismic intensity, *Annali di Geofisica*, Vol. 38, pp. 805-810.

Mouroux, P., Bertrand, E., Bour, M., Le Brun, B. Depinios, S., Masure, P. (2004) An advanced approach to earthquake risk scenarios with applications to different European towns. *Proceedings of 13th World Conference on Earthquake Engineering*, Vancouver, Canada.

NCSE-02 (2002) Norma de construcción sismorresistente: Parte general y edificación, Española. Subcomisión Permanente de Normas Sismorresistentes, Real Decreto 997/2002. Boletín Oficial del Estado del 27 de septiembre de 2002.

NIKER B3.1. (2010) Inventory of earthquake-induced failure mechanisms related to construction types, structural elements, and materials. *New integrated knowledge based approaches to the protection of cultural heritage from earthquake-induced risk*, Università di Padova, Italy. Project No. 244123.

Pujades, L.G., Barbat A.H., Gonzalez-Drigo R., Avila J., Lagomarsino S. (2010) Seismic performance of a block of buildings representative of the typical construction in the Eixample district in Barcelona (Spain). *Bulletin of Earthquake Engineering*, Online: 17 September 2010, DOI:10.1007/s10518-010-9207-5, pp. 1-19.

Roca, P. (2010) Ancient rules and classical approaches, Course Notes – Advanced Masters on the Structural Analysis of Historical Constructions.

Silva, J. (2011) Seismic Analysis of Local Collapse Mechanisms for Typical Masonry Buildings from Barcelona's Eixample District, *Master's Thesis*, Universitat Politècnica de Catalunya, Spain.

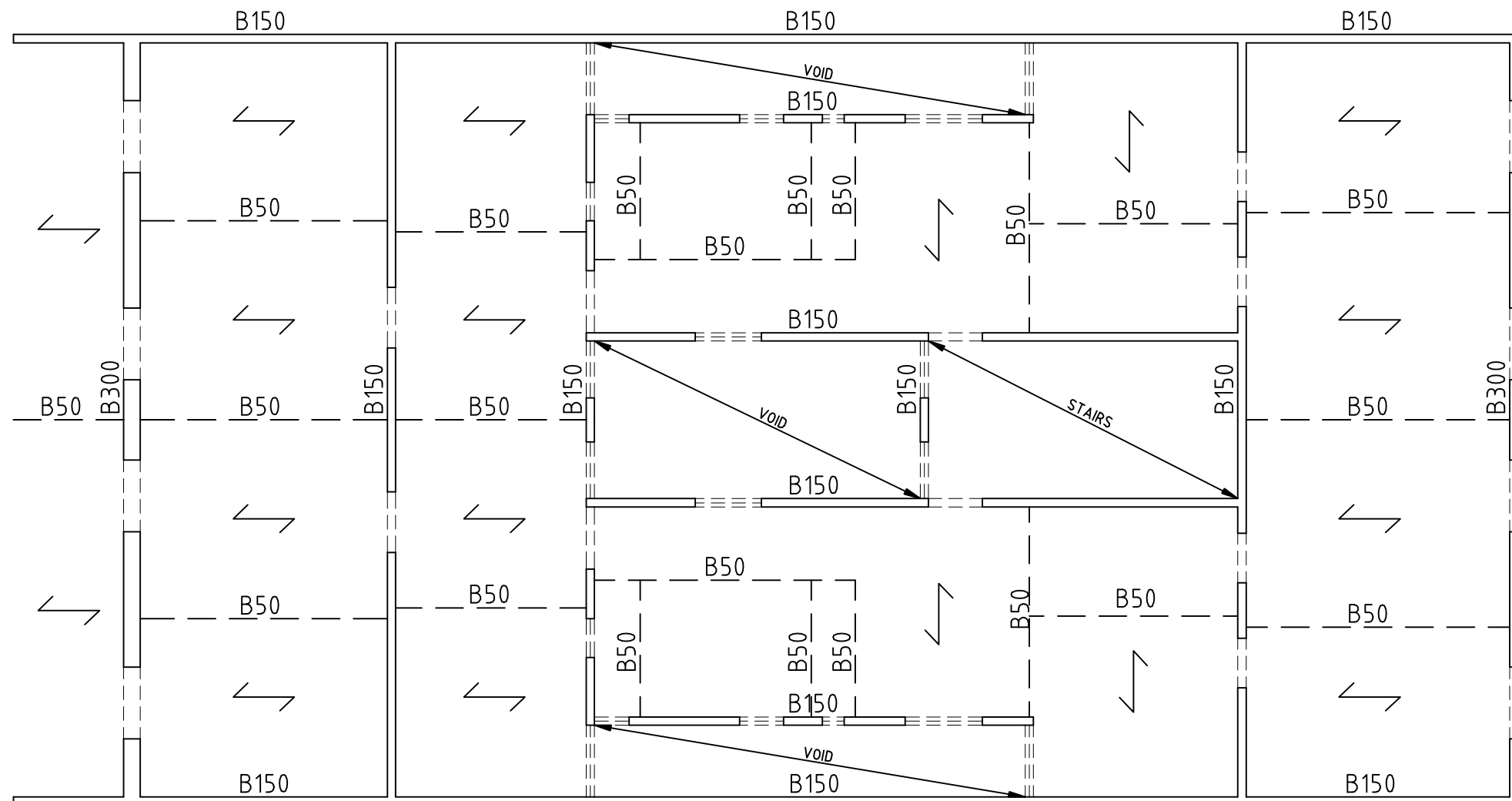
10. APPENDICES

10.1 Appendix A

The following AutoCad drawing is provided of the building at 629 Gran Via de la Catalanes, Barcelona:

Table 10.1: Drawing Register

Drawing Number	Drawing Title	Revision
S01	Typical Floor Plan	A



TYPICAL FLOOR PLAN

SCALE 1 : 100

LEGEND

- ↙ - DENOTES SPAN DIRECTION OF FLOOR JOISTS, SPACED AT APPROX. 450mm CTS.
- ==== - DENOTES DOORWAY OPENING.
- ==== - DENOTES WINDOW OPENING.
- B150 - DENOTES 150mm THICK LOAD BEARING BRICKWORK WALL. (300mm THICKNESS AT GROUND FLOOR)
- B300 - DENOTES 300mm THICK LOAD BEARING BRICKWORK WALL. (600mm THICKNESS AT GROUND FLOOR)
- B50 - DENOTES 50mm THICK NON LOAD BEARING BRICKWORK PARTITION WALL.

Issue	Description	Drawn	Chk.	Appd.	Date
1	FINAL ISSUE				15.07.11

Project SEISMIC PERFORMANCE OF A TYPICAL EIXAMPLE BUILDING BARCELONA, SPAIN	Designed by	C. POTTER	Project No.	Drawing No.	Rev.
	Drawn by	C. POTTER			
	Date	JULY 2011			
	Scale	1:100 @ A3			
Title TYPICAL FLOOR PLAN	Status	FINAL	-	S01	A